

**COMPUTER MODELING  
OF NEUROMODULATION IN THE  
MANAGEMENT OF  
CHRONIC PAIN**

**Ljubomir Manola**

**PhD dissertation committee:**

**Promotor:**

prof. dr. ir. Peter Veltink

**Assistant-promotor:**

dr. Jan Holsheimer

**Members:**

prof. dr. Enrico Marani, Universiteit Twente, The Netherlands

prof. dr. Bart Nuttin, MD, Katholieke Universiteit Leuven,  
Belgium

prof. dr. ir. Kees Slump, Universiteit Twente, The Netherlands

prof. dr. tech. Dejan Popović, University of Belgrade, Serbia  
& Aalborg Universitet, Denmark

The research described in the thesis was performed in the Biomedical Signals and Systems Group at the University of Twente, The Netherlands. In part, this research was financially supported by Advanced Bionics - a Boston Scientific Company, which is gratefully acknowledged.

**Title:** Computer modeling of neuromodulation in the management of chronic pain

**Author:** Ljubomir Manola

**ISBN:** 90-365-2357-5

**Printed by:** Wöhrmann Print Service, Zutphen, The Netherlands

**Copyright © 2006, Ljubomir Manola**

**COMPUTER MODELING  
OF NEUROMODULATION IN THE  
MANAGEMENT OF  
CHRONIC PAIN**

**DISSERTATION**

to obtain  
the doctor's degree at the University of Twente,  
under the authority of the rector magnificus,  
prof. dr. W.H.M. Zijm,  
on account of the decision of the graduation committee,  
to be publicly defended  
on Wednesday, June 14, 2006 at 15.00

by

**Ljubomir Manola**

born on March 14, 1977  
in Belgrade, Serbia

This dissertation is approved by:

prof. dr. ir. Peter Veltink

dr. Jan Holsheimer

“Fortitudo ac decus”  
Gladiatore

To:  
*Life, nature and their wonders*



## Acknowledgments

This thesis is the ultimate result of a four year research carried out in the Biomedical Signals & Systems group at the University of Twente, The Netherlands. Surely, a lot of time has been invested in the research and writing of the articles and this thesis. However, I also had the opportunity to see the world and learn things about life. I like to say: “I do not live to work, but rather work to live”. This means that I have interacted a lot with my environment and met many nice, unique people, some of which I would like to mention here. All these people, directly or indirectly, constitute an important part of my life.

I cannot help beginning with Jan Holsheimer, my daily supervisor, with whom the ‘dutch chapter of my life’ began. Working with Jan was a pleasure from the first day and there was not a single day (in four years) that it was different. He is an excellent person, that guided me in a gradual, relaxed and ‘stress-free’ way. But Jan is much, much more than my colleague and teacher of research and science. I could always approach Jan for advice or help on anything and I did not need to beat around the bush when I had a question or request. I always felt like I was addressing a friend. Together with his wife, Ria, they accepted, supported and surrounded me with an entire sea of kindness. I feel that my integration in the dutch society was more successful thanks to them. They were persistent and patient with practicing ‘nederlands’ with me, especially Ria, and certainly large credits for my passing the state exam on dutch language goes to them. The three of us spent treasured times just chatting or having serious discussions in (english or dutch), strolling or cycling, enjoying nice food that Ria would usually make, tasting wines, going to conferences together... I will remember this time with joy lifelong. But above all, I feel like Jan and Ria are my dutch family! Bedankt voor alles – ik hou van jullie!

My favorite greek person is Dimitrios Kotiadis. We started as colleagues and housemates, but we quickly developed a strong friendship and we even consider each other a brother. Memorable trips to Rhodes, England, Switzerland, making ‘masterpieces’ of food together, going out, drinking, chasing ragazze or just fooling around in our flat and later in Macandra was just part of the enormous time we spent together during four years. Naturally, we had some disputes over time, but we always managed to sort things out and to strengthen the trust in each other even further. Dimitri, thank you for believing and trusting in me on many occasions, for supporting me many times, giving me advice, making fun of each other, thank you for waking up that cook in me, for teaching me many things and for making my life in a foreign country certainly easier.

Dimitri’s family, especially Cpt. Ilias and Lynette, accepted me as a family member and I certainly had lots of reasons to feel that way. Family

Kotiadis, my greeks, thank you also for all the kindness and hospitality you gave to me!

At work, whenever I approached Peter Veltink, Jan Buitenweg and Enrico Marani with a scientific problem, they would always use their first available time slot to consider it and would always tackle it with utmost interest and focus, as if it was their own burning question. I value their advice and help. Work aside, Peter also showed a strong human line and helped me sort out a number of (administration) problems. Peter, thank you for always finding time to listen to me, regardless of how busy you were, and for helping me!

Wies, our secretary, is another person who was always very kind and helpful. Wies, thank you!

Having Remy and Daniel for roommates at work guaranteed that not a single day at work would be boring, the same or fully productive... I appreciate our 'anti-RSI' strategy so much. Guys, thanks for all the fun that we had in and out of the office!

My master students Bas Roelofsen and Lisette Harting deserve special credits for the work they did, a part of which was included in this thesis.

Big thanks go to Wilbert Wesselink, my predecessor on project, for providing me advice and explanations whenever I asked.

I thank everyone in the BSS group, for being nice and kind colleagues - I am proud and honored to have been a part of this group! I also apologize if I bothered you with my singing - it's safe to take out your earplugs now...

I also thank prof. Popović, my former supervisor, for boosting my interest in biomedical engineering with his easygoing and humourous, yet brilliant approach. Thank you also for giving me valuable advices, promptly, whenever I asked.

Living in Macandra and going to the international parties exposed me to a large number of different and interesting people. With many of them I made friends and we explored Holland together and had lots of fun. It wasn't easy to witness their departures and farewells from Enschede. I'd like to mention and thank Macandra gang from my first year among which my Italians Piero, Pippone, Luca, Alessio then Faten, Preeti and Norwegians, then Dyego, Sandra, Kerry and, from the last Macandra period, Pietro-the-Generale, Marco, Carmela&Carmela, Sonia, Karina and other Russians, Luca, Damiano, Uroš, Mila... Outside Macandra, I'd like to thank Linda, Emanuela, Blas, Eric, Sebastian, Bente, Jillian, Estelle, Richie, my 'greek society' and people from Smit (parties). Special thanks go to Colleen and Michael with whom Dimitrios and I spent lots of fun and quality time.

Of course, the Serbian population here deserves a special credit. Guys, I think we did a good job in supporting each other here! Many times I got a useful advice from you especially those who spent longer time here. Zikislave & Tijana, Miloše, Rastislave, Duško, Boki, Dragana & Blažo, Vojče & Sofka, Smiljanići, Potići, Dragone, Zorane & Tanja, Tanja T., Nataša, Ana I., Jelena, Borise & Jelena, Dragana & Chedo, my 'srpčići', I enjoyed the spirit of Serbia



we managed to keep up here and I thank you for that. The members of our basketball squad, thanks for great games.

Skating, windsurfing, riding, climbing, capoeira, tennis etc... though I found them very attractive, none of these kept my attention as long as salsa and latino dances did. It's not only about latin music, but the entire atmosphere that surrounds it. I spent hours in lessons and parties by Rico Latino developing my own 'serbian Lou' style of dancing that I will carry with me wherever I go further. Dancing and socializing in salsa worked as an anti-stress medicine for me. I thank all my 'salseras e salseros' for fantastic atmosphere and great dances.

Finally, I thank Marija, a girl that walked into my life recently, for having a great time together and for understanding and supporting me in this final stage...

The very last thanks goes to my family, my sister Ana, my mother Mila and my father Predrag who gave me tons of love and support my whole life. I know that the criticism you express sometimes for my choices (in life) is because you care and wish all the best for me. I also know that it was quite a change and not easy for you to see me only a couple of weeks per year but I also know that you do understand, especially at this moment, that it was for my own benefit and that I had a fantastic, intensive and successful chapter in life. Zato hvala vam za sve i znam da mogu isto i ubuduće da očekujem.

To conclude, all these people had a different impact on me in the previous four years and contributed in a different way to my being here. Therefore, I thank them all once again for helping me to be who I am and where I am!

Ljubomir

Enschede, 14. May 2006.

## Table of CONTENTS

<b>Glossary</b> .....	<b>11</b>
<b>CHAPTER 1</b> .....	<b>13</b>
Introduction to clinical neuromodulation techniques and computer modeling of their effects	
<b>CHAPTER 2</b> .....	<b>35</b>
Technical performance of percutaneous and laminectomy leads analyzed by modeling	
<b>CHAPTER 3</b> .....	<b>55</b>
Technical performance of percutaneous leads for spinal cord stimulation: a modeling study	
<b>CHAPTER 4</b> .....	<b>77</b>
Theoretical investigation into longitudinal electrical field steering in spinal cord stimulation	
<b>CHAPTER 5</b> .....	<b>97</b>
Modelling motor cortex stimulation for chronic pain control: electrical potential field, activating functions and responses of simple nerve fibre models	
<b>CHAPTER 6</b> .....	<b>119</b>
Anodal vs cathodal stimulation of motor cortex: a modeling study	
<b>CHAPTER 7</b> .....	<b>145</b>
Final remarks	
<b>Summary</b> .....	<b>153</b>
<b>Samenvatting</b> .....	<b>155</b>
<b>Curriculum vitae</b> .....	<b>159</b>
<b>List of publications</b> .....	<b>160</b>

**Glossary of anatomical and clinical terms  
(alphabetical order)**

CS	– central sulcus
CSF	– cerebrospinal fluid
DM	– dura mater
DCs	– dorsal columns
DRs	– dorsal roots
GM	– gray matter
LAM	– laminectomy lead
MCS	– motor cortex stimulation
PCG	– precentral gyrus
PERC	– percutaneous lead
SCS	– spinal cord stimulation
WM	– white matter



# **Chapter 1**

**Introduction to clinical neuromodulation techniques  
and computer modeling of their effects**

## 1.1. Neuromodulation

According to the International Neuromodulation Society, neuromodulation (NM) is defined as the therapeutic alteration of activity in the central, peripheral or autonomic nervous systems, electrically or pharmacologically, by means of implanted devices.

Some applications of NM found more readily their way into clinical practice and are nowadays well-established and widely used despite the fact that their mechanisms of action are often not well understood. NM can be achieved by focal administration of neurochemicals (chemical neuromodulation e.g. intrathecal drug pumps) or by applying electrical stimulation (electro-neuromodulation). Some NM applications related to pain are the scope of this thesis and are therefore discussed in greater detail below. The identified clinical indications of electro-NM are neuropathic pain (either of central or peripheral origin) [12, 33, 80], limb ischaemia (peripheral vascular disease) [4], cardiac ischaemia (angina) [17], spasticity (hyperreflexia), motor disorders (tremor, dyskinesia, dystonia) [8], psychiatric disorders (obsessive-compulsive disorder [56], depression [20], Gilles de la Tourette syndrome [77]), epilepsy [20], neurogenic incontinence [9, 66], auditive deficit (tinnitus) [18] with other indications still emerging. Stimulation is applied at the afferent side or within the central nervous system. The targets may be: spinal cord (dorsal columns (DCs) and/or dorsal roots (DRs)), basal ganglia, thalamus, motor cortex, cerebellum, vagal nerve, trigeminal nerve, occipital nerve, lumbo-sacral spinal nerves, peripheral nerves. A main application of NM is still chronic pain treatment, in particular pain of neuropathic origin.

## 1.2. Chronic pain

There are two types of chronic pain:

- *Nociceptive pain* – occurs as a response of cutaneous afferents to tissue damage near their receptors. It is well localized and lasts only as long as tissue damage causes activation of the pain receptors. Additionally, a prolonged activation of the receptors may cause a change in transfer function of the pain pathway.
- *Neuropathic pain* – follows trauma, dysfunction or pathological changes in the neural system itself (most frequently in the periphery) [58]. A relationship between the neural damage and the onset of neuropathic pain is not found. The pain is characterized by abnormal, unpleasant sensations (dysesthesia), a painful response to non-noxious stimuli (allodynia), and/or an exaggerated response to noxious stimuli (hyperalgesia) and the persistence of pain after removal of the stimuli [40]. Apart from the physiological component, a strong psychological component of pain perception is also present [69]. The quality of life of the affected individual is often seriously deteriorated. Sometimes the

persistence and severity of neuropathic pain may even lead to suicidal inclinations.

By means of neuromodulation it is possible to change the altered transfer function of the impaired neural circuitry so as to normalize its function back within its natural range. Because of the limited invasiveness and reversibility of the therapy, neuromodulation is preferred over neuroablative procedures. Neuromodulation is trialed when the pain condition proves to be refractory to other treatments (physical therapy, pharmacological treatment, surgical intervention) although there are reports indicating that an earlier application would actually increase the success rate [35, 55].

Neuromodulation can be attempted to target any part of the peripheral or central nervous system (that interacts with pain pathway) depending on the location and the complexity of pain [72]:

- Transcutaneous electrical nerve stimulation (TENS) – stimulates only the nerve fibers in the vicinity of the lead
- Peripheral nerve stimulation (PNS) – stimulates nerve fibers originating distally from the stimulation site
- Spinal nerve stimulation - stimulates nerve fibers originating from a single dermatome (usually lumbar or sacral dermatomes which are difficult to target by SCS)
- Spinal cord stimulation (SCS) – stimulates nerve fibers originating from a single or multiple dermatomes caudal to the stimulation site
- Thalamic stimulation – not so successful and almost abandoned
- Motor cortex stimulation – stimulates neural structures that induce analgesia in primarily central (poststroke) and trigeminal pain syndromes.

In this thesis, spinal cord stimulation and motor cortex stimulation as clinical NM techniques for the management of chronic, intractable, neuropathic pain are addressed.

### **1.3. Spinal cord stimulation (SCS)**

#### **Historical background**

In 1965, Melzack and Wall presented their ‘gate-control’ theory of pain transmission in the spinal cord [41]. Motivated by this theory, Shealy and colleagues [67] implanted a lead subdurally on the dorsal side of the spinal cord in a cancer patient, whose pain was alleviated by the application of electrical stimuli. The particular patient responded well to the stimulation and a new therapy was born although nociceptive pain is now considered a poor indication for SCS treatment. In the following years, Shealy and colleagues implanted a number of patients having different indications [68]. Other centers adopted the technique too and applied it in various pain conditions with variable success. This variation in success was primarily due to a lack of proper selection criteria for SCS candidates, poor clinical experience, insufficient training and technical

problems/insufficiencies of the early SCS systems (lead fracture, dislocation, insulation failure) [7, 69]. Therefore, the therapy was almost abandoned in the early 1980s. However, improvements in the design of the equipment (i.e. increased reliability and versatility), implantation procedure, patient selection criteria, defining the strategy for screening and follow-up of the patients caused a better understanding of the mechanisms and better training of the physicians that led to SCS regaining popularity, both in USA and Europe [7].

### **Mechanism of action**

Although the theory of Melzack and Wall [41] was challenged [32, 45] and modified even by the authors themselves [78] its basic idea still persists: the interaction of noxious and non-noxious stimuli (originating from the same dermatome) exists in the dorsal horn of the spinal cord. Their relative strength determines whether the ascending signal will be perceived as pain or not. Thus, an excessive noxious input (mediated by small A $\delta$ - or C-fibers) to the dorsal horn neural network would open the 'gate' and result in pain perception. Conversely, the activation of large, cutaneous, mechanoreceptive fibers (A $\beta$ ) inhibits the activity of the interneurons in the dorsal horns thus closing the 'gate' which in turn diminishes/abolishes pain perception. Theoretically, pain perception may also occur when the A $\beta$  input to the dorsal horn is reduced and the noxious input is at its normal level. The 'gate-control' theory is schematically shown in **Figure 1**.

The exact mechanism of analgesia is not yet known [21, 34, 42, 52, 60, 69]. A number of theories has been proposed:

- SCS causes a direct blocking of the impulses signaling pain [13]
- Supraspinal mechanisms (thalamus, reticulo-spinal loops) [57]
- Changes in the autonomic system responses (in heart and limb ischaemia) [42]
- Normalization of the disturbed function of neurotransmitters [40, 42]

It is likely that the mechanism of action is complex and involves a combination of the aforementioned (and possibly additional) neurophysiological mechanisms. A proof that it is no placebo effect [69] was important for the survival of the clinical SCS. When SCS is applied, a tingling sensation called *paresthesia* (presumably due to orthodromic transmission of the activated dorsal column fibers) is felt in the corresponding dermatomes. Ideally, this sensation substitutes the uncomfortable dysesthesia, felt when pain prevails. Achieving paresthesias in the painful dermatomes is a necessary, although not a sufficient, condition for pain relief. It is considered to be a statistically significant predictor of the success of the therapy [1, 7, 52, 69].



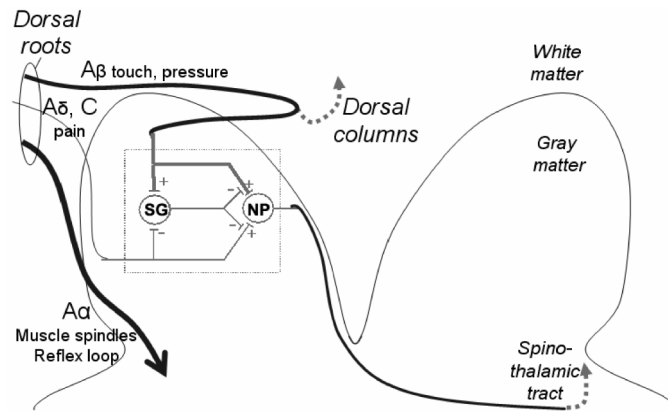


**Figure 1.** Schematic of the ‘gate-control’ theory: suppression of the pain signal transmission in the dorsal horn circuitries of the spinal cord through the activity of large, mechanoreceptive fibers. NP – nucleus proprius. SG – substantia gelatinosa. (Courtesy of Prof. P. Veltink, University of Twente, The Netherlands).

Bearing in mind the position of the lead in the dorsal epidural space, large, myelinated nerve fibers in the DRs and in the superficial parts of the DCs are most likely stimulated directly in SCS [31]. When the large DC fibers originating from certain dermatomes are stimulated, paresthesia is perceived in those dermatomes. Similarly, by stimulating large, myelinated fibers in the DRs, paresthesia is felt in part of the corresponding dermatome. However, the DRs also contain large, myelinated nerve fibers involved in reflex loops whose stimulation may induce undesired discomfort/motor responses and stimulation must be below the discomfort threshold (DT) in order to avoid these effects. Favorably, the stimulation threshold of these proprioceptive fibers is somewhat higher than the threshold of the most excitable DR fibers [24]. The *therapeutic range* is defined as the ratio between the discomfort threshold and the threshold for which initial paresthesia is perceived (paresthesia threshold (PT)). With a different lead position and configuration (number and polarity of poles), the therapeutic range can be extended and, with it, the chance for the success of therapy (see further in this chapter).

Although it is possible to achieve the same effects by stimulating the appropriate peripheral nerves, SCS has shown more versatility than PNS, spinal nerve stimulation and TENS. A relatively easy accessibility of the spine and representation of all dermatomes caudal to the level of implantation [71] (**Figure 2A**) makes SCS a convenient choice, especially if complex, multi-dermatomal pain should be treated.

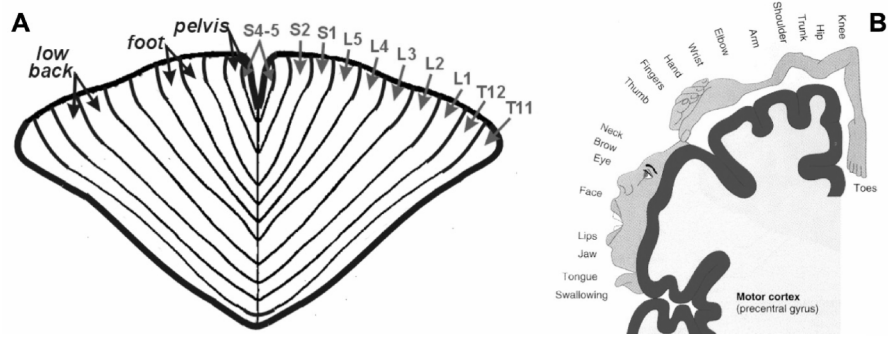


**Figure 2.** Somatotopic organization of: A) Dorsal columns at the low-thoracic level (Smith and Deacon [71] modified by Holsheimer [30]) and B) Brodmann area 4 of the motor cortex (adapted from Penfield [62]). These presentations are approximations because significant overlap of adjacent body part projections exists.

### Clinical indications and efficacy

Chronic, neuropathic pain responds favorably to SCS treatment [52, 69]. In contrast, nociceptive pain does not show a good response to SCS and is not considered to be a positive indication for it (despite reports of a few cases that did actually respond). Success of SCS when treating pain associated with angina pectoris and ischaemic (upper or lower) limb pain (peripheral vascular disease) is almost certain. There are reports that, in addition to alleviating the accompanying pain, SCS also ameliorates the disease condition by reducing ischaemia through vasodilatation. It is not yet clear which one is the primary effect of stimulation [52, 69]. The second group in which success of SCS therapy is less certain but still very likely consists of reflex sympathetic dystrophy (complex regional pain syndrome I), causalgia (complex regional pain syndrome II), peripheral nerve lesion, stump pain, cauda equina damage and nerve root avulsion. Patients diagnosed with failed back surgery syndrome (FBSS), failed neck surgery syndrome (FNSS), phantom limb pain and spinal cord injury have less, but still fair chances for improvement. Failed surgery syndromes are often difficult to diagnose but are the most commonly encountered chronic pain syndromes [15, 76]. However, they may not only be of neuropathic but also nociceptive etiology, the latter not being likely to respond to SCS. Axial pain (low back or neck) seems to be difficult to treat, presumably because of the nociceptive component that may be involved. In addition, the fibers originating from the low back region seem to be located in the lateral parts of the DCs (for the low-thoracic level where most implants are done) [30]. This may cause their stimulation threshold to be above the DT which makes their stimulation unfeasible without causing adverse effects. The failed surgery syndromes remain challenging to tackle and because of the high incidence they represent an attractive issue for the SCS approach.

Studies to assess the efficacy of SCS are difficult to design. The methods of assessment and interpretation of the results are not unified across clinical centers performing these studies. The studies cannot be double-blinded because the patients feel paresthesias. Perhaps the most disappointing fact is that there is *no objective measurement of pain relief*. All studies have to rely on patient's subjective perception of pain and memory about it at the moment of current and previous questionings (visual analogue scale - VAS). This is especially problematic as pain perception involves a psychological component and it is not uncommon that pain patients are emotionally distressed [69]. In addition, the VAS scores may not be fully reliable [14]. A more objective approach is to map the paresthesia and pain coverage through patient interactive computer systems [6, 50] and to assess changes in the quality of life. Therefore, it is not surprising that percentages of pain relief are not consistent and vary from center to center and from series to series. All do, however, show that the initial pain relief is greater than the long-term success and that there are economical benefits of SCS. However, as a recent Cochrane review on studies about efficacy of SCS concludes, there have hardly been any prospective, randomized, controlled studies performed. Therefore, no sufficient evidence is available to assess the benefits of SCS in chronic pain treatment [38]. Turner et al. reported similar conclusions in their review and they proposed guidelines for study design, assessment and reporting [76].

#### **Implantation and technical aspects**

An SCS system comprises a lead, a cable and a pulse generator (**Figure 3**). All components are implanted. The *lead* is an insulating bar or plate on which multiple metal contacts are mounted, usually as one or more linear arrays. Unlike the early implants, the leads are now placed in the epidural space, next to the dura mater (**Figure 5A**). In this way cerebrospinal fluid (CSF) leakage and morbidity are avoided. Two lead types are used in SCS practice nowadays: *paddle (surgical)* and *catheter (percutaneous) leads*. Paddle leads are implanted via a laminectomy or a laminotomy and are fixed by suturing techniques. Both interventions are fairly complex and invasive, but provide direct visual control of the lead position. Catheter leads are inserted percutaneously using Tuohy needles under fluoroscopic guidance. Although the latter technique is surgically less demanding and less traumatic for the patient, both techniques require a high degree of skillfulness, carefulness and experience. Percutaneous leads were originally introduced for temporary trial stimulation but, because of their convenience, were later introduced for chronic implantation as well. The characteristics of paddle and percutaneous leads are summarized in **Table 1**.

**Table 1.** Characteristics of paddle and percutaneous leads: advantages and disadvantages.

Lead type:	Advantages	Disadvantages
<b>Paddle</b>	<ul style="list-style-type: none"> <li>• Placed under visual guidance</li> <li>• Direct contact with dura mater</li> <li>• Low migration rate</li> <li>• Choice of orientation</li> <li>• Larger volume, reduces distance to the cord by pressing dura ventrally [53]</li> </ul>	<ul style="list-style-type: none"> <li>• Complex implantation procedure</li> <li>• Significantly invasive</li> <li>• Frequent postoperative pain [69]</li> <li>• Access to spinal segments either proximal or distal to the laminotomy</li> </ul>
<b>Percutaneous</b>	<ul style="list-style-type: none"> <li>• Easy to implant</li> <li>• Minimally invasive</li> <li>• Little trauma</li> <li>• Access to multiple spinal segments</li> </ul>	<ul style="list-style-type: none"> <li>• No direct visual guidance in placement, fluoroscope needed</li> <li>• Larger migration rate [64]</li> <li>• Dorsoventral position in epidural space hard to control</li> <li>• Eventual stimulation of fibers in the ligamentum flavum [53]</li> </ul>

The early leads were hampered by frequent wire fracturing. Using different material and design this problem has been reduced nowadays. Similarly, newer percutaneous leads have better positional stability in the epidural space due to better materials and new anchoring techniques. This resulted in less incidence of lead migration [51, 81].

In trial stimulation the lead cable is externalized and connected to an external programmable pulse generator. It is performed to screen the patients and to map paresthesia coverage, but also to provide the physician and the patient with an objective basis to decide whether to opt for permanent implantation of the SCS system. By mimicking a permanent device it allows clinicians to assess the pain relief in multiple postures in daily routines and optimize the stimulation over the trial period that may last from a few days up to 2 months. After the trial period it is decided whether to implant the permanent SCS system. The disadvantages of the trial procedure are the risk of infection because of the transcutaneous cable and the need for two procedures [52]. Another drawback



**Figure 3.** SCS equipment: a pulse generator, a pair of cables and a pair of leads. (Courtesy of Advanced Bionics – a Boston Scientific Company, Valencia, CA, USA).

of trial stimulation is that the test lead is removed and a new one (often different type i.e. plate or percutaneous with different contact size and/or spacing) are inserted. The permanent lead may not be placed in exactly the same position as the removed temporary lead. This means that one cannot expect the permanent lead to perform exactly the same as the temporary one. Therefore, optimization of the contact combination and of the stimulating parameters has to be repeated with the permanent lead. Usually, trial stimulation is required to claim the reimbursement of the implant. The *pulse generator* delivers pulses of a preselected amplitude, duration and rate that get transferred through the contacts into the surrounding tissues. There are radiofrequency(RF)-powered and fully implantable, battery powered pulse generators. With technical advances that extended the capacity of the batteries the RF-powered pulse generators are becoming obsolete. This is especially true since the devices belonging to the newest generation are RF-rechargeable and fully implantable.

Most pulse generators include just one output channel i.e. one positive and one negative voltage [48]. All anodal contacts are connected to the positive output and all cathodal contacts to the negative output (**Figure 4**).

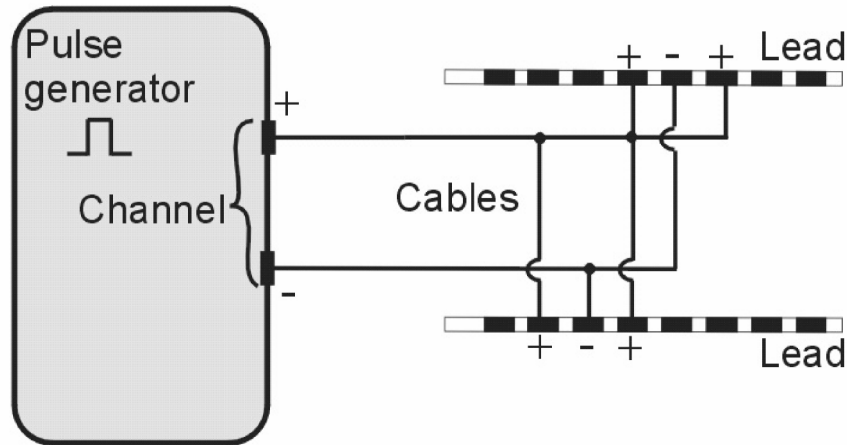


**Figure 4.** Pulse generator and its connection with two leads. Multiple contacts are connected to a single channel. All connected anodes have the same electrical potential just as all connected cathodes.

The flexibility of programming and control has improved, by introducing multiple generator channels, developing user-friendly interfaces, enabling independent control of the channels, making powerful programmers that use artificial neural networks [54] or other engineering concepts to help to optimize the stimulating contact configuration within a limited time. Either *constant current* or *constant voltage pulses* may be delivered to a lead contact, the former providing a better control and robustness to local tissue impedance changes [1].

The key manufacturers of the SCS systems are all based in the USA:

- Medtronic Inc., Minneapolis, MN, USA
- Advanced Bionics - a Boston Scientific Company, Valencia, CA, USA
- Advanced Neuromodulation Systems – a St. Jude Medical Company, Plano, TX, USA

#### **Positioning and programming the lead**

Following implantation, various contacts are connected as an anode (positive polarity, +) or a cathode (negative polarity, -) to the pulse generator, in order to select the contact combination giving most overlap of paresthesia coverage with pain topography. All combinations are tested with the same pulsewidth and pulse rate. The best combinations are further optimized by testing them with different amplitudes, pulse widths and pulse rates. Typically, these range within 33-120 Hz, 0.5-5 Volt and 100-500  $\mu\text{sec}$ , respectively [69].

On/off cycling is used to prolong the battery life. The position of the cathode(s) is the most critical one because the activation of DC and DR fibers occurs in its vicinity. This means that the spinal level and mediolateral position (with respect to the spinal cord ('physiological') midline, not the radiological midline) of the cathode(s) determines in which dermatome(s) paresthesias can be felt and positioning of the lead must be based upon the somatotopic organization of the DCs (**Figure 2A**). It can be considered, as a rule of thumb, that the lead should be positioned two vertebrae rostral to the uppermost spinal segment corresponding to a painful dermatome and ipsilateral or medial for unilateral and bilateral pain, respectively [69]. Although, the stimulation outcome is roughly determined by the cathode, the presence of nearby anodes modulates paresthesia coverage. In accordance with this principle, patients preferred bipolar stimulation with a small contact spacing over bipolar stimulation with a large contact spacing [36]. Similarly, tripolar stimulation was preferred over monopolar and bipolar [49]. These clinical findings were confirmed by theoretical studies [26, 27]. As mentioned previously, some contact combinations are favorable for stimulation of the DCs, whereas some favor stimulation of the DRs. It was also observed that with an increased distance from the lead to the spinal cord, the threshold for stimulation of the DCs increases more steeply than the threshold for the stimulation of the DRs [26]. By choosing a bipolar or tripolar (guarded cathode) combination as well as reducing the lead-to-cord distance, the threshold ratio for the stimulation of the DRs and DCs can be maximized, which would in turn enhance the recruitment of the DCs and increase paresthesia coverage. This may make a difference, for instance, in FBSS if activation of the fibers originating from the low-back region is achieved this way.

Thanks to the augmented interfacing between the pulse generator and users, a large number of anode-cathode combinations can be examined within a reasonable time. This is mandatory because the number of combinations to test has become extremely large since modern systems tend to include at least 8 contacts (2x4 or 1x8), or even more since the dual (or even triple) contact arrays are getting increasingly popular [2]. To some extent a systematic approach can be used, because narrow bipoles and tripoles are frequently selected by patients [3, 49]. With an improved design and versatility of latest generation of pulse generators (e.g. multiple independently-controlled channels, current-control etc.), a knowledge-based 'shaping' of the imposed electrical field may be possible. This may be done in such a way as to evoke certain physiological effects or even compensate for the suboptimal lead position or its dislodgment. In this way, not only does it matter which contact is programmed as an anode, cathode or is disconnected, but also the ratio of voltage/current applied to the contacts is important. This reduces the testing to only one or two longitudinal or transverse tripoles. The concept of shaping and steering the electric field was introduced, tested and proven in the Transverse Tripole System (TTS) using

dual-channel voltage pulse generator [29]. Also in **Chapter 4** of this thesis a new approach for electrical field steering that uses these concepts is presented. Unfortunately, still a majority of the SCS systems have the following shortcomings: lead contact spacing too large (7-10 mm) to obtain optimal paresthesia coverage, poor control of (medio-lateral and dorso-ventral) position of percutaneously placed leads, voltage instead of current-controlled stimulation, single channel stimulation (no independent driving of the contacts), if dual channel stimulation is used pulses are delivered alternately by each channel. With the knowledge available in the literature, SCS systems could have been improved at a faster pace and more than it has been done.

#### **1.4. Motor cortex stimulation (MCS)**

##### **Historical background**

Unlike SCS, MCS for chronic pain management is a relatively new and still emerging clinical technique, performed only in a few centers worldwide (Japan, France, Sweden, Germany, Netherlands, Belgium). The idea about a possible influence of cortical stimulation on pain perception emerged from Penfield's observation that sensory responses could be provoked by motor cortex stimulation [37]. In the early 1990s, MCS was introduced as a clinical technique by Tsubokawa and colleagues [75] for patients with thalamic pain whereas Meyerson and his team used it in patients with neuropathic facial pain [44]. Neurosurgeons in France also acknowledged the technique and proposed several improvements [46, 63].

##### **Mechanism of action**

In order to optimize the therapy it is necessary to improve the understanding of the physiological mechanisms underlying pain relief by MCS. PET scan studies showed an increase in regional cerebral blood flow in the ipsilateral thalamus, cingulate gyrus, orbito-frontal cortex and brainstem [19, 63], but no increase in the motor cortex itself. This may be either due to an insufficient resolution of the PET scanners or to absence of activation of cortical neurons following electrical stimulus. An explanation for the latter could be that the activated cortical axons primarily have inhibitory synaptic connections with other neurons in the motor cortex. The neural elements that may be directly activated by MCS may either be large, myelinated nerve fibers or soma-dendritic elements in the cortex. From chronaxie and refractory period measurements during experiments in which motor responses were measured, Hanajima et al. concluded that nerve fibers are activated [22]. In contrast to SCS, anodal stimulation may also directly activate neurons, namely cortical pyramidal cells of which the dendritic tree is directed towards the anode [5, 65]. However, the way MCS suppresses pain remains unknown just as the elements that are directly stimulated by a stimulus pulse and neuronal circuits and neurophysiological mechanisms involved [43, 47].



### **Clinical indications**

In the clinical studies on MCS about 350 patients have been reported worldwide [43]. So far, central pain (secondary to a cerebral lesion) and neuropathic facial pain (secondary to a trigeminal nerve lesion) have been identified as indications for MCS, using a >50% pain relief as a criterion [10, 43, 47]. These types of pain are difficult to treat and are often refractory to contemporary pharmacotherapy. SCS is neither an option for these pain syndromes. Some success in the treatment of neuropathic pain syndromes related to limbs and trunk are also reported. These include phantom limb pain, spinal cord lesion pain, brachial plexus injury and peripheral nerve lesion [10, 47]. Using MCS treatment for these pain conditions may be justified only when SCS has failed to give satisfactory results. Apart from treatment of neuropathic pain, MCS might find a second application in relieving movement disorders [61] and enhancing poststroke rehabilitation [11].

### **Technique**

Following a craniotomy, a contact grid or linear array is brought on the dura mater. The central sulcus between the motor cortex and the somatosensory cortex is identified by the polarity reversal in the somatosensory potentials evoked by median nerve stimulation. To confirm its identification magnetic resonance imaging techniques are usually used. Once the motor cortex is identified, the representation of the painful body part within the motor cortex is localized by its stimulation and the recording of motor evoked potentials (MEP) in the EMG of a muscle in that body part. As in SCS, a number of anode-cathode combinations is tested and the cathode of the combination giving the largest MEP is selected for chronic stimulation. According to Penfield [62], motor cortex (just as sensory) has a somatotopic representation of all parts of the body (**Figure 2B**). Nevertheless, this representation differs among individuals and is prone to neural plasticity and thus necessitates mapping each patient's motor cortex individually. One or two linear contact arrays, usually the Resume (Medtronic Inc.), are placed across (and about perpendicular) to the central sulcus (**Figure 5B**) and sutured to the dura [47].

Usually, bipolar stimulation is applied by programming the contact over or close to the cortical representation of the painful body part as a cathode and programming one of the contacts posteriorly as an anode. The pulse amplitude used in MCS ranges from 1.5 to 10 Volt (but always below motor threshold), pulse width from 90 to 450  $\mu$ sec and stimulation rate between 40 and 100 Hz [10]. The on/off cycling mode may be used for the same reason as in SCS. To provide the stimulation pulses, fully implantable pulse generators similar to those used in SCS are applied. Only few complications were reported, among which epidural hematoma and pulse generator pocket infection.

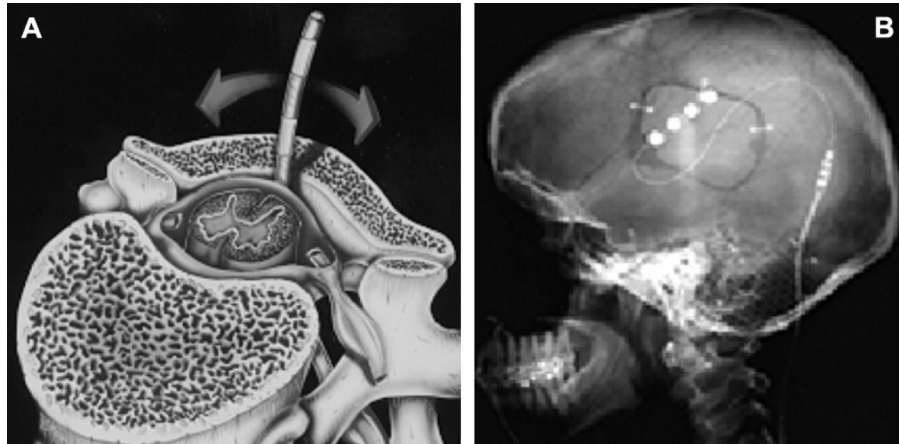


**Figure 5.** Placement of: A) A percutaneous lead for SCS in the dorsal epidural space (Courtesy of Medtronic Inc., Minneapolis, MN, USA) and B) A surgical lead for MCS under the skull bone (Courtesy of Prof. J-P. Nguyen, Hôpital Henri Mondor, Créteil, France).

## 1.5. Computer modeling

### Role of computer modeling

Computer modeling is a powerful tool that is utilized when it is difficult or impossible to perform an empirical study on animals or patients. However, any model is a simplification of reality and the degree of simplification depends on the computer power and on the choice of details that will be represented in the model. Care should be taken to carefully select parameters that are of importance for the modeled process and those that are not. Favorably, with an increased processing capacity of contemporary computers, more demands can be imposed on models, sometimes resulting in an increased complexity. However, a higher complexity may mean more (unknown) parameters to be chosen and does not guarantee a more useful model!

The goal of modeling as performed in the studies of this thesis is to extend knowledge about the immediate effects of the stimuli on neural tissue in the vicinity of the stimulating contacts. Combined with empirical methods this approach may help to determine which lead, stimulus, tissue and spatial parameters are important and how they affect stimulation of the particular neural structures (e.g. [26, 27]). Once the neural elements directly activated by the therapy are known, a part of the pain relieving chain is identified and this may help to elucidate the mechanism behind suppression of pain perception. On the other hand, if neural elements that should be targeted in order to obtain a successful treatment are known, modeling may reduce the effort and time

needed to optimize the stimulation parameters that will lead to improvement of the therapy outcome [28]. These improvements among others are needed as the success rate of the therapy (SCS and MCS) is rather low. E.g. the current criteria for a ‘good’ result of therapy (both SCS and MCS) are often that at least 50% of patients have a greater than 50% pain relief as indicated on VAS. With all restrictions of the assessment procedures (discussed previously), a good therapy should still yield a greater percentage of success.

### **Volume conductor and neural model**

The first SCS models were made by Coburn and Sin in 1980s [16, 70]. A decade later, our group (University of Twente), introduced a more complex and accurate SCS model [73]. The model was later validated [23, 74] and it was used to identify the most important parameters for stimulation [26, 27] as well as a new lead design [29, 59]. Recently, a MCS model was introduced [39]. Although still in an early stage, it already shed some light on the effects of electrical stimuli applied to the motor cortex (see **Chapter 5** and **Chapter 6**).

A SCS model consists of a 3D volume conductor model of part of the spinal cord including leads inserted in the epidural space (see **Chapter 2** and **Chapter 3**). The geometry of the model was made so as to fit data obtained from transverse MRI scans of the human spine at three different vertebral levels [25]. The tissue conductivities were either obtained from the literature or from measurements and approximation techniques (see **Chapter 2**). After defining potential difference(s) or current(s) between contact(s), the 3D electrical potential field was calculated using a red-black Gauss-Seidel numerical method with a variable overrelaxation factor. This field represents the driving force for stimulation of the neural structures in the model. Responses of DC and DR nerve fiber models were simulated. The fiber models used are compartmental models whose geometrical and electrical characteristics were chosen such that a behavior similar to that of human sensory fibers is mimicked [79]. The fibers were situated according to their anatomical position. In this way, it is predicted which fibers respond to a stimulus of a given amplitude when applied by the simulating contact combination.

Similarly, a MCS model comprises a 3D volume conductor representing the precentral gyrus and surrounding sulci, whose geometries and tissue conductivities were taken from the available (human) data (see **Chapter 5**). The electrical field imposed in the precentral cortex region below the epidural lead was calculated and subsequently the response of the neurons in the precentral gyrus was simulated. Both myelinated nerve fibers parallel and perpendicular to the cortical layers were modeled. It was shown that the group of fibers perpendicular to the cortical layers does not have a unified response to the stimulus, primarily due to their different orientations in respect to the contact surface (see **Chapter 6**). In addition, these fibers originate from the pyramidal cell bodies located closer to the contact. The presence of these cell bodies in the models modified the excitation threshold for some of these fibers. The lack of

knowledge on morphology, position and electrical characteristics of the cortical neural structures as well as scarce data on tissue conductivities, thickness of the CSF between the pia and dura mater under the implanted lead makes the model less accurate. Therefore, further improvements and validation of the MCS model are essential before model predictions can be incorporated in clinical practice.

### **1.6. Outline of the thesis**

In this thesis, computer modeling as a tool to explore the immediate biophysical effects of electrical stimulation in SCS and MCS is described. In **Chapter 2** the technical performance of percutaneous and paddle SCS leads having a similar contact spacing is compared. Leads commonly used in clinical practice were modeled and their performance was evaluated by their ability to recruit multiple large, myelinated fibers in the DCs and DRs, with a discussion on presumed implications on paresthesia coverage. The performance of several percutaneous leads with different contact spacing, as used in SCS practice, is evaluated in **Chapter 3** of the thesis. In addition, the influence of the medio-lateral and dorso-ventral lead position within the epidural space as well as the influence of the dorsal CSF thickness was explored. The performance of two leads inserted in parallel ('dual-lead') in the epidural space was compared against the performance of the corresponding single lead. In **Chapter 4** an electronically controlled method to smoothly steer the cathodal electrical field rostrally or caudally along the spinal cord is presented. The effects on primarily DR fiber recruitment achieved by this steering are reported. **Chapter 5** introduces and describes our first model of MCS. Initial results related to electrical field distribution, nerve fiber activating functions and the response of simple fiber models are presented. In addition, the influence of some geometrical parameters of the volume conductor model on the stimulus-induced electrical field and excitation threshold was assessed. In **Chapter 6** a refined MCS model and a more realistic model of the pyramidal neuron is presented. The sensitivity of its excitation threshold to different spatial, morphometric and electrical parameters, as well as to the thickness of the CSF and to precentral gyrus geometry was calculated. Finally, the modeling predictions were validated with empirical results, both from animal experiments and clinical trials.

## REFERENCES

- 1 Alo KM and Holsheimer J. New trends in neuromodulation for the management of neuropathic pain. **Neurosurgery**. 50:690-704, 2002
- 2 Alo KM, Recko V and Chornov J. Four year follow-up of dual electrode spinal cord stimulation for chronic pain. **Neuromodulation**. 5:79-88, 2002
- 3 Alo KM. Spinal cord stimulation for complex pain: initial experience with a dual electrode, programmable, internal pulse generator. **Pain Practice**. 3:31-38, 2003
- 4 Amann W, Berg P, Gersbach P, Gamain J, Raphael JH, *et al*. Spinal cord stimulation in the treatment of non-reconstructable stable critical leg ischaemia: results of the european peripheral vascular disease outcome study (SCS-EPOS). **Eur J Vasc Endovasc Surg**. 26:280-286, 2003
- 5 Amassian V, Stewart M, Quirk G and Rosenthal J. Physiological basis of motor effects of a transient stimulus to cerebral cortex. **Neurosurgery**. 20:74-93, 1987
- 6 Barolat G, Massaro F, He J, Zeme S and Ketcik B. Mapping of sensory responses to epidural stimulation of the intraspinal neural structures in man. **J Neurosurg**. 78:233-239, 1993
- 7 Barolat G. Current status of epidural spinal cord stimulation. (Review). **Neurosurg Q**. 5:98-124, 1995
- 8 Benabid AL. Deep brain stimulation for Parkinson's disease. **Curr Opin Neurobiol**. 13:696-706, 2003
- 9 Bosch JLHR and Groen J. Sacral (S3) segmental nerve stimulation as a treatment for urge incontinence in patients with detrusor instability: Results of chronic electrical stimulation using an implantable neural prosthesis. **J Urol**. 154:504-507, 1995
- 10 Brown JA and Barbaro NM. Motor cortex stimulation for central and neuropathic pain: current status. (Review). **Pain**. 104:431-435, 2003
- 11 Brown JA, Lutsep H, Cramer SC and Weinand M. Motor cortex stimulation for enhancement of recovery after stroke: case report. **Neurol Res**. 25:815-818, 2003
- 12 Burchiel KJ, Anderson VC, Brown FD, Fessler RG, Friedman WA, *et al*. Prospective, multicenter study of spinal cord stimulation for relief of chronic back and extremity pain. **Spine**. 21:2786-2794, 1996
- 13 Campbell JN. Examination of possible mechanisms by which stimulation of the spinal cord in man relieves pain. **Appl Neurophysiol**. 44:181-186, 1981
- 14 Carlsson AM. Assessment of chronic pain. I. Aspects of reliability and validity of the visual analogue scale. **Pain**. 16:87-101, 1983
- 15 Cherkin DC, Deyo RA, Loeser JD, Bush T and Waddell G. An international comparison of back surgery rates. **Spine**. 19:1201-1206, 1994
- 16 Coburn B. Electrical stimulation of the spinal cord: two-dimensional finite element analysis with particular reference to epidural electrodes. **Med Biol Eng Comput**. 18:573-584, 1980
- 17 De Jongste MJL, Nagelkerke D, Hooyshuur CM, Journee HL, Meyler PWJ, *et al*. Stimulation characteristics, complications and efficacy of spinal cord

- stimulation systems in patients with refractory angina: a prospective feasibility study. **Pace**. 17:1751-1760, 1994
- 18 De Ridder D, De Mulder G, Verstraeten E, van der Kelen K, Sunaert S, *et al*. Primary and secondary auditory cortex stimulation for intractable tinnitus. **Otorhinolaryngol Relat Spec**. 68:48-55, 2006
- 19 Garcia-Larrea L, Peyron R, Mertens P, Gregoire MC, Lavenne F, *et al*. Positron emission tomography during motor cortex stimulation for pain control. **Stereotact Funct Neurosurg**. 68:141-148, 1997
- 20 Groves DA and Brown VJ. Vagal nerve stimulation: a review of tis applications and potential mechanisms that mediate its clinical effects. **Neurosci Biobehav Rev**. 29:493-500, 2005
- 21 Gybels J and van Roost D. Spinal cord stimulation for the modification of dystonic and hyperkinetic conditons: A critical review. In: Recent Achievements in Restorative Neurology; Book 1: Upper motor neuron functions and dysfunctions. Basel: Karger, 1985: 56-70.
- 22 Hanajima R, Ashby P, Lang AE and Lozano AM. Effects of acute stimulation through contacts placed on the motor cortex for chronic stimulation. **Clin Neurophysiol**. 113:635-641, 2002
- 23 He J, Barolat G, Holsheimer J and Struijk JJ. Perception threshold and electrode position for spinal cord stimulation. **Pain**. 59:55-63, 1994
- 24 He J, Barolat G and Ketcik B. Stimulation usage range for chronic pain management. **Analgesia**. 1:75-80, 1995
- 25 Holsheimer J, Den Boer JA, Struijk JJ and Rozeboom AR. MR assessment of the normal position of the spinal cord in the spinal canal. **Am J Neuroradiol**. 15:951-959, 1994
- 26 Holsheimer J, Struijk JJ and Tas NR. Effects of electrode geometry and combination on nerve selectivity in spinal cord stimulation. **Med Biol Eng Comput**. 33:676-682, 1995
- 27 Holsheimer J and Wesselink WA. Optimum electrode geometry for spinal cord stimulation: the narrow bipole and tripole. **Med Biol Eng Comput**. 35:493-497, 1997
- 28 Holsheimer J. Computer modelling of spinal cord stimulation and its contribution to therapeutic efficacy. **Spinal Cord**. 36:531-540, 1998
- 29 Holsheimer J, Nuttin B, King GW, Wesselink WA, Gybels JM, *et al*. Clinical evaluation of paresthesia steering with a new system for spinal cord stimulation. **Neurosurgery**. 42:541-547, 1998
- 30 Holsheimer J. Does dual lead stimulation favor stimulation of the axial lower back? (Editorial). **Neuromodulation**. 3:55-57, 2000
- 31 Holsheimer J. Which neuronal elements are activated directly by spinal cord stimulation. **Neuromodulation**. 5:25-31, 2002
- 32 Iggo A. Critical remarks on the gate control theory. In: Janzen R. Pain. London: Churchill Livingstone, 1972: 127-128.
- 33 Kemler MA, Reulen JP, Barendse GA, van Kleef M, de Vet HC, *et al*. Impact of spinal cord stimulation on sensory characteristics in complex regional pain syndrome type I: a randomized trial. **Anesthesiology**. 95:72-80, 2001

- 34 Krames ES. Mechanisms of action of spinal cord stimulation. In: Waldman SD. *Interventional Pain Management*. Philadelphia: WB Saunders, 2001: 561-565.
- 35 Kumar K, Toth C, Nath R and Laing P. Epidural spinal cord stimulation for treatment of chronic pain: some predictors of success. A 15 year experience. **Surg Neurol**. 50:110-121, 1998
- 36 Law JD. Spinal stimulation: Statistical superiority of monophasic stimulation of narrowly separated longitudinal bipoles having rostral cathodes. **Appl Neurophysiol**. 46:129-137, 1983
- 37 Lende R, Kirsch W and Druckman R. Relief of facial pain after combined removal of precentral and postcentral cortex. **J Neurosurg**. 34:537-543, 1971
- 38 Mailis-Gagnon A, Furlan AD, Sandoval JA and Taylor R. Spinal cord stimulation for chronic pain. The Cochrane Database of Systematic Reviews. Issue 3. Art No.: CD003783.pub2. DOI: 10.1002/14651858.CD003783.pub2, 2004
- 39 Manola Lj, Roelofsen BH, Holsheimer J, Marani E and Geelen J. Modelling motor cortex stimulation for chronic pain control: electrical potential field, activating functions and responses of simple nerve fibre models. **Med Biol Eng Comput**. 43:335-343, 2005
- 40 Medtronic Pain Therapies. Neurostimulation for the management of chronic neuropathic pain. (Monograph). UC200501509 EE NB6422EE, 2005
- 41 Melzack R and Wall PD. Pain mechanisms: a new theory. **Science**. 150:971-978, 1965
- 42 Meyerson B and Linderoth B. Spinal cord stimulation: mechanisms of action in neuropathic and ischaemic pain. In: Simpson BA. *Electrical Stimulation and the Relief of Pain* (Pain research and clinical management series). Elsevier, 2003: 161-182.
- 43 Meyerson B. Motor cortex stimulation - effective for neuropathic pain but the mode of action remains illusive. (Editorial). **Pain**. 118:6-7, 2005
- 44 Meyerson BA, Lindblom U, Lind G and Herregodts P. Motor cortex stimulation as treatment of trigeminal neuropathic pain. **Acta Neurochir Suppl**. 58:150-153, 1993
- 45 Nathan PW. The gate control theory of pain. A critical review. **Brain**. 99:123-158, 1976
- 46 Nguyen J-P, Lefaucheur J-P, Decq P, Uchiyama T, Carpentier A, *et al*. Chronic motor cortex stimulation in the treatment of central and neuropathic pain. Correlations between clinical, electrophysiological and anatomical data. **Pain**. 82:245-251, 1999
- 47 Nguyen J-P, Lefaucheur J-P and Keravel Y. Motor cortex stimulation. In: Simpson B. *Electrical Stimulation and the relief of Pain* (Pain Research and Clinical Management). Elsevier, 2003: 197-209.
- 48 North R, Kidd D, Olin J and Sieracki J. Spinal cord stimulation electrode design: prospective, randomized, controlled trial comparing percutaneous and laminectomy electrodes - Part I: Technical outcomes. **Neurosurgery**. 51:381-390, 2002
- 49 North RB, Ewend MG, Lawton MT and Piantadosi S. Spinal cord stimulation for chronic, intractable pain: superiority of 'multi-channel' devices. **Pain**. 44:119-130, 1991

- 50 North RB, Nigrin DJ, Fowler KR, Szymanski RE and Piantadosi S. Automated 'pain drawing' analysis by computer-controlled, patient interactive neurological stimulation system. **Pain**. 50:51-57, 1992
- 51 North RB, Kidd DH, Zahwak M, James CS and Long DM. Spinal cord stimulation for chronic, intractable pain: experience over two decades. **Neurosurgery**. 32:384-395, 1993
- 52 North RB and Roark GL. Spinal cord stimulation for chronic pain. (Review). **Neurosurg Clin N Am**. 6:145-155, 1995
- 53 North RB, Lanning A, Hessels R and Cutchis PN. Spinal cord stimulation with percutaneous and plate electrodes: side effects and quantitative comparisons. **Neurosurg Focus**. 2:1-5, 1997
- 54 North RB, McNamee JP, Wu L and Piantadosi S. Artificial neural networks: application to electrical stimulation of the human nervous system. **Neurosurg Focus**. 2:1-5, 1997
- 55 North RB. Spinal cord stimulation: patient selection. In: Burchiel KJ. Surgical management of pain. New York: Thieme Medical Publishers, 2002: 527-534.
- 56 Nuttin B, Gabriels LA, Cosyns PR, Meyerson BA, Andreewitch S, *et al*. Long-term electrical capsular stimulation in patients with obsessive-compulsive disorder. **Neurosurgery**. 52:1263-1272, 2003
- 57 Nyquist JK and Greenhoot JH. Responses evoked from the thalamic centrum medianum by painful input: Suppression by dorsal funiculus conditioning. **Exp Neurol**. 39:215-222, 1973
- 58 Oakley J. Spinal cord stimulation for neuropathic pain. In: Simpson BA. Electrical Stimulation and the Relief of Pain (Pain research and clinical management series). Elsevier, 2003: 87-109.
- 59 Oakley J, Espinosa F, Burchiel K, Bothe H, McKean J, *et al*. Transverse tripolar spinal cord stimulation: results of an international multicenter study. **Neuromodulation**. 9:(in press), 2006
- 60 Oakley JC and Prager JP. Spinal cord stimulation. Mechanisms of action. **Spine**. 27:2574-2583, 2002
- 61 Pagni CA, Altibrandi MG, Bentivoglio A, Caruso G, Cioni B, *et al*. Extradural motor cortex stimulation (EMCS) for Parkinson's disease. History and first results by the study group of the Italian neurosurgical society. **Acta Neurochir Suppl**. 93:113-119, 2005
- 62 Penfield W and Rasmussen T. The cerebral cortex of man. A clinical study of localization of function., New York: The Macmillan Comp., 1950.
- 63 Peyron R, Garcia-Larrea L, Deiber MP, Cinotti L, Convers P, *et al*. Electrical stimulation of precentral cortical area in the treatment of central pain: electrophysiological and PET study. **Pain**. 62:275-286, 1995
- 64 Racz GB, McCarron RF and Talboys P. Percutaneous dorsal column stimulator for chronic pain control. **Spine**. 14:1-4, 1989
- 65 Rothwell J. Techniques and mechanisms of action of transcranial stimulation of the human motor cortex. **J Neurosci Methods**. 74:113-122, 1997
- 66 Schmidt RA. Applications of neurostimulation in urology. **Neurol Urodynam**. 7:585-592, 1988



- 67 Shealy CN, Mortimer JT and Reswick JB. Electrical inhibition of pain by stimulation of the dorsal columns: preliminary clinical report. **Anesth analg.** 46:489-491, 1967
- 68 Shealy CN. Six years' experience with electrical stimulation for control of pain. **Adv Neurol.** 4:775-782, 1974
- 69 Simpson BA. Spinal cord stimulation. **Pain Rev.** 1:199-230, 1994
- 70 Sin WK and Coburn B. Electrical stimulation of the spinal cord: a further analysis relating to anatomical factors and tissue properties. **Med Biol Eng Comput.** 21:264-269, 1983
- 71 Smith MC and Deacon P. Topographical anatomy of the posterior columns of the spinal cord in man. The long ascending fibers. **Brain.** 107:671-698, 1984
- 72 Stanton-Hicks M and Salamon J. Stimulation of the central and peripheral nervous system for the control of pain. **J Clin Neurophysiol.** 14:46-62, 1997
- 73 Struijk JJ, Holsheimer J, van Veen BK and Boom HBK. Epidural spinal cord stimulation: calculation of field potentials with special reference to dorsal column nerve fibers. **IEEE Trans Biomed Eng.** 38:104-110, 1991
- 74 Struijk JJ, Holsheimer J, Barolat G, He J and Boom HBK. Paresthesia thresholds in spinal cord stimulation: a comparison of theoretical results with clinical data. **IEEE Trans Rehab Eng.** 1:101-108, 1993
- 75 Tsubokawa T, Katayama Y, Yamamoto T, Hirayama T and Koyama S. Chronic motor cortex stimulation in patients with thalamic pain. **J Neurosurg.** 78:393-401, 1993
- 76 Turner JA, Loeser JD, Deyo RA and Sanders SB. Spinal cord stimulation for patients with failed back surgery syndrome or complex regional pain syndrome: a systematic review of effectiveness and complications. **Pain.** 108:137-147, 2004
- 77 Visser-Vandewalle V, Ackermans L, van der Linden C, Temel Y, Tijssen MA, *et al.* Deep brain stimulation in Gilles de la Tourette's syndrome. **Neurosurgery.** 58:(in press), 2006
- 78 Wall PD. The gate control theory of pain mechanisms: A re-examination and re-statement. **Brain.** 101:1-18, 1978
- 79 Wesselink WA, Holsheimer J and Boom HBK. A model of the electrical behaviour of myelinated sensory nerve fibres based on human data. **Med Biol Eng Comput.** 37:228-235, 1999
- 80 Wetzel TF, Hassenbusch S, Oakley JC, Willis KD, Simpson RK, *et al.* Treatment of chronic pain in failed back surgery patients with spinal cord stimulation: a review of current literature and proposal for future investigation. **Neuromodulation.** 3:59-74, 2000
- 81 Young RF. Brain and spinal stimulation: how and to whom! **Clin Neurosurg.** 35:429-447, 1989



# Chapter 2

## Technical performance of percutaneous and laminectomy leads analyzed by modeling

Ljubomir Manola • Jan Holsheimer

Institute for Biomedical Technology, Department of Electrical Engineering,  
University of Twente, The Netherlands

### Abstract

**Objective.** To compare the technical performance of laminectomy and percutaneous spinal cord stimulation leads with *similar* contact spacing by computer modeling.

**Method.** Monopolar and tripolar (guarded cathode) stimulation with both lead types in a low-thoracic spine model was simulated using UT-SCS software. Dorsal column and dorsal root fiber thresholds were calculated as well as the area of recruited fibers in the dorsal columns, the rostrocaudal span of recruited dorsal root fibers and the energy consumption at discomfort threshold.

**Results.** Tripolar stimulation is superior to monopolar stimulation in the recruitment of the dorsal columns, a percutaneous lead recruiting a ~15% larger dorsal column area than a laminectomy lead. This difference is reduced when the contact spacing of the lead models is the same. A percutaneous lead with significant wire impedance (140 Ohms) consumes ~115-240% more energy, whereas the same lead with negligible wire impedance consumes ~40-85% more energy. A deterioration of all performance parameters is predicted when a percutaneous lead is placed more dorsally in the epidural tissue.

**Conclusion.** When positioned next to the dura mater, a percutaneous lead has a similar performance (fiber recruitment in the dorsal columns and the dorsal roots) as a laminectomy lead with a similar contact spacing, but a substantially higher energy consumption. The superior clinical performance of the laminectomy lead is most probably due to the difference in volume and insertion technique of the two lead types.

---

\* Published in *Neuromodulation*, 7:231-241, 2004.

## 2.1. Introduction

Spinal cord stimulation (SCS) is a clinical method used to alleviate various chronic, neuropathic pain syndromes such as failed back surgery syndrome (FBSS), complex regional pain syndrome (CRPS), peripheral nerve injury, etc. Some vascular disorders accompanied by pain, e.g. peripheral vascular disease and angina can also be treated by SCS [1, 3, 19, 21]. The mechanism underlying SCS was postulated by Melzack and Wall in 1965 [15]. They hypothesized a ‘gate-control’ mechanism, stating that stimulation of large cutaneous mechanoreceptive fibers inhibits pain pathways towards the brain, thus reducing pain perception. At any level of the spinal cord, such fibers (originating from the dermatomes up to that level) are grouped in the dorsal columns (DCs) by their segment of origin [20]. The presence of fibers from many dermatomes at a single spinal level and their topographic arrangement makes the DCs eligible for this therapy.

In order to fully benefit from SCS, a complete and consistent coverage of the painful body area(s) with tingling sensations (paresthesiae) must be achieved [1, 3, 16, 19]. For complex pain management the DCs should be targeted, as their stimulation may elicit paresthesiae in multiple dermatomes. However, insufficient paresthesia coverage or its loss is a commonly encountered problem in SCS. Another limitation is the simultaneous stimulation of large proprioceptive fibers in one or few dorsal roots (DRs), which results in uncomfortable sensations and/or motor effects.

Several parameters that influence the extent of DC and DR fiber recruitment were identified by Holsheimer et al. [10]: the thickness of the dorsal cerebrospinal fluid layer (dCSF) which was assumed to be identical to the distance between the epidural lead and the spinal cord, the distance between lead contacts, the contact length and the contact combination (e.g. monopolar, bipolar, tripolar...).

So far, two approaches have routed their way into clinical practice and led to different SCS lead designs: surgical, or laminectomy (LAM) leads and percutaneous (PERC) leads. Implantation of a PERC lead is simple and less invasive, yet control of its position is difficult and maintenance over time less likely, so revisions are needed more frequently [17, 18, 26]. The abundance of different SCS lead types available on the market shows that an optimal lead has not yet been designed and that their development has to be continued.

Recently, a few clinical studies aimed to compare the therapeutic and technical performance of the most common LAM and PERC leads, which have a similar longitudinal geometry (9-10 mm center-to-center contact spacing) [17, 18, 26]. This modeling study aims to quantify and compare the technical performance of the two lead types from a theoretical point of view.

## 2.2. Methods

### Computer model

In order to simulate the effects of stimulation, the UT-SCS software developed at the University of Twente [12, 22-24] was used. This software enables the construction of models and the calculation of both the imposed electrical field and the response of myelinated nerve fiber models. Each model consists of two parts: 1) a 3D volume conductor model of the anatomical structures and the anodal and cathodal contacts and 2) myelinated nerve fiber model(s).

We chose to model a low-thoracic segment, being a common level for SCS implants. Its transverse section is shown in **Figure 1**.

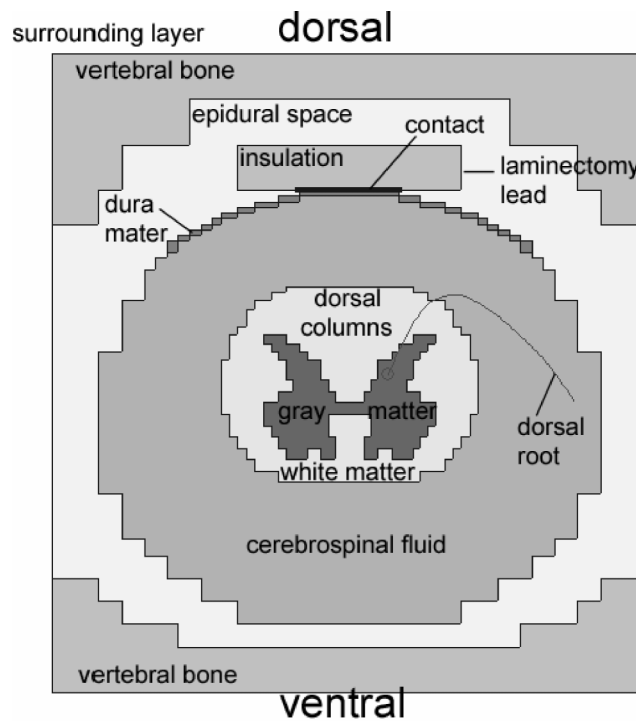


**Figure 1.** Transverse section of an UT-SCS spinal cord model with an epidural LAM lead.

The geometric properties of the model were based on transverse magnetic resonance imaging scans of the spine [8]. Due to the considerable inter-subject variability of dCSF at a low-thoracic level, we made models with a dCSF

equaling 2.0, 3.2 and 4.4 mm, thus covering its estimated range [8, 13]. The rostrocaudal, mediolateral and ventrodorsal dimensions of the models were 60, 24 and 26 mm, respectively. The electrical conductivities of the various structures in the model were taken from Struijk et al. [24], except for the dura mater and surrounding layer values. These conductivities were chosen to be 0.6 and 0.005 S/m, respectively, thus matching recent impedance measurements [2]. Anodal and cathodal contacts were modeled for each lead type as described below and were placed dorsomedially in the epidural space of the model as shown in **Figure 1**. In monopolar stimulation the boundary of the model served as the anode. In order to determine the imposed electric field, the Laplace equation was solved. This equation was first discretized using a finite difference method and the resulting set of equations was solved using a Gauss-Seidel numerical method with variable overrelaxation. As the layered structure of the volume conductor defines a 3D grid, the solution to the electric field potentials was obtained at these grid points.

A myelinated nerve fiber model was defined at its anatomical position and its response to the applied field was calculated using potentials at the positions of its Ranvier nodes, obtained by interpolation of the grid potentials. The fibers were modeled according to McNeal [14], with modifications as described by Wesselink et al. [27]. The two types of fibers modeled in this study had the following characteristics:

- 1) *DC fibers* (without collaterals) with a diameter of 12  $\mu\text{m}$  in the median 66% of the DCs and linearly increasing to 15  $\mu\text{m}$  at the lateral sides of the DCs, thus mimicking the presence of DC collaterals near the bifurcation of the corresponding DR fibers [5, 22].
- 2) *DR fibers* with a diameter of 15  $\mu\text{m}$ , with an ascending and a descending 12  $\mu\text{m}$  DC fiber with collaterals attached. Since a low-thoracic segment was modeled, we chose to model the ‘type A1’ DR fiber, as described in [24].

Monophasic rectangular pulses with a pulsewidth of 210  $\mu\text{sec}$  were applied and the threshold voltage to excite a specific fiber model was determined. By varying the dorsoventral position of the DC fiber model, the depth within the DCs at which it was not excited anymore by a given pulse amplitude was determined for all mediolateral fiber positions. In this way, the outer part of the DCs in which fibers were stimulated by the applied stimulus at discomfort threshold (DT) was calculated and named ‘*maximum recruited DC area*’. The line bordering the dorsal part of the DCs containing stimulated fibers was named ‘*recruitment contour*’ (see **Figure 3**). Similarly, by varying the rostrocaudal position of the DR fiber model, a range within which this fiber model was excited by the applied stimulus at DT was calculated. We named this range ‘*maximum span of DR recruitment*’.

### SCS lead models

The Pisces Quad 3487A lead (Medtronic Inc.) and the Resume 3587A lead (Medtronic Inc.) were modeled and named ‘PERC’ lead and ‘LAM’ lead, respectively. Since the center-to-center contact distance of these leads is slightly different, a hypothetical ‘wide PERC’ lead, having the Resume center-to-center distance (10 mm instead of 9 mm), was also modeled. The main geometrical characteristics of these leads are summarized in **Table 1**.

**Table 1.** . Main geometric characteristics of the modeled leads

Lead type	designation	contact length [mm]	center-to-center distance [mm]	active contact area [mm <sup>2</sup> ]
Pisces Quad 3487A	PERC	3	9	11.96
Resume 3587A	LAM	4	10	12.56
Pisces Quad with 10 mm center-to-center spacing	wide PERC	3	10	11.96

A LAM contact has a round, planar shape, whereas a PERC contact has a hollow, cylindrical shape. We modeled them as a polygonal surface on an insulating paddle and as four rectangular surfaces around an insulating square bar, respectively, setting their dimensions so as to approximate their active areas. In **Figure 2** the lead models and their dimensions are shown.

Monopolar (-) and tripolar (guarded cathode, + - +) contact combinations were modeled. The lead position was always symmetrical with respect to the spinal cord (physiological) midline (which in all our models coincides with the radiological midline). The leads were placed just behind the dura mater, which is generally the most favorable position in clinical applications – easy to achieve by modeling, but not guaranteed with PERC leads in clinical practice. In addition, we positioned the PERC lead deeper in the epidural space, namely at a 0.2, 0.4, 0.8 and 1.2 mm distance behind the dura mater, while retaining its position symmetrical to the spinal cord midline.

It was assumed that the stimulation pulses are applied by a single, voltage-controlled stimulator, forcing the two anodes in tripolar stimulation to have the same electrical potential.

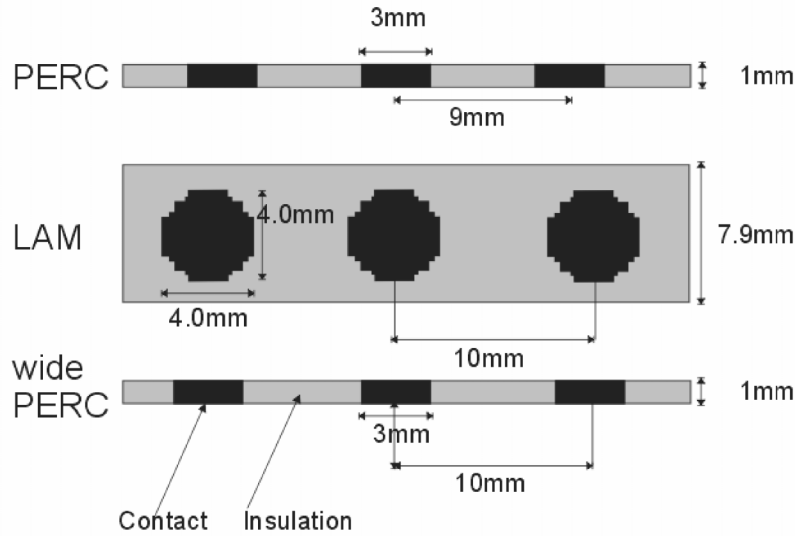


**Figure 2.** 2D projections of the lead models. PERC – percutaneous Pisces Quad lead; LAM – laminectomy Resume lead; wide PERC – percutaneous Pisces Quad lead with the same center-to-center contact spacing as Resume (10 mm).

### Model output parameters

In order to compare the performance of the leads, the following output parameters were used:

$V_{PT}$ [V]	<i>paresthesia threshold (PT)</i> : the voltage to be applied between the positive and negative outputs of the stimulator in order to activate the lowest threshold fiber, being either a DC fiber or a DR fiber (depending on lead geometry, contact combination and dCSF)
$V_{DT}$ [V]	<i>discomfort threshold (DT)</i> : the voltage to be applied between the stimulator outputs at initial stimulation of proprioceptive DR fibers; according to clinical data this threshold was set at 140% of the lowest DR fiber threshold [7]
DT/PT [-]	<i>threshold ratio</i> , the ratio of discomfort and paresthesia threshold
$Z_{tis}$ [Ohm]	<i>tissue impedance between anode(s) and cathode(s)</i> : $Z_{tis} = Z_{Cath}$ and $Z_{tis} = Z_{Cath} + 0.5 Z_{Anod}$ for a monopolar and a tripolar (guarded cathode) combination respectively
$Z_w$ [Ohm]	<i>wire impedance</i> between a lead contact and a stimulator output



$Z_G$ [Ohm]	<i>load impedance ‘seen’ between the stimulator outputs: <math>Z_G = Z_{tis} + Z_W</math> and <math>Z_G = Z_{tis} + 1.5 Z_W</math> for a monopolar and a tripolar combination, respectively.</i>
$I_{PT}$ [mA]	<i>impressed current at paresthesia threshold: <math>I_{PT} = V_{PT}/Z_G</math></i>
$I_{DT}$ [mA]	<i>impressed current at discomfort threshold: <math>I_{DT} = V_{DT}/Z_G</math></i>
$E_{DT}$ [μJ]	<i>energy per pulse at DT delivered by the stimulator; <math>E_{DT} = V_{DT} * I_{DT} * T</math>, where T is the pulsewidth, being 0.21 msec in all simulations</i>
$S_{RA}$ [mm <sup>2</sup> ]	<i>maximum recruited DC area – DC area recruited at DT</i>
depth [mm]	<i>depth of recruited area – depth on the spinal cord midline at DT</i>
span [mm]	<i>maximum span of DR recruitment: rostrocaudal span of recruited DR fibers at DT.</i>

In contrast to the low wire impedance of the Resume 3587A lead ( $Z_W = 16$  Ohms), the value of the Pisces Quad 3487A wire impedance was substantially larger (140 Ohms). Accordingly, these values were incorporated in the calculations with the LAM, PERC and wide PERC leads. Note that the new Pisces Z Quad family with a negligible wire impedance has recently been marketed (see Discussion).

### 2.3. Results

#### PERC vs. LAM lead characteristics

The model output parameters with the leads placed symmetrically to the spinal cord midline in models with dCSF = 3.2 mm are summarized in **Table 2**.

**Table 2.** Output parameters of the models with dCSF = 3.2 mm; acronyms are defined in ‘Model output parameters’.

Parameter	LAM mono	LAM tri	PERC mono	PERC tri	wide PERC tri
$S_{RA}$ [mm <sup>2</sup> ]	0.7	3.3	1	3.8	3.5
depth [mm]	0.19	0.63	0.29	0.74	0.67
DT/PT [-]	1.4	1.7	1.4	2	1.9
span [mm]	7.1	5.7	7.1	5.5	5.7
$Z_{tis}$ [Ohm]	191	136	266	247	250
$Z_G$ [Ohm]	207	160	406	457	460
$I_{PT}$ [mA]	2.5	2.45	2.6	2.3	2.3
$I_{DT}$ [mA]	3.5	4.2	3.7	4.6	4.3
$V_{PT}$ [V]	0.52	0.39	1.09	1.05	1.06
$V_{DT}$ [V]	0.73	0.68	1.5	2.11	1.98
$E_{DT}$ [μJ]	0.54	0.60	1.16	2.04	1.79

In this table it is shown that in tripolar stimulation a PERC lead recruits a ~15% larger and ~17% deeper DC area than a LAM lead does at DT, whereas a wide PERC lead performs just slightly better than a LAM lead. In monopolar stimulation a PERC lead recruits a ~42% larger DC area at DT than a LAM lead. The recruitment contours for monopolar and tripolar stimulation are shown in **Figure 3A** for a LAM lead and in **Figure 3B** for a PERC lead. As shown in this figure, the recruited DC area is significantly smaller in monopolar than in tripolar stimulation for both leads. In **Figure 4A** the influence of dCSF on the recruited DC area is shown. In all cases the recruited DC area decreases as dCSF is increased.

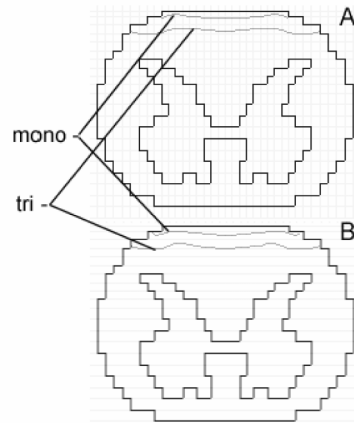


**Figure 3.** Recruitment contours in the DCs at monopolar and tripolar stimulation with a LAM (**A**) and PERC (**B**) lead; model with dCSF = 3.2 mm. PERC – Pisces Quad, LAM – Resume lead.

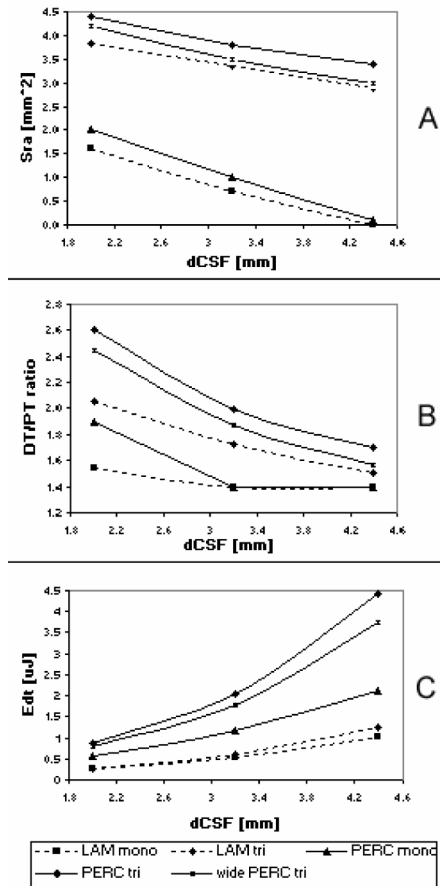


**Figure 4.** Calculated recruited DC areas at DT ( $S_{RA}$ ) (A), threshold ratio (DT/PT ratio) (B) and energy per pulse (210  $\mu$ sec pulse width) at DT ( $E_{DT}$ ) (C) of different leads and contact combinations as a function of dCSF. The meanings of the parameters are explained in Methods section. Mono – monopolar combination, tri – tripolar combination. For acronyms see Table 1.

Similar to  $S_{RA}$ , the DT/PT ratio is largest in tripolar stimulation with a PERC lead, as shown in Table 2 and Figure 4B. The wide PERC lead has a 5% lower DT/PT ratio, whereas the ratio of the tripolar LAM lead is ~15% less at dCSF = 3.2 mm. Monopolar stimulation gives by far the lowest DT/PT ratio, close or equal to 1.4, indicating preferential DR recruitment. In all cases, the DT/PT ratio decreases as dCSF is increased as shown in Figure 4B.

All three lead models have a similar span of DR recruitment, larger in monopolar stimulation ( $\sim 7.1$  mm) than in tripolar stimulation ( $\sim 5.7$  mm). The span is slightly larger with a larger center-to-center distance of the contacts (wide PERC tri and LAM tri vs. PERC tri), as shown in **Table 2**.

Tissue impedances  $Z_{tis}$  as ‘seen’ between contacts and load impedances  $Z_G$  are also summarized in **Table 2**. As shown, a PERC lead has a higher tissue impedance than a LAM lead, regardless of the contact combination ( $\sim 40\%$  for a monopole and  $\sim 80\%$  for a tripole). Due to a considerable difference in wire impedance between LAM and PERC leads, the difference is even more pronounced when the load impedance  $Z_G$  is considered ( $\sim 100\%$  for a monopolar and  $\sim 190\%$  for a tripolar combination).

Currents needed to achieve paresthesia and discomfort threshold, respectively, have up to 10% higher values for PERC as compared to LAM leads, as shown in **Table 2**. By contrast, PERC leads require a much higher voltage in order to achieve paresthesia and discomfort thresholds ( $V_{PT}$  and  $V_{DT}$  in **Table 2**). This is primarily due to their higher  $Z_G$  value. As a consequence, more energy is consumed when a PERC lead is used for stimulation. The energy per pulse delivered by the pulse generator at DT ( $E_{DT}$ ) is higher by  $\sim 115\%$  and  $\sim 240\%$  for monopolar and tripolar stimulation, respectively (**Table 2**).  $E_{DT}$  rises when dCSF is increased, as shown in **Figure 4C**. This tendency is more pronounced with PERC leads than with LAM leads.

#### **Dorsoventral position of PERC lead**

While most current is directed towards the highly conductive CSF layer when the lead is next to the dura mater (**Figure 5A**), current is distributed fairly uniformly in the vicinity of the dorsally displaced PERC lead (**Figure 5B**). This results in a substantial difference in the magnitudes of the labeled iso-current density lines in **Figure 5** ( $22 \mu\text{A}/\text{mm}^2$  in (A) and  $1 \mu\text{A}/\text{mm}^2$  in (B)), having similar positions in the models, namely just at the dorsolateral border of the DCs. As a consequence, a deterioration of performance parameters is observed when the lead is displaced dorsally, as shown in **Table 3**.

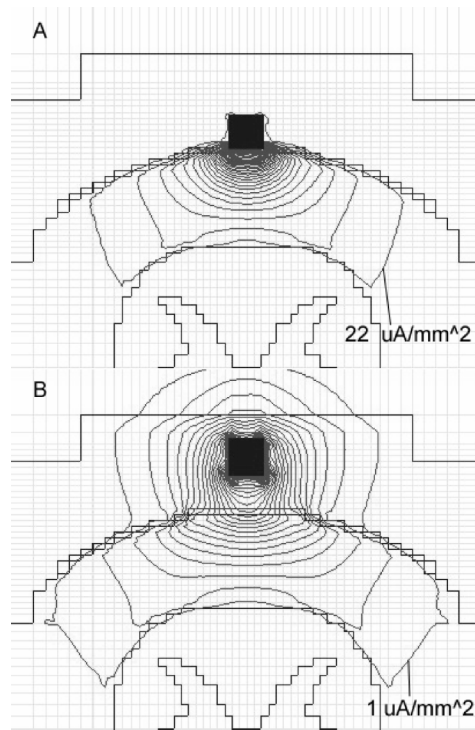


**Figure 5.** Iso-current-density lines in a transverse section of the model with a PERC lead 0 mm (A) and 1.2 mm (B) dorsal to the dura; 50 iso-current-density lines are equally spaced in the range up to the maximum current density in tripolar stimulation at 1V. The numbers indicate the lowest value of the displayed contours (in  $\mu\text{A}/\text{mm}^2$ ).

The recruited DC area at DT ( $S_{RA}$ ) is decreased as the lead is displaced dorsally. The reduction in its size is  $\sim 20\%$  when the lead is moved from a position just behind the dura to 1.2 mm deep in the epidural space. Under the same conditions,  $I_{PT}$  and  $I_{DT}$  are increased by  $\sim 80\%$  and  $\sim 40\%$ , respectively, which consequently lead to a decrease of the DT/PT ratio by  $\sim 20\%$ . Because the corresponding increase of  $Z_G$  is  $\sim 425\%$ ,  $V_{PT}$  and  $V_{DT}$  are increased by  $\sim 840\%$  and  $\sim 645\%$ , respectively, whereas  $E_{DT}$  is increased by  $\sim 980\%$ . A slight increase in recruited rostrocaudal DR span ( $\sim 10\%$ ) is also present.

**Table 3.** Model output parameters of a PERC lead displaced dorsally from a midline position next to the dura mater (0.0 mm); model with dCSF = 3.2 mm.

Dura - to - lead distance [mm]	0.0	0.2	0.4	0.8	1.2
$S_{RA}$ [mm <sup>2</sup> ]	3.8	3.5	3.4	3.2	3.0
$I_{PT}$ [mA]	2.3	2.7	3.0	3.6	4.1
$I_{DT}$ [mA]	4.6	4.95	5.4	5.95	6.55
DT/PT [-]	2	1.85	1.8	1.7	1.6
$Z_G$ [Ohm]	457	1310	1710	2146	2399
$V_{PT}$ [V]	1.05	3.54	5.13	7.73	9.84
$V_{DT}$ [V]	2.11	6.48	9.18	12.77	15.71
$E_{DT}$ [ $\mu$ J]	2.0	6.7	10.4	16.0	21.6
DR span [mm]	5.5	5.7	5.7	5.9	6.0

However, in addition to the low conductivity of the epidural tissue surrounding the lead entirely, these simulation results are also influenced by the increased lead-to-spinal cord distance. By comparing the results of tripolar PERC stimulation with dCSF = 4.4 mm and the lead next to the dura with the results of tripolar PERC stimulation with dCSF = 3.2 mm and the lead displaced dorsally into the epidural tissue by 1.2 mm, only the influence of the epidural space is left as both leads have the same lead-to-spinal cord distance. Under these conditions the dorsally displaced lead has a  $\sim 12\%$  smaller  $S_{RA}$ , a  $\sim 6\%$  lower DT/PT ratio, a  $\sim 400\%$  higher  $V_{DT}$  and a  $\sim 390\%$  higher  $E_{DT}$ .

## 2.4. Discussion

The aim of this modeling study was to compare the technical performance of the LAM and PERC leads most commonly used in SCS practice. Several clinical studies addressing the same issue were published in the past [17, 18, 26].

### DC and DR fiber recruitment

We calculated that a PERC lead in tripolar combination, positioned symmetrically to the spinal cord midline and next to the dura, recruits the largest DC area. By increasing the spacing between the contacts (wide PERC), the ability of the lead to recruit DC fibers is diminished. In fact, the larger the contact spacing, the weaker the influence of the anodes on the cathodal field is, so that the performance of the tripole approaches the performance of a monopole in all respects, as shown in **Table 2**. Moreover, a wide PERC lead recruits a slightly larger DC area than a tripolar LAM lead (having the same contact distance) - the difference getting smaller with increasing dCSF. This

implies that the main lead parameter determining DC fiber recruitment in tripolar (and bipolar) stimulation, is the center-to-center contact distance.

In the absence of anodal contacts (monopolar stimulation), the contact shape plays an important role: a LAM lead recruits a smaller DC area than a PERC lead. Because a LAM lead has wider contacts than a PERC lead (4 mm max vs. 1 mm in the models), these contacts are closer to the DRs, thus resulting in a lower DR fiber threshold and a reduced DT/PT ratio (**Figure 4B**). This, in turn, results in a smaller  $S_{RA}$  in monopolar stimulation with a LAM lead than with a PERC lead (**Figure 4A**), especially when dCSF is small. Similarly, the difference in  $S_{RA}$  when stimulating tripolarly with a LAM lead and a wide PERC lead is due to a difference in their contact shape (**Figure 4A**).

It is, however, important to realize that a larger recruited DC area does not necessarily lead to a higher overlap of the pain area with paresthesiae. As Feirabend et al. [4] have shown, the density of large fibers ( $\geq 10.7 \mu\text{m}$ ) in the superficial part of the human DCs at  $T_{11}$  is  $\sim 110$  fibers/ $\text{mm}^2$ . Using this data and the calculated recruited DC area in tripolar stimulation with a LAM lead, we estimated that a mean of  $\sim 15$  fibers in each of 12 dermatomes ( $T_{11-12}$ ,  $L_{1-5}$ ,  $S_{1-5}$ ) would be recruited. Depending on the actual positions of these few fibers, the 12% larger recruited DC area in PERC tripolar stimulation may or may not include 1-2 additional stimulated fibers from each dermatome compared to LAM tripolar stimulation. For comparison, the parts of the DCs recruited by tripolar LAM and PERC leads are shown in the same plots (**Figure 6**). The shaded parts represent the difference between the recruited areas with each dCSF and hence the part of the DCs that may contain additional fibers recruited by the PERC lead. In conclusion, the size of the calculated  $S_{RA}$  and pain relief are not necessarily proportional, although statistically there will be a correlation.

The span of DR recruitment ranges from 5.2 – 8.1 mm, having its maximum value when monopolar stimulation is applied and dCSF is large. Because the mean rostrocaudal length of a low-thoracic spinal segment is  $\sim 10$  mm, not even all filaments (rootlets) of a single DR will be recruited at DT. Depending on the cathode position relative to the spinal segments, a number of rootlets belonging to one or two adjacent segments may be recruited on each side.

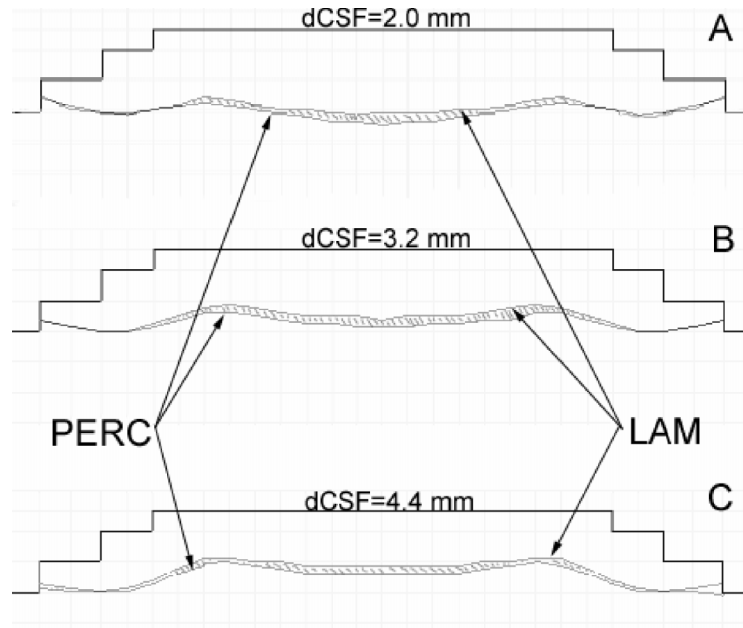


**Figure 6.** Calculated max. recruited DC areas for LAM (Resume) and PERC (Pisces Quad) tripolar stimulation with dCSF = 2.0 mm (A), 3.2 mm (B) and 4.4 mm (C). The part of the DCs representing the difference between the PERC and LAM recruited area is shaded.

### Energy consumption

The currents needed to achieve PT and DT, respectively, do not differ substantially among the modeled leads. In contrast, the corresponding voltages needed at the stimulator output differ significantly (**Table 2**). This is primarily due to the following factors:

- 1) owing to a different contact shape of LAM and PERC leads and their different insulation design, the intrinsic tissue impedance  $Z_{tis}$  of a PERC lead is larger by ~40% (monopole) and ~80% (tripole).
- 2) a considerable wire impedance ( $Z_w = \sim 140$  Ohms) increases the load impedance of a PERC lead additionally. Despite nearly identical currents, the substantially larger load impedance of a PERC lead results in a larger voltage at the stimulator output, both at PT and DT.

Consequently, the energy per pulse delivered by the stimulator is substantially larger with a PERC lead. Note that a reduction in wire impedance would reduce the energy dissipation, thus decreasing the energy to be delivered by the stimulator. The Quattrode lead (Advanced Neuromodulation Systems Inc.) and the Pisces Z Quad lead (Medtronic Inc.) have a similar contact shape and intercontact distance as the PQ lead, but a negligible wire impedance, therefore



consuming less energy. We calculated that the voltage and the energy per pulse delivered at DT to a PERC lead increase by ~55% and ~85% when the wire impedance is increased from 0 to 140 Ohms for monopolar and tripolar stimulation, respectively.

When a battery powered IPG is used, battery life and therefore energy consumption are of great interest. In that sense, LAM leads with a low wire impedance are superior. However, it should be noted that energy consumption of the stimulation pulses does not influence battery life proportionally. Apart from the energy consumption per pulse and the pulse rate, additional specifications such as continuous (bias) current drain of the stimulator are needed in order to estimate battery longevity. Therefore, we could not readily conclude on the difference in battery longevity of the IPGs coupled with a LAM and a PERC lead, as North et al. did [18].

### Comparison with clinical data

Villavicencio et al. in their clinical study reported greater improvement in VAS scores when the Resume lead as opposed to the Pisces Quad lead was used [26]. North et al. [17] and particularly North et al. in a prospective, randomized, controlled study [18], reported that LAM leads (Resume, Medtronic Inc.) produce significantly better coverage of pain areas by SCS induced paresthesiae, and consume less power than PERC leads (Pisces Quad, Medtronic Inc.). How do our modeling data compare to these clinical results?

Some of the available clinical data [18] and the corresponding modeling values are summarized in **Table 4** (note that the empirical data are related to the “usage amplitude” which is slightly below the value of  $V_{DT}$ ).

As shown, our modeling results have the same trend as the clinical results and the values we calculated are close to, or are even within the range of empirical data. However, modeling shows that a PERC lead is capable of recruiting a larger area in the DCs than a LAM lead, both in monopolar and tripolar stimulation. Despite the probabilistic relation between the recruited DC area and the extent of pain relief (see above), we can still conclude that PERC leads should, in a statistical sense, provide a better pain control than LAM leads with the same contact combination. There are two aspects that may explain this discrepancy between clinical and theoretical results:

- a) In our modeling study we assumed that the PERC lead was next to the dura mater, a position which is not guaranteed in real situations. Unlike the rostrocaudal and mediolateral position of a PERC lead, its dorsoventral position in the epidural space is not under control. As we have shown by modeling, dorsal displacement of the PERC lead affects its performance in a negative sense. A distance of only 0.4 mm between the dura and the PERC lead results in a reduction of its recruited area to a value as obtained by the LAM lead (see **Table 2** and **Table 3**). Unlike PERC leads, LAM leads are positioned next to the

dura mater under visual control and are generally secured to the dura [17, 19, 26].

- b) Due to the substantial volume of its paddle (12.6-fold the volume of a PERC lead of the same length) and its rigid, flat shape, a LAM lead most probably pushes the dura ventrally, thus reducing dCSF as discussed [11, 17, 26]. The reduced dCSF increases the preference for DC fiber recruitment, as has previously been calculated [9, 10].

Although under identical conditions a PERC lead would most probably perform somewhat better than a LAM lead in terms of pain control, it is likely that, once implanted, the LAM lead is the one performing better, as has been reported [17, 18, 26].

**Table 4.**  $V_{DT}$  values of LAM (Resume) and PERC (Pisces Quad) leads. Measured values are actually “usage amplitudes” (somewhat lower than  $V_{DT}$ ) and are presented as mean  $\pm$  standard deviation. Modeled values are presented as a range obtained for dCSF = 2.0 mm - 4.4 mm. Contact combination (i.e. mono-, bi-, tri-) and the sample size (n) are included in parentheses,. Source of data is also specified.

Data source	North et al. [18]	Our modeling data
$V_{DT}$ LAM [V]	1.44 $\pm$ 0.89 (bi-, n = 12)	0.5 - 1.0 (mono-) 0.48 - 0.97 (tri-)
$V_{DT}$ PERC [V]	2.68 $\pm$ 0.96 (bi-, n = 12)	1.05 - 2.03 (mono-) 1.41 - 3.09 (tri-)
Ratio PERC/LAM	1.86	2.23 - 2.03 (mono-) 2.94 - 3.15 (tri-)

Both the modeling and clinical studies show that a LAM lead has a lower  $V_{DT}$  than a PERC lead (see **Table 4**). However, there is a large difference in means and standard deviations of the two clinical studies by North et al. [17, 18], which makes it difficult to compare clinical and theoretical data. Nevertheless, the theoretical  $V_{DT}$  values are lower than the measured ones. This difference may be due to various aspects:

- 1) The leads were implanted from T8 to T12 with a majority implanted more rostrally within this range. According to Holsheimer et al. [8, 13], dCSF at this level may well range from  $\sim$ 2.5 mm up to  $\sim$ 7.5 mm with a mean value of  $\sim$ 4 – 4.5 mm. This range is somewhat higher than the one we assumed when modeling a low-thoracic segment, which, in turn, should have resulted in higher calculated  $V_{DT}$  values.

- 2) We did not model the influence of the dura displacement by the implanted LAM lead. This would have resulted in a reduction of the calculated  $V_{DT}$  of the LAM lead.
- 3) Since it is likely that the mean depth of the implanted PERC leads in the epidural space was more than zero, the calculated  $V_{DT}$  values would have been higher (**Table 3**). It is worth noting that, because the maximum voltage output of an IPG is 10.5 V (Itrel, Medtronic Inc.), a stimulator coupled with a PERC lead positioned at more than  $\sim 0.5$  mm dorsal to the dura would not allow stimulation up to  $V_{DT}$  (**Table 3**).
- 4) A lead position slightly asymmetrical to the spinal cord midline results in a reduced  $V_{DT}$ , because a DR fiber has a lower stimulation threshold value ( $V_{DR}$ ) due to its position being closer to the lead [9].
- 5) SCS was made with bipolar combinations, whereas we modeled monopolar and tripolar stimulation. In order to test the influence of the contact combination on  $V_{DT}$ , we simulated bipolar stimulation with a PERC lead and  $dCSF = 3.2$  mm. Compared to tripolar stimulation with a PERC lead and the same  $dCSF$ , this resulted in a  $\sim 22\%$  increase of  $V_{DT}$ . Therefore, bipolar stimulation requires higher voltages than tripolar stimulation. By contrast, bipolar stimulation gave a  $\sim 20\%$  smaller recruited DC area than tripolar stimulation under the same conditions.
- 6) We modeled a pulsewidth of 210  $\mu\text{sec}$ , whereas this parameter was set at 500  $\mu\text{sec}$  in the clinical studies [17, 18]. According to the strength-duration relationship, stimulation with longer pulses results in lower threshold currents and voltages. Additional simulation of tripolar PERC and LAM stimulation with  $dCSF = 3.2$  mm and a pulsewidth of 500  $\mu\text{sec}$  showed that  $V_{DT}$  was  $\sim 15\%$  lower as compared to stimulation with a 210  $\mu\text{sec}$  pulsewidth, in both cases.
- 7) The measured samples of “usage amplitudes” (slightly below  $V_{DT}$ ) were characterized by their mean and standard deviation [17, 18], which means that a normal distribution was assumed. However, the  $V_{DT}$  population most likely has a skew distribution [9, 25], which means that the samples should be characterized by their median and not by their mean [6]. For the skewed distribution of  $V_{DT}$  the median value is lower than the mean (due to positive skewness) [9, 25]. Hence, a more reliable estimate of the samples of “usage amplitude” (and thus  $V_{DT}$ ) would have been lower.

In summary, the discrepancy between the empirical and calculated values of  $V_{DT}$ , as shown in **Table 4**, would have been reduced by aspects 1, 3 (only PERC lead), 5 and 7, whereas aspects 2 (LAM lead only), 4 and 6 would have had the opposite effect. In addition, some model parameters may need some adjustments.

## **2.5. Conclusions**

Computer modeling predicts that a PERC lead, positioned next to the dura mater would intrinsically provide slightly better pain control than a LAM lead in the same position. However, in clinical practice, a LAM lead gives better results, both because of the dura displacement towards the spinal cord and a high probability of residing next to the dura. The similar performance of the PERC and LAM lead is primarily determined by their similar center-to-center contact spacing (9 mm and 10 mm, respectively). Finally, a LAM lead needs less energy for stimulation which is primarily due to its lower load impedance.

## REFERENCES

- 1 Alo K and Holsheimer J. New trends in neuromodulation for the management of neuropathic pain. **Neurosurgery**. 50:690-704, 2002
- 2 Alo K, Varga C, Krames E, Prager J and Bradley K. Variability of contact impedance by vertebral placement in spinal cord stimulation. San Francisco, CA: 2004.
- 3 Barolat G. Current status of epidural spinal cord stimulation. **Neurosurg Q**. 5:98-124, 1995
- 4 Feirabend H, Choufoer H, Ploeger S, Holsheimer J and van Gool J. Morphometry of human superficial dorsal and dorsolateral column fibres: significance to spinal cord stimulation. **Brain**. 125:1137-1149, 2002
- 5 Fyffe R. Afferent fibers. In: Davidoff R. Handbook of the Spinal Cord. New York: Dekker, 1984: 79-136.
- 6 Glantz S. Primer of Biostatistics., 5th edn. New York: McGraw-Hill., 2002.
- 7 He J, Barolat G and Ketcik B. Stimulation usage range for chronic pain management. **Analgesia**. 1:75-80, 1995
- 8 Holsheimer J, Den Boer J, Struijk J and Rozeboom A. MR assessment of the normal position of the spinal cord in the spinal canal. **Am J Neuroradiol**. 15:951-959, 1994
- 9 Holsheimer J, Barolat G, Struijk J and He J. Significance of the spinal cord position in spinal cord stimulation. **Acta Neurochir (Suppl)**. 64:119-124, 1995
- 10 Holsheimer J, Struijk J and Tas N. Effects of electrode geometry and combination on nerve fiber selectivity in spinal cord stimulation. **Med Biol Eng Comput**. 33:676-682, 1995
- 11 Holsheimer J and Wesselink W. Effects of anode-cathode configuration on paresthesia coverage in spinal cord stimulation. **Neurosurgery**. 41:654-660, 1997
- 12 Holsheimer J. Computer modelling of spinal cord stimulation and its contribution to therapeutic efficacy (Review). **Spinal Cord**. 36:531-540, 1998
- 13 Holsheimer J and Barolat G. Spinal geometry and paresthesia coverage in spinal cord stimulation. **Neuromodulation**. 1:129-136, 1998
- 14 McNeal D. Analysis of a model for excitation of myelinated nerve. **IEEE Trans Biomed Eng**. 23:329-337, 1976
- 15 Melzack R and Wall P. Pain mechanisms: a new theory. **Science**. 150:971-978, 1965
- 16 North R, Ewend M, Lawton M and Piantadosi S. Spinal cord stimulation for chronic, intractable pain: superiority of "multi-channel" devices. **Pain**. 44:119-130., 1991
- 17 North R, Lanning A, Hessels R and Cutchis P. Spinal cord stimulation with percutaneous and plate electrodes: side effects and quantitative comparisons. **Neurosurg Focus**. 2:1-5, 1997
- 18 North R, Kidd D, Olin J and Sieracki J. Spinal cord stimulation electrode design: prospective, randomized, controlled trial comparing percutaneous and laminectomy electrodes - Part I. Technical outcomes. **Neurosurgery**. 51:381-390, 2002

- 19 Simpson B. Spinal cord stimulation. **Pain Rev.** 1:199-230, 1994
- 20 Smith M and Deacon P. Topographical anatomy of the posterior columns of the spinal cord in man. The long ascending fibres. **Brain.** 107:671-698, 1984
- 21 Stanton-Hicks M and Salamon J. Stimulation of the central and peripheral nervous system for the control of pain. **J Clin Neurophysiol.** 14:46-62, 1997
- 22 Struijk J, Holsheimer J, van der Heide G and Boom H. Recruitment of dorsal column fibers in spinal cord stimulation: influence of collateral branching. **IEEE Trans Biomed Eng.** 39:903-912, 1992
- 23 Struijk J, Holsheimer J, Barolat G, He J and Boom H. Paresthesia thresholds in spinal cord stimulation: a comparison of theoretical results with clinical data. **IEEE Trans Biomed Eng.** 1:101-108., 1993
- 24 Struijk J, Holsheimer J and Boom H. Excitation of dorsal root fibers in spinal cord stimulation: a theoretical study. **IEEE Trans Biomed Eng.** 40:632-639, 1993
- 25 Tulgar M, Barolat G and Ketcik B. Analysis of parameters for epidural spinal cord stimulation. 1. Perception and tolerance thresholds resulting from 1100 combinations. **Stereotact Funct Neurosurg.** 61:129-139, 1993
- 26 Villavicencio A, Leveque J, Rubin L, Bulsara K and Gorecki J. Laminectomy versus percutaneous electrode placement for spinal cord stimulation. **Neurosurgery.** 46:399-406, 2000
- 27 Wesselink W, Holsheimer J and Boom H. A model of the electrical behaviour of myelinated sensory nerve fibers based on human data. **Med Biol Eng Comput.** 37:228-235, 1999

# Chapter 3

## **Technical performance of percutaneous leads for spinal cord stimulation: a modeling study**

Ljubomir Manola • Jan Holsheimer • Peter Veltink

Institute for Biomedical Technology, Department of Electrical Engineering,  
University of Twente, The Netherlands

### **Astract**

**Objective:** To compare the technical performance of different percutaneous lead types for Spinal Cord Stimulation.

**Methods:** Using UT-SCS (University of Twente Spinal Cord Stimulation) software, lead models having similar characteristics as Pisces Quad 3487A, Pisces Compact 3887 and Pisces Plus 3888 lead (Medtronic Inc., Minneapolis, MN), and the AB SC2108 lead (Advanced Bionics Corp., Valencia, CA) were simulated in a monopolar and a tripolar (guarded cathode) combination on a single lead, placed just outside the dorsal dura mater and both centered on the spinal cord midline and at 1 mm lateral. The influence of displacing a lead dorsally in the epidural fat was examined as well. Finally, dual leads both aligned and offset were modeled. Several parameters were calculated to allow a quantitative comparison of the performances.

**Results:** When programmed as a guarded cathode, the AB SC2108 lead recruits nerve fibers in a ~25% larger dorsal column area than the Pisces Quad 3487A. However, the AB SC2108 has a ~160% higher energy consumption. The performance of the Pisces Compact 3887 is in-between them, whereas the Pisces Plus 3888 is suitable only for dorsal root stimulation. Displacing a single lead off midline or dorsally decreases its ability to recruit fibers in the dorsal columns. Similarly, dual-lead combinations are less capable when compared to single leads centered on the spinal cord midline just outside the dura mater.

**Conclusions:** Complex pain syndromes are treated best with a lead having a small contact spacing, being programmed as a tripole (guarded cathode) and centered on the spinal cord midline just outside the dura mater, because dorsal column fiber recruitment is more extensive than with any other combination, including dual-leads. Improved recruitment of dorsal column fibers is accompanied by increased energy consumption.

---

\* Published in *Neuromodulation*, 8:88-99, 2005.

### 3.1. Introduction

According to the ‘gate-control’ theory, postulated by Melzack and Wall [17], stimulation of large cutaneous mechanoreceptive fibers causes relief of chronic, neuropathic pain. As the dorsal columns of the spinal cord contain such fibers originating from various body areas (dermatomes), they were chosen as a target of electrical stimulation, leading to the clinical method named dorsal column stimulation (DCS), or spinal cord stimulation (SCS) for the management of chronic, intractable pain. In order to fully benefit from SCS, a complete and consistent coverage of the painful body areas with tingling sensations (paresthesiae) must be achieved [1].

Although paresthesia and pain relief may be elicited by stimulation of cutaneous A $\beta$  fibers in both dorsal columns (DCs) and dorsal roots (DRs), the latter may only induce paresthesiae in a few dermatomes (segmental or radicular paresthesia), whereas DC stimulation may elicit paresthesiae in many dermatomes. In clinical practice, however, the management of particularly complex pain syndromes (Complex Regional Pain Syndrome - CRPS, Failed Back Surgery Syndrome - FBSS) is often hampered by an incomplete paresthesia coverage and an insufficient pain relief. A second drawback of DR stimulation is that apart from cutaneous A $\beta$  fibers these roots hold large proprioceptive fibers whose stimulation elicits uncomfortable sensations and motor responses. It is, therefore, favorable to apply SCS such that the recruitment of the fibers in the DCs is maximized [11].

Unfortunately, DR fibers may be activated first or even exclusively in SCS, as concluded by Coburn [5, 24] and Struijk et al. [24]. However, this is vastly influenced by a patient’s anatomy at the spinal segment where the lead is implanted and by the utilized contact combination as well. In the modeling study by Holsheimer et al. [10] the geometric parameters determining a preference for either DC or DR stimulation have been identified being the thickness of the dorsal cerebrospinal fluid layer (dCSF, the contact length, the center-to-center distance between contacts, and the contact combination. It was concluded that the preferential activation of DC fibers is advanced most in tripolar (“guarded cathode”) stimulation, a small dCSF and a small contact length and distance. In contrast, the preferential recruitment of DRs is advanced most in monopolar stimulation, a wide dCSF and a long contact. Regarding lead geometry, the center-to-center contact distance is actually the relevant parameter.

In a study that followed, a lead combination having a high preference for DC fiber stimulation and a limited energy consumption, was identified. An optimal lead should have contacts about 1.5 mm long, spaced by about 2.5 mm (center-to-center distance of approximately 4 mm), and programmed as a guarded cathode (tripole), as proposed by Holsheimer and Wesselink [13].



Modern SCS therapy requires multidermatomal, complex pain treatment with long-term beneficial effects. In order to achieve this goal, different lead designs were and are still being developed. The advances in technology also enabled the design of improved stimulators, capable of advanced stimulation techniques. However, the problems of non-optimal lead placement and lead migration are not yet solved. The technological innovations on one side and the need to solve the problem of lead migration and changing pain patterns on the other side, led to multiple-lead (particularly dual-lead) stimulation in which contacts of multiple leads are connected to either a single pulse generator ('*single mode*') or to two pulse generators giving pulses to contacts on each lead alternately ('*dual mode*').

The goal of this modeling study is to quantitatively compare the performance of several percutaneous lead types. Furthermore, effects of a non-optimal lead placement and the performance of several dual-lead combinations are addressed.

### 3.2. Methods

#### Computer model

In this study, the computer software and a simulation model developed at the University of Twente (UT-SCS) [8, 22-24] were used to calculate the response of neural targets to the applied electrical stimulation. The model consists of: 1) 3D models of a spinal cord segment and implanted stimulating contacts and 2) nerve fiber models. The 3D volume conductor model incorporates the geometries and electrical conductivities of the modeled anatomical structures. A transverse cross-section of the model, with all the compartments labeled, is shown in **Figure 1**.

The geometry of the models was based on transverse magnetic resonance imaging scans of various spinal segments [9]. The electrical conductivities of the various compartments were the same as used by Struijk et al. [22], except for the values of the dura mater and the surrounding layer, which were adjusted to match recent lead contact impedance data [3]. Anodal and cathodal contacts were modeled and placed in the dorsal epidural space of the model. In monopolar stimulation the boundary of the model served as the anode. A finite difference method and an iterative red-black Gauss-Seidel algorithm with variable over-relaxation were used to numerically solve the discrete form of the Laplace equation, resulting in the solution to the imposed electrical potential field.

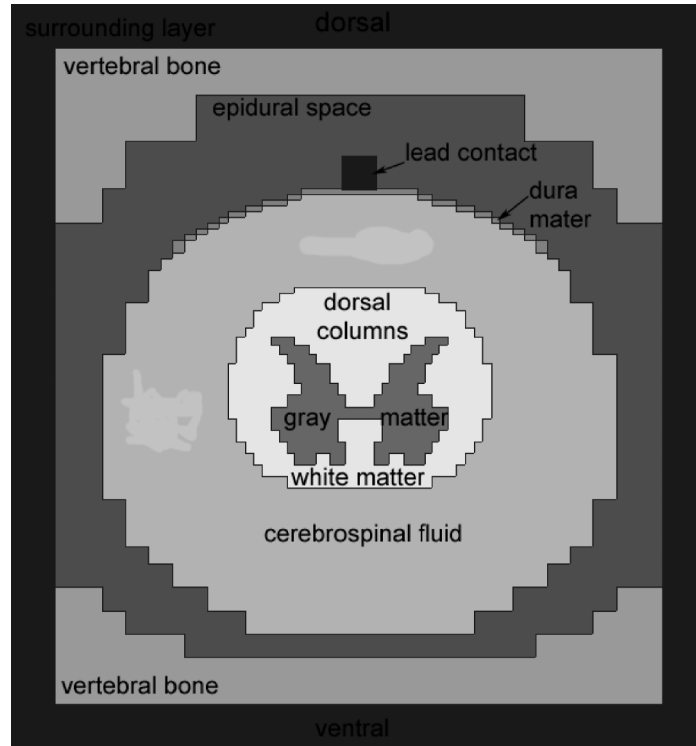


**Figure 1.** Transverse cross-section of an UT-SCS spinal cord model with a percutaneous lead placed just outside the dura mater and centered on the spinal cord midline. The model compartments are designated.

Myelinated nerve fiber models were defined at their anatomical positions in the volume conductor. The 3D field potentials at the positions of their nodes of Ranvier were used to calculate the fiber response to the applied stimulus pulse. A McNeal fiber model [16], modified as described by Wesselink et al. [25], was used to calculate the threshold voltage to be applied by a specific combination of contacts in order to recruit any specific fiber.

Because most SCS leads are implanted at a low-thoracic level, we used the low-thoracic model in this study. The model was 60, 24 and 26 mm in the rostrocaudal, mediolateral and dorsoventral direction, respectively. It consisted of 56x64x80 cubic volume compartments forming a grid. This was more than in previous models [23], hence a better resolution near the contact sites, needed to model various contact combinations accurately, was obtained. As the variability of the dCSF is substantial at a low-thoracic level, we made three models with a dCSF of 2.0, 3.2 and 4.4 mm, respectively, thus covering the estimated range of dCSF at that level [9, 14].

The nerve fiber models used in this study had the following standard diameters:

*DC fibers* (without collaterals): 12  $\mu\text{m}$  in the median 66% of the DCs and linearly increasing to 15  $\mu\text{m}$  at the lateral borders, thus mimicking the lower fiber threshold due to the presence of DC collaterals near the bifurcation of the corresponding DR fibers [6, 22].

*DR fibers*: 15  $\mu\text{m}$ , with an ascending and a descending 12  $\mu\text{m}$  DC fiber with collaterals attached. Since a low-thoracic segment was modeled, we chose to model the ‘type A1’ DR fiber, as described by Struijk et al. [24].

Monophasic rectangular voltage pulses with a pulse width of 0.21 msec were applied and the threshold voltage to excite a specific fiber model could be determined. Furthermore, by varying the dorsoventral position of the DC fiber model, the depth within the DCs at which it was just excited by the applied stimulus was determined for all fiber positions from median to lateral on both sides. In this way, the dorsal area of the DCs in which fibers were stimulated by the applied stimulus at discomfort threshold (DT – see Evaluation parameters) was calculated and named ‘*maximum recruited DC area*’. The line bordering the dorsal part of the DCs containing stimulated fibers was named ‘*recruitment contour*’ (see **Figure 5**). Similarly, by varying the rostrocaudal position of the DR fiber model, a span within which this fiber model was excited by the applied stimulus at DT was calculated. We named this range ‘*maximum span of DR recruitment*’.

### **Percutaneous SCS lead types**

Due to frequent confusion in using the terms ‘lead’, ‘electrode’ and ‘contact’, these terms will be used consistently according to the following definitions proposed by North et al. [20]:

‘**contact**’: an electrically conductive surface from which current passes into the tissue, being a cathode (-) or an anode (+) depending on the output connector of the pulse generator to which it is connected.

(**percutaneous**) ‘**lead**’: a linear array of 4 or 8 contacts mounted at one end of a flexible, insulating tube, and connected with insulated wires to a connector at the other end.

‘**electrode**’: this term is confusing, because in literature it is used to indicate both ‘contact’ and ‘lead’; therefore, this term is avoided.

The modeled percutaneous leads are presented in **Table 1**.

**Table 1.** Main characteristics of the modeled percutaneous leads

Lead type	Acronym	Contact length [mm]	Center-Center distance [mm]
Medtronic Pisces Plus 3888	PP	6	18
Medtronic Pisces Quad 3487A	PQ	3	9
Medtronic Pisces Compact 3887	PC	3	7
Advanced Bionics AB SC2108	AB	3	4

The cylindrical contacts with a diameter of 1.27 mm were modeled as four rectangular surfaces around an insulating square bar. The length of the contacts was always chosen to be the same as in real contacts. The two transverse dimensions of a contact were chosen to be 1.0 mm each, providing a close approximation of the surface area of each contact type. The insulation in-between and inside the contacts was modeled as a low-conductive (0.0001 S/m) compartment. Monopolar (-) and tripolar (guarded cathode, + - +) contact combinations were modeled, because theoretically the stimulation effects of these combinations differ most [10]. Tripolar combinations were modeled on both single and dual leads.

Single leads were positioned in a model in various ways: 1) centered on the spinal cord ('physiological') midline, next to the dura mater; 2) centered on the spinal cord midline, but more dorsally in the epidural space; 3) displaced laterally by 1 mm off the spinal cord midline.

Dual lead models were placed symmetrically to the spinal cord midline at a 3 mm center-to-center separation just outside the dura mater and either aligned or offset by half the contact separation. The only exception was the offset dual PQ programmed as a single tripole (cathode on one, two anodes on the other lead), where the lateral separation was 2.5 mm with asymmetric leads in order to obtain a nearly symmetrical recruited DC area.

All tripolar combinations we modeled are shown in **Figure 2**. It was assumed that the stimulation pulses were delivered by a single constant voltage pulse generator, which means that with any combination all active anodes had the same electrical potential, as well as all active cathodes involved.

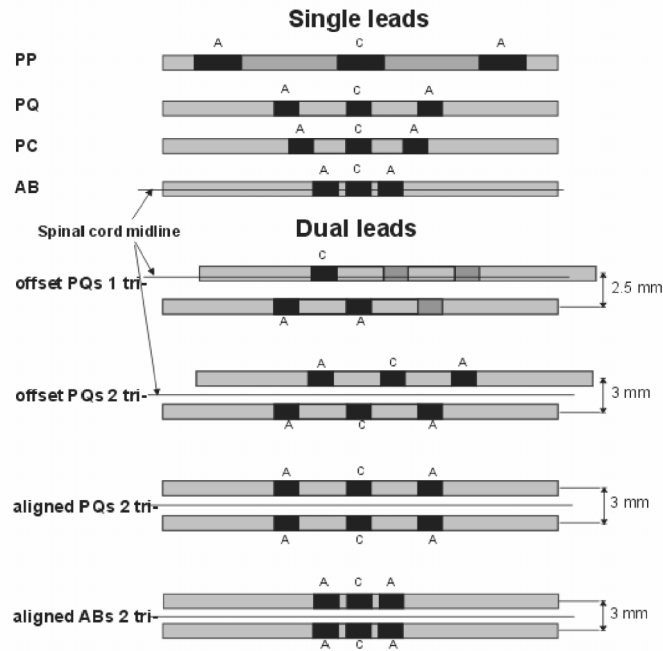


**Figure 2.** Schematic presentation of the modeled tripolar combinations on single and dual-leads; c: cathode, a: anode. PP – Pisces Plus 3888, PQ – Pisces Quad 3487A, PC – Pisces Compact 3887, AB – AB SC2108.

**Evaluation parameters**

To allow a quantitative comparison of the performance of the various lead types and contact combinations, several model output parameters were calculated. These parameters are defined below.

- $V_{PT}$  [V]**      *paresthesia threshold (PT)*: the voltage to be applied between the positive and negative outputs of the stimulator in order to activate the lowest threshold fiber, being either a DC fiber or a DR fiber (depending on lead geometry, contact combination and dCSF as discussed before)
- $V_{DT}$  [V]**      *discomfort threshold (DT)*: the voltage to be applied between the stimulator outputs at initial stimulation of supposedly large proprioceptive DR fibers; according to clinical data this threshold was set at 140% of the lowest DR fiber threshold [7].
- DT/PT [-]**      *threshold ratio*: the ratio of discomfort and paresthesia threshold
- $Z_{tis}$  [Ohm]**      *tissue impedance, between anode(s) and cathode(s)*:  $Z_{tis} = Z_{Cath}$  and  $Z_{tis} = Z_{Cath} + 0.5 Z_{Anod}$  for a monopolar and a tripolar (guarded cathode) combination, respectively

$Z_W$ [Ohm]	wire impedance between a lead contact and a stimulator output
$Z_G$ [Ohm]	load impedance, seen between stimulator outputs: $Z_G = Z_{tis} + Z_W$ and $Z_G = Z_{tis} + 1.5 Z_W$ for a monopolar and a tripolar combination, respectively
$I_{PT}$ [mA]	injected current at paresthesia threshold: $I_{PT} = V_{PT} / Z_{tis}$
$I_{DT}$ [mA]	injected current at discomfort threshold: $I_{DT} = V_{DT} / Z_{tis}$
$E_{DT}$ [μJ]	energy per pulse at DT delivered by the stimulator; $E_{DT} = V_{DT} * I_{DT} * T$ , where T is the pulse width, being 0.21 msec in all simulations
$S_{RA}$ [mm <sup>2</sup> ]	maximum recruited DC area: DC area recruited at DT
depth [mm]	depth of the recruited area at DT, determined at the center of the recruitment contour.
span [mm]	maximum span of DR recruitment: rostrocaudal span of recruited DR fibers at DT.

### 3.3. Results

#### Single lead on spinal cord midline, next to dura mater

All four single lead models (PP, PQ, PC and AB in **Figure 2**), positioned on the spinal cord midline and just outside the dura mater were modeled in both a monopolar and a tripolar combination. Tissue impedance  $Z_{tis}$  and load impedance  $Z_G$  of each lead model are shown in **Table 2**. According to empirical data, we used a wire impedance of 140 Ohm per wire when calculating  $Z_G$  for the Pisces leads. Similarly, an impedance of 3 Ohm per wire was used when calculating  $Z_G$  for the AB leads.

**Table 2.** Calculated impedances (in Ohm) of the various leads in a model with dCSF=3.2 mm.  $Z_{tis}$  and  $Z_G$  designate tissue and load impedance, respectively. Wire impedance ( $Z_W$ ) is also specified.

Lead type	PP	PQ	PC	AB
$Z_W$	140	140	140	3
$Z_{tis}$ (mono)	198	266	266	266
$Z_G$ (mono)	338	406	406	269
$Z_{tis}$ (tri)	174	247	241	211
$Z_G$ (tri)	384	457	451	216

Because the contact area of PP is nearly twice as large (~24 mm<sup>2</sup>) as the areas of PQ, PC and AB (~12 mm<sup>2</sup>), its  $Z_{tis}$  is substantially lower. Due to the large wire impedance of the Pisces leads, their total load impedance is considerably larger than the tissue impedance. Variations of dCSF have only a minor effect on the tissue impedance  $Z_{tis}$  of any lead. A reduction of dCSF from 4.4 mm to 2.0 mm results in an average increase of  $Z_{tis}$  by 6.5%.

As shown in **Figure 3A**, the maximum recruited DC area is larger in tripolar than in monopolar stimulation with the same lead and it decreases as dCSF is increased. Moreover, this area is increased when in tripolar stimulation the center-to-center spacing is reduced. Accordingly, the area is largest ( $5.3 \text{ mm}^2$ ) in tripolar AB stimulation with the smallest dCSF (2.0 mm) and is zero in monopolar PP stimulation with a dCSF exceeding 4 mm. Unlike the recruited area, the maximum span of DR recruitment is larger in monopolar than in tripolar stimulation with the same lead and increases as dCSF is increased (**Figure 3B**). The maximum span is achieved with monopolar PP stimulation (9 mm), whereas the minimum is obtained with tripolar AB stimulation (3.3 mm).

The opposite effects of both contact spacing and dCSF on the maximum recruited DC area and the maximum DR span are also shown in **Figure 4**. The increase of the maximum recruited DC area levels off, when the contact distance gets smaller (**Figure 4A**), whereas the maximum span of DR recruitment is reduced (**Figure 4B**).

In **Table 3** a comparison of various evaluation parameters of the four (single) lead types is presented. It is shown that the lead with the smallest contact distance (AB) has the highest DT/PT ratio,  $S_{RA}$  and DC recruitment depth and thus most likely the largest paresthesia coverage. However, it also requires the highest current and by far the highest energy for stimulation.

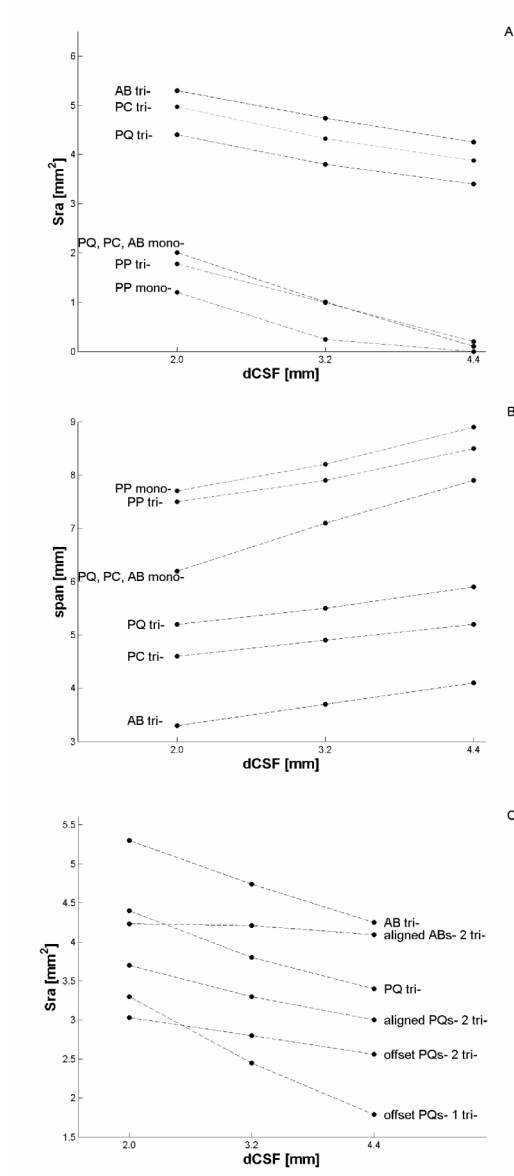


**Figure 3.** Max. recruited DC area (A) and max. span of DR recruitment (B) as a function of dCSF in monopolar and tripolar stimulation with a single lead centered on the spinal cord midline and max. recruited DC area in tripolar stimulation with dual leads and the corresponding single leads as a function of dCSF (C); for acronyms see Figure 2.



**Table 3.** % difference (+ or -) in evaluation parameter values of the PP, PC and AB leads as compared to the PQ lead, for which absolute values are given (tripolar stimulation, dCSF = 3.2 mm). Acronyms are in accordance with definitions introduced in the text.

Lead type		PQ (100%)	PP (±%)	PC(±%)	AB(±%)
$V_{PT}$	[V]	1.05	8.6	- 0.9	- 34.2
$V_{DT}$	[V]	2.11	- 25.6	18	11.4
$I_{PT}$	[mA]	2.3	26.1	0.0	43.5
$I_{DT}$	[mA]	4.6	- 10.9	19.6	137.0
DT/PT	[-]	2	- 30.0	19.0	65.0
$S_{RA}$	[mm <sup>2</sup> ]	3.8	- 73.9	13.7	24.7
depth (DC)	[mm]	0.74	- 58.1	10.8	20.3
span (DR)	[mm]	5.5	43.6	- 10.9	- 32.7
$E_{DT}$	[μJ]	2.04	- 34.3	41.7	162.7
$Z_{tis}$	[Ohm]	247	- 29.6	- 2.4	- 14.6

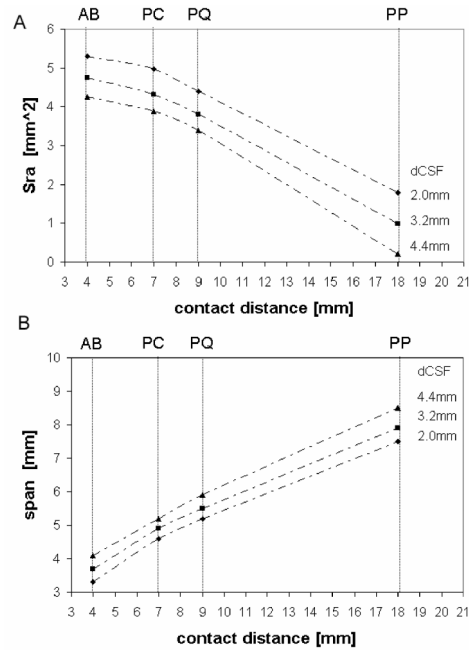


**Figure 4.** Max. recruited DC area (A) and max. span of DR recruitment (B) as a function of the center-to-center contact distance in tripolar stimulation with a single lead centered on the spinal cord midline and different dCSF values. Only PP lead has a different contact length (see Table 2); for acronyms see Figure 2.

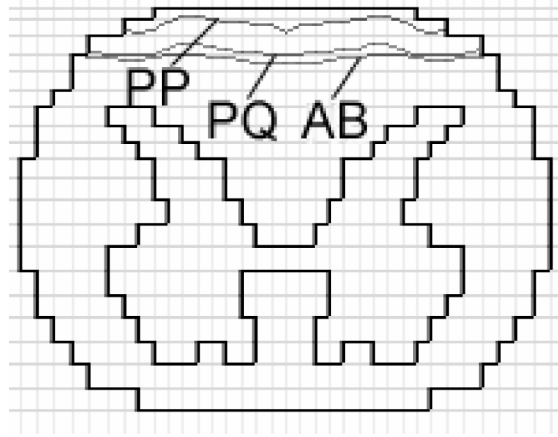


**Figure 5.** Transverse section of the spinal cord with recruitment contours indicating the max. recruited DC area in tripolar stimulation with the PQ, PP and AB lead centered on the spinal cord midline and dCSF = 3.2 mm; for acronyms see Figure 2.

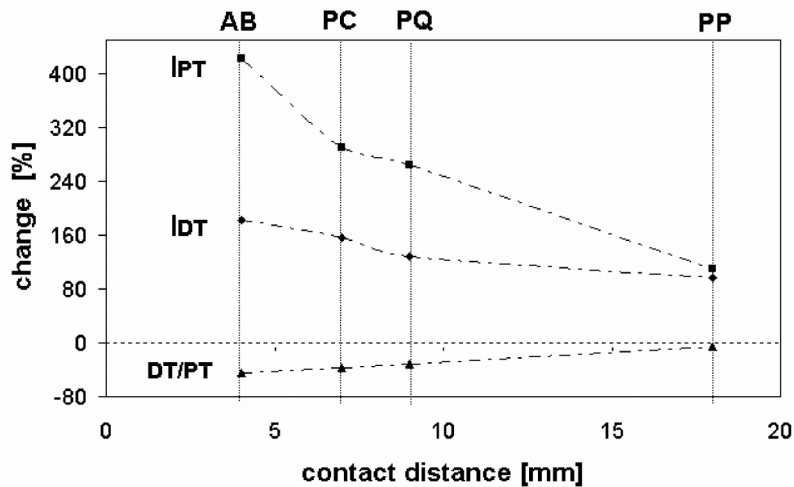


**Figure 6.** % change of the injected current at paresthesia threshold ( $I_{PT}$ ), injected current at discomfort threshold ( $I_{DT}$ ) and threshold ratio (DT/PT) when dCSF is increased from 2.0 mm to 4.4 mm for the modeled leads ordered by their center-to-center contact distance; value obtained with dCSF equaling 2.0 mm represents reference 100%; for acronyms see Figure 2.

The shapes of the recruited areas in the DCs at DT are presented in **Figure 5** for the PQ, PP and AB leads in tripolar stimulation.

The sensitivity of evaluation parameters to a change in dCSF is increased when the contact distance is reduced, i.e. the smaller the contact

distance, the larger is the (percentage) change when dCSF is increased from 2.0 to 4.4 mm for e.g.  $I_{PT}$ ,  $I_{DT}$  and DT/PT ratio as shown in **Figure 6**.

#### Single leads 1mm off spinal cord midline, next to dura mater

In order to examine the influence of an asymmetric lead position, each single lead was placed with its axis 1.0 mm off the spinal cord midline and just outside the dura mater, in both a monopolar and a tripolar combination.

A displacement of a lead off the midline results in a considerable reduction of  $V_{DT}$ ,  $I_{DT}$ , DT/PT,  $E_{DT}$ ,  $S_{RA}$  and its depth, as shown in **Table 4**.

**Table 4.** % change (+ or -) in evaluation parameter values for single leads 1.0 mm off midline as compared to the corresponding spinal cord midline lead position. Results for tripolar stimulation with dCSF = 3.2 mm are presented. Acronyms are in accordance with definitions introduced in the text.

Lead type	PQ (±%)	PP (±%)	PC(±%)	AB(±%)
$V_{PT}$	0.0	- 14.9	0.0	1.4
$V_{DT}$	- 19.4	- 15.3	- 33.3	- 25.9
$I_{PT}$	0.0	- 15.2	0.0	- 1.5
$I_{DT}$	- 19.6	- 16.1	- 21.8	- 27.5
DT/PT	- 20.0	0.0	- 21.8	- 26.1
$S_{RA}$	- 46.3	- 94.9	- 39.8	- 39.5
depth (DC)	- 37.8	- 77.4	- 30.5	- 29.2
span (DR)	- 3.6	- 3.8	- 4.1	- 5.4
$E_{DT}$	- 35.2	- 28.5	- 48.2	- 46.0
$Z_{tis}$	1.2	1.1	1.7	1.4

All these effects are due to the fact that an asymmetrically placed lead is closer to the DR fibers on one side (see Discussion). Moreover, the shape of the recruited DC area is highly asymmetrical, 70-100% being in the DC on the lead side. This result stresses the importance of a perfect midline lead position for an adequate bilateral pain relief.

At  $V_{PT}$  the DC fiber recruitment starts at the dorsal border near the mediolateral position of the lead and spreads bilaterally and ventrally when the stimulation voltage is increased. The amount of asymmetry of the recruited areas is similar, except for a complete unilaterality in PP lead stimulation which is due to its small DT/PT ratio.

Similar relations between the recruited areas of the various single leads as shown in **Figure 3A** are evident, except that their absolute values are reduced by nearly 50% when the leads are 1 mm off the midline.

### Single lead on spinal cord midline, deeper in the epidural space

Unlike surgical SCS leads usually being fixed to the dura mater, the dorsoventral position of a percutaneous lead in the dorsal epidural space can usually not be controlled. Therefore, we modeled the influence of the dorsoventral position of a single PQ lead, programmed as a tripole and positioned symmetrically to the spinal cord midline.

When the lead is displaced dorsally from a position next to the dura mater, an increasing deterioration of performance parameters occurs, as we have presented in more detail in a previous publication [15].

### Dual leads (single mode)

Because SCS with two closely spaced percutaneous leads is getting increasingly popular in the management of chronic, neuropathic pain, we also modeled tripolar stimulation with dual staggered and aligned PQ leads, and with dual aligned AB leads (see **Figure 2**: ‘offset tri-PQ’, ‘offset 2 tri-PQ’, ‘2 aligned tri-PQ’, ‘2 aligned tri-AB’).

**Table 5.** Parameter values of tripolar stimulation with dual and single PQ and AB leads. The data of dual leads are given as % difference (+ or -) of the corresponding single lead values (presented with their absolute values). Results of simulations with dCSF = 3.2 mm

Lead type	single PQ tri- (100%)	align PQs 2 tri- (±%)	offset PQs 1 tri- (±%)	offset PQs 2 tri- (±%)	single AB tri- (100%)	align ABs 2 tri- (±%)
$V_{PT}$ [V]	1.05	- 35.2	+34.3	- 8.6	0.69	- 29
$V_{DT}$ [V]	2.11	- 44.1	34.6	- 33.6	2.35	- 42.5
$I_{PT}$ [mA]	2.3	+11.3	+34.8	+68.7	3.3	+15.2
$I_{DT}$ [mA]	4.6	-3.0	+33.7	+21.7	10.9	- 4.6
$DT/PT$ [-]	2	-13.0	0.0	- 27.5	3.3	- 18.5
$S_{RA}$ [mm <sup>2</sup> ]	3.8	- 13.2	- 35.5	- 26.3	4.74	- 11.2
depth (DC) [mm]	0.74	- 20.3	- 24.3	- 35.1	0.89	- 16.9
span (DR) [mm]	5.5	- 1.8	- 9.1	+7.3	3.7	0.0
$E_{DT}$ [μJ]	2.04	- 46.1	+79.4	- 19.1	5.36	- 45.0
$Z_G$ [Ohm]	457	- 42	+0.8	- 45	216	- 40

Due to bilateral, off midline lead positions, these leads are closer to the DRs than a midline lead. Consequently, DR fiber thresholds are reduced as compared to DC fiber thresholds, thus reducing the DT/PT ratio. As shown in **Table 5** and **Figure 3C** all simulated dual-lead combinations recruit a smaller maximum DC area with a smaller depth than the corresponding single lead combinations. Load impedances of the dual-leads with two tripoles programmed are

substantially reduced due to the parallel connection of the leads to the pulse generator.

The maximum span of DR recruitment of a dual-lead tripole is not substantially different from the span of the corresponding single lead tripole. This is due to the fact that the lead geometry, particularly the cathodal length on either side, is identical. In contrast to the aligned tripoles, the offset tripoles will likely recruit different groups of rootlets on either side.

### 3.4. Discussion

#### **Preferential stimulation of DC vs. DR fibers**

The aim of this modeling study was to predict which percutaneous SCS lead is most appropriate to be applied in patients with complex chronic pain syndromes such as CRPS and FBSS and which one is most appropriate to manage segmental pain, taking into account the large variability of dCSF among subjects. In a previous paper it has already been shown that a tripolar combination (guarded cathode) favors stimulation of DC fibers most, whereas a monopole (cathode) stimulates DR fibers preferentially [10].

From this modeling study we conclude that a single AB lead programmed as a guarded cathode and placed at the spinal cord midline just outside the dura mater performs best in terms of recruitment of DC fibers. Leads with a larger contact distance perform worse. Under identical conditions the DC areas recruited by the PC and PQ lead are approximately 8% and 19% smaller. Monopolar stimulation with any lead gives even less DC recruitment, similar to the performance of the PP lead programmed as a tripole. In fact, due to its large contact distance (18 mm) the tripolar PP combination performs virtually as a monopole for all realistic dCSF values. The performance of the AB lead is in accordance with the results by Holsheimer and Wesselink [13], who proposed a similar lead design.

In contrast, a monopolar PP combination recruits the largest span of DR filaments (rootlets), being 8-9 mm. At a common low-thoracic stimulation level (vertebrae T11-T12) the mean length of the corresponding spinal cord segments is about 10 mm, which means that not even all filaments of a single DR would be recruited at DT. Depending on the rostrocaudal position of the cathode, part of the filaments of two adjacent spinal cord segments may be recruited. In clinical practice the span of recruited DR fibers is often enlarged by programming two adjacent contacts as cathodes, thus virtually increasing the cathodal length and thereby the preferential stimulation of DR fibers. By modeling the PQ and the AB lead programmed as a dual cathode ( - - ) we obtained an increase in the maximum span of DR recruitment of about 100% and 20%, respectively, when compared to a single cathode case. In this way paresthesia may be elicited in 2-3 adjacent dermatomes. Anyhow, mere DR stimulation would not result in a wide paresthesia coverage (only 1-2 segments). Moreover, there is an inverse, nearly linear relation between the

recruited DC area and the span of DR recruitment, so that an improved DC recruitment implies a diminished DR recruitment and vice versa. Therefore, leads (programmed to be) efficient in the management of complex pain syndromes are less efficient in the treatment of segmental pain.

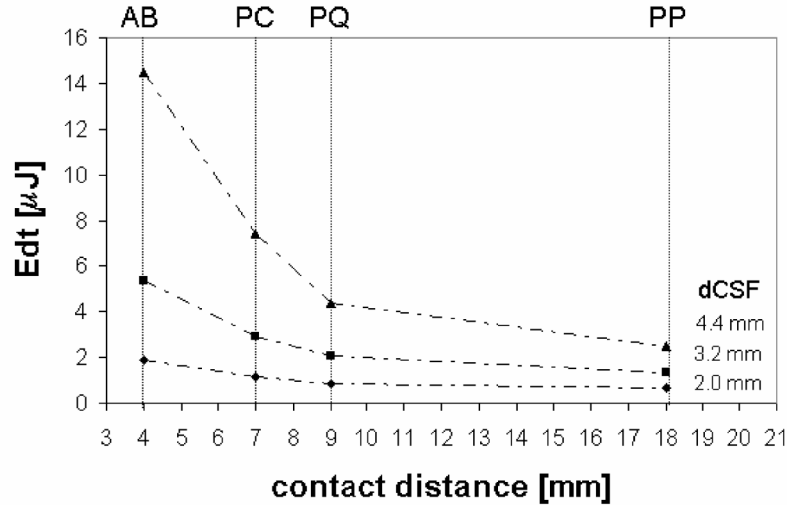


**Figure 7.** Energy consumption as a function of the modeled leads center-to-center contact distance; for acronyms see Figure 2.

#### DC fiber recruitment and energy consumption

Unfortunately, improved DC recruitment is accompanied by a substantial increase in energy consumption, particularly when using the AB lead. This is due to the proximity of anodes and cathodes, resulting in a more confined electric field. Accordingly, more current needs to be supplied for the excitation of nerve fibers in the DCs (and DRs).  $I_{PT}$  of the AB lead is 40% higher than  $I_{PT}$  of the PQ lead. Due to the strongly increased DT/PT ratio,  $I_{DT}$  of the AB lead exceeds the corresponding value of the PQ lead by 140%, whereas its  $S_{RA}$  is just 25% larger. With the PC lead  $I_{DT}$  and  $S_{RA}$  are increased by 20% and 14%, respectively, as compared to the PQ lead (see **Table 3**).

The larger  $S_{RA}$  of the AB lead as compared to the PQ (and PC) lead may be a significant factor for the efficacy of the therapy. As the contact distance of a lead gets smaller the cost in terms of energy consumption rises more steeply (**Figure 7**) than the recruited area (**Figure 4A**) and a trade off has to be made. Therefore, the increased energy consumption of AB leads make a RF-system or an implantable stimulator with a rechargeable battery more suitable to use.

### **Effects of asymmetrical lead position**

By displacing a single lead off the spinal cord midline, its performance deteriorates. The maximum recruited DC area is decreased and asymmetrical with its major part on the lead side. In clinical practice the probability of a perfect midline position of the lead as in our models is not so high and hence the performance will generally get worse, as predicted by modeling.

In the treatment of unilateral or asymmetrical pain an asymmetrical lead position can be favorable because paresthesia will most likely be focused on those dermatomes represented in the DC on the same side. If so, the lead should be intentionally guided so as to lay aside the spinal cord midline [4].

Although the maximum span of DR recruitment on the lead side does not change, the current needed is lower than with the lead in a midline position. An asymmetrical lead position can, however, only be used in the treatment of unilateral segmental pain.

### **Effects of dorsoventral epidural lead position**

By displacing a lead dorsally, preserving its midline, symmetrical position, the overall performance deteriorates. When the lead is positioned just outside the dura mater it has thin dura and a highly conductive CSF layer on one side, which directs most current towards the target nerve fibers. By positioning the lead deeper in the low conductive epidural space, the load impedance is increased and more equally distributed around a contact. Accordingly, an increasing part of the current flows dorsally and laterally in the epidural space and does not contribute to the stimulation of DC and DR fibers. Moreover, this current may well recruit fibers located in the ligamentum flavum, as hypothesized by North et al. [19].

### **Dual vs. single lead performance**

All modeled tripolar, dual lead combinations in single mode perform worse than the corresponding tripolar combination on a single, midline lead. Their DT/PT ratios are generally smaller. Their maximum recruited DC areas are smaller and  $I_{DT}$  is generally similar or higher (in case of staggered leads).  $I_{PT}$  is also higher with dual leads. Because more contacts are connected in parallel to the stimulator when two tripoles are used, they have a lower load impedance and less energy consumption.

In clinical studies, however, both an improved [2] and a worse [18, 21] performance of dual-leads in comparison to single leads are reported. In our modeling study we did not take into account that by inserting a lead in the epidural fat tissue the volume of the epidural space is increased, which may push the dura mater anteriorly and thereby reduce dCSF. In this way a dual (or triple) lead may reduce the distance between the leads and the spinal cord more than a single lead, as discussed by Holsheimer and Wesselink [12]. According to the results of this modeling study, a smaller dCSF results in a larger recruited

DC area and most likely an increased paresthesia coverage, resulting in better clinical results.

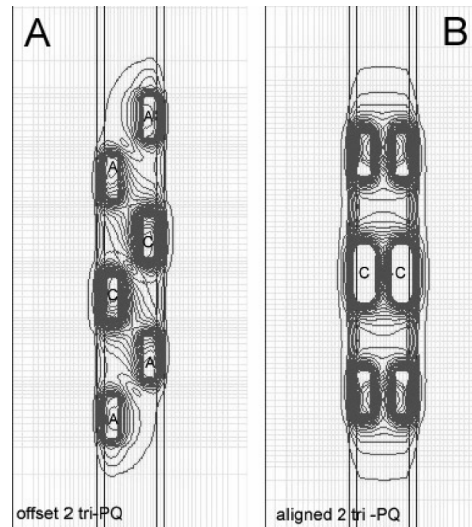


**Figure 8.** Iso-current-density lines in a coronal plane intersecting the dorsal CSF layer; dual offset leads (**A**) and dual aligned leads (**B**), programmed as dual tripoles.

The two offset PQ lead combinations have a worse performance than the aligned PQ lead combination, despite the fact that their rostrocaudal center-to-center contact distance is reduced by 50%. This is due to the fact that the preferred rostrocaudal current component (the direction of DC fibers) is reduced by approximately 17% (**Figure 8A**) in comparison to aligned PQ leads (**Figure 8B**). A larger current is thus required for stimulation. Consequently, offset leads recruit an even smaller and less deep DC area (**Figure 3C**) and have a larger  $I_{DT}$  and  $I_{PT}$  than aligned leads.

Finally, the performance of two tripoles programmed to be simultaneously active on the dual-leads (single mode) as we modeled is not to be mistaken for the performance of two tripoles programmed alternately on the dual leads (dual mode) as often used in SCS. Due to a separation in time of pulses applied to the tripoles programmed on each lead, there is no superposition of the electrical fields and no compound effect of the tripoles on the fiber recruitment. In fact, dual mode stimulation is identical to having a single lead positioned on either side of the midline, as we modeled for just one side. As in single mode, a dual lead in dual mode performs worse than a single lead placed on the spinal cord midline.



**Other similar percutaneous leads**

Although we addressed several specific leads, the results apply to all percutaneous leads with similar contact geometries and spacing. These include the Quattrode 3153 and 3143 (Advanced Neuromodulation Systems). The latter have identical contact lengths and spacings as the PQ and the PC lead, respectively, resulting in a similar performance when the same contact combinations are used. Due to the larger diameter of the Quattrodes (1.6 mm) their tissue impedance will be somewhat lower. Moreover, these leads have a low wire impedance, thus reducing energy consumption. Similarly, the recently released Pisces Z family leads (Medtronic Inc.) with the same contact characteristics as the corresponding leads from the Pisces family have a low wire impedance thus reducing energy consumption too.

**3.5. Conclusions**

- 1) For maximum stimulation of the DCs, the best lead is a lead with closely spaced contacts programmed as a guarded cathode (+ - +) and centered on the spinal cord midline just outside the dura mater;
- 2) For maximum stimulation of the DRs, the best combination is a monopole (cathode) programmed on a lead having long contacts (or a lead with two adjacent cathodes);
- 3) The recruitment of fibers in the DCs and DRs is inversely related;
- 4) Increased energy consumption is the cost to be paid for a better performance;
- 5) Leads positioned aside the spinal cord midline should be used for the treatment of unilateral, primarily segmental pain;
- 6) Any lead should be placed immediately outside the dura. A position deeper in the epidural fat results in a strong deterioration of its performance;
- 7) A single tripole exactly on the spinal cord midline performs better than any dual lead combination, either in single, or in dual mode.

A clinical study comparing the performance of percutaneous leads would be useful to verify the modeling results and to help finding an optimal lead for SCS.

---

**Acknowledgements**

The authors gratefully thank Advanced Bionics Corporation (Valencia, CA, USA) for their grant to support this research.

**REFERENCES**

- 1 Alo K and Holsheimer J. New trends in neuromodulation for the management of neuropathic pain. **Neurosurgery**. 50:690-704, 2002
- 2 Alo K, Redko V and Chornov J. Four year follow-up of dual electrode spinal cord stimulation for chronic pain. **Neuromodulation**. 5:79-88, 2002
- 3 Alo K, Varga C, Krames E, Prager J and Bradley K. Variability of contact impedance by vertebral placement in spinal cord stimulation. San Francisco, CA: 2004.
- 4 Barolat G, Massaro F, He J, Zeme S and Ketcik B. Mapping of sensory responses to epidural stimulation of the intraspinal neural structures in man. **J Neurosurg**. 78:233-239, 1993
- 5 Coburn B. A theoretical study of epidural electrical stimulation of the spinal cord - Part II. Effects on long myelinated fibers. **IEEE Trans Biomed Eng**. 40:632-639, 1985
- 6 Fyffe R. Afferent fibers. In: Davidoff R. Handbook of the Spinal Cord. New York: Dekker, 1984: 79-136.
- 7 He J, Barolat G and Ketcik B. Stimulation usage range for chronic pain management. **Analgesia**. 1:75-80, 1995
- 8 Holsheimer J and Struijk J. How do geometric factors influence epidural spinal cord stimulation? A quantitative analysis of computer modeling. **Stereotact Funct Neurosurg**. 56:234-239, 1991
- 9 Holsheimer J, Den Boer J, Struijk J and Rozeboom A. MR assessment of the normal position of the spinal cord in the spinal canal. **Am J Neuroradiol**. 15:951-959, 1994
- 10 Holsheimer J, Struijk J and Tas N. Effects of electrode geometry and combination on nerve fiber selectivity in spinal cord stimulation. **Med Biol Eng Comput**. 33:676-682, 1995
- 11 Holsheimer J. Effectiveness of spinal cord stimulation in the management of chronic pain. Analysis of technical drawbacks and solutions. **Neurosurgery**. 40:990-996, 1997
- 12 Holsheimer J and Wesselink W. Effects of anode-cathode configuration on paresthesia coverage in spinal cord stimulation. **Neurosurgery**. 41:654-660, 1997
- 13 Holsheimer J and Wesselink W. Optimum electrode geometry and combination on nerve fiber selectivity in spinal cord stimulation. **Med Biol Eng Comput**. 33:676-682, 1997
- 14 Holsheimer J and Barolat G. Spinal geometry and paresthesia coverage in spinal cord stimulation. **Neuromodulation**. 1:129-136, 1998
- 15 Manola L and Holsheimer J. Technical performance of percutaneous and laminectomy leads analyzed by modeling. **Neuromodulation**. 7:231-241, 2004
- 16 McNeal D. Analysis of a model for excitation of myelinated nerve. **IEEE Trans Biomed Eng**. 23:329-337, 1976
- 17 Melzack R and Wall P. Pain mechanisms: a new theory. **Science**. 150:971-978, 1965

- 18 North R, Fowler K, Nigrin D and Szymanski R. Patient-interactive computer-controlled neurological stimulation system: clinical efficacy in spinal cord stimulator adjustment. **J Neurosurg.** 76:967-972, 1992
- 19 North R, Lanning A, Hessels R and Cutchis P. Spinal cord stimulation with percutaneous and plate electrodes: side effects and quantitative comparisons. **Neurosurg Focus.** 2:1-5, 1997
- 20 North R, Kidd D, Olin J and Sieracki J. Spinal cord stimulation electrode design: prospective, randomized, controlled trial comparing percutaneous and laminectomy electrodes - Part I. Technical outcomes. **Neurosurgery.** 51:381-390, 2002
- 21 North RB, Kidd DH, Olin J, Sieracki JN and Petrucci L. Spinal cord stimulation for axial low back pain: a prospective controlled trial comparing 16-contact insulated electrodes with 4-contact percutaneous electrodes. **Neuromodulation.** 9:56-67, 2006
- 22 Struijk J, Holsheimer J, van der Heide G and Boom H. Recruitment of dorsal column fibers in spinal cord stimulation: influence of collateral branching. **IEEE Trans Biomed Eng.** 39:903-912, 1992
- 23 Struijk J, Holsheimer J, Barolat G, He J and Boom H. Paresthesia thresholds in spinal cord stimulation: a comparison of theoretical results with clinical data. **IEEE Trans Biomed Eng.** 1:101-108., 1993
- 24 Struijk J, Holsheimer J and Boom H. Excitation of dorsal root fibers in spinal cord stimulation: a theoretical study. **IEEE Trans Biomed Eng.** 40:632-639, 1993
- 25 Wesselink W, Holsheimer J and Boom H. A model of the electrical behaviour of myelinated sensory nerve fibers based on human data. **Med Biol Eng Comput.** 37:228-235, 1999



# Chapter 4

## Theoretical Investigation into Longitudinal Electrical Field Steering in Spinal Cord Stimulation

Ljubomir Manola<sup>1</sup> • Jan Holsheimer<sup>1</sup> • Peter H. Veltink<sup>1</sup> • Kerry Bradley<sup>2</sup> • David Peterson<sup>2</sup>

<sup>1</sup>) Institute for Biomedical Technology, Department of Electrical Engineering, University of Twente, The Netherlands; <sup>2</sup>) Advanced Bionics Corporation, Valencia, CA, USA

### Abstract

**Objective.** In spinal cord stimulation (SCS) for chronic pain management, precise longitudinal positioning of the cathode is crucial to generate electrical field capable of targeting the neural elements involved in pain relief. Presently used methods have a poor spatial resolution and lack postoperative flexibility needed for fine tuning and reprogramming the stimulation field after lead displacement or changes in pain pattern. We describe a new method, “*electrical field steering*”, to control paresthesia in SCS. The method takes advantage of newer stimulator design and a programming technique allowing for ‘continuous’ adjustment of contact combination while controlling stimulation *current* for each contact *separately*.

**Methods.** Using computer modeling we examined how stimulation of dorsal column (DC) and dorsal root (DR) fibers was influenced by changing the current ratio of the cathodes of a dual (- -) and a guarded dual cathode (+ - - +) configuration programmed on a percutaneous lead with 9 and 4 mm center-to-center contact spacing.

**Results.** A cathodal current ratio could be found for which DC or DR fiber recruitment and thus likely the paresthesia coverage was maximized. The DR threshold profiles shifted longitudinally, thus following the shift in the electrical field during steering. The profiles had constant shape when contact spacing was small and changed shape for wider contact separation. Generally, the wider contact separation provided less DC and more DR fiber recruitment.

### **Conclusions.**

- By means of cathodal steering on a longitudinal contact array the group of excited DC and DR fibers and thus paresthesia coverage in SCS can be controlled.
- With widely spaced contacts, superposition of the electrical field from each steering contact is limited.
- To precisely control segmental paresthesia (DR stimulation), a small contact spacing is necessary.

## 4.1. Introduction

### Background context

Spinal Cord Stimulation (SCS) is a well-established clinical technique for the treatment of chronic, otherwise intractable pain. The pain associated syndromes that can be treated include peripheral neuropathy, peripheral vascular disease, angina, phantom limb pain, complex regional pain syndrome, failed back surgery syndrome (low-back pain), segmental pain etc [2, 22]. Melzack and Wall postulated that stimulation of large myelinated cutaneous fibers relieves pain by inhibiting the transmission of the pain signals towards the brain (“gate-control theory”) [17]. The position of the epidural cathodal contact(s) relative to the neural targets located in the dorsal columns (DCs) and dorsal roots (DRs) primarily determines which fibers will be stimulated. The anodal contacts only modulate the gross effects of cathodal stimulation by e.g. increasing the therapeutic range of stimulation [13] and thereby the extent of paresthesia coverage. In addition, the paresthesia coverage is affected by the position of the anodes with respect to the cathode(s) and their impedances (when a single-channel, constant-voltage pulse generator is used).

The clinical procedure consists of inserting lead(s) in the dorsal epidural space percutaneously or surgically. The ‘optimal’ rostrocaudal level of the lead is roughly determined by manipulating the lead position and using test stimulation intraoperatively. In the postoperative test stimulation procedure, the contact combination giving maximum coverage of the pain with paresthesia [1] is determined for each patient using his/her feedback on paresthesia coverage and subjective pain relief. In order to have satisfactory pain relief it is crucial to stimulate tactile fibers originating from the entire painful body area(s) (dermatome(s)) [1, 13, 18]. By varying the longitudinal position of the lead (“trolling”) and thereby the cathode position and the stimulation-induced electrical field, the population of fibers recruited in the DCs and DRs (and thus paresthesia coverage) can be varied. By programming a different or additional contact as a cathode, the stimulation-induced electrical field can be modified even more, thus allowing for some flexibility. However, tuning of the electrical field depends on the spatial resolution of the contact array (center-to-center spacing) and the ability of the stimulator to drive multiple contacts independently. For some pain patterns, such as chronic low-back pain (when stimulating low-thoracically, the target nerve fibers are located in the lateral aspects of the DCs [10]), a smooth shift of the cathodal field may be necessary to target the “sweet-spot” in the low-thoracic region. Similarly, treatment of segmental pain (DR stimulation) may also require a fine control of the longitudinal position of the stimulation-induced field.

Sweeney et al. [27] and Veraart et al. [28] considered and confirmed experimentally that by simultaneously applying variable currents to a longitudinal guarded cathode and a transversely-opposed (‘steering’) anode in a cuff electrode, the stimulation-induced field can be changed and the selectivity

of peripheral nerve stimulation improved. Goodall et al. [3] concluded that selectivity in peripheral nerve stimulation can be changed by changing the current ratio of the longitudinal and transverse anodes in the cuff electrode. Struijk and Holsheimer proposed an SCS system to smoothly shift the electrical field mediolaterally using a dual-channel stimulator coupled with a transversely oriented guarded cathode [26]. Clinical studies that followed have shown that the electrical field and thereby paresthesia coverage can be shifted as has theoretically been predicted by computer modeling [9, 21, 30]. Similarly, using a single, percutaneous lead Oakley et al. demonstrated the ability to shift paresthesia in a comfortable fashion with patient feeling paresthesia continuously [20].

### **Purpose**

In this paper we describe a method to electronically shift the stimulation field longitudinally and thus fiber recruitment and paresthesia in SCS. We named this method “electrical field steering”. It takes advantage of newer programming techniques that became available with new stimulator designs. The method is similar to the one applied by Oakley et al. [20]. The effects of electrical field steering on DC and DR fiber recruitment were investigated using computer modeling and were primarily related to the contact spacing on a single, percutaneous longitudinally oriented lead. The possibility to electronically shift the stimulation field is extremely important as it would allow postoperative fine-tuning of the locations where paresthesias are perceived without the need to change the lead position. Preliminary results of this study have been previously reported [15].

### **4.2. Methods**

In order to evaluate the effects of the proposed field steering technique on the electrical potential field and the recruitment of nerve fibers, computer simulations were performed using the University of Twente – Spinal Cord Stimulation (UT-SCS) software [7, 24]. Each model consisted of a 3D volume conductor, an array of lead contacts and nerve fiber models.

#### **Volume conductor model**

A 3D model of the low-thoracic region (T10-T12) was used. The dimensions of the modeled anatomical compartments (spinal cord, dural sac, epidural space, etc.) were taken from an MRI study on spinal cross-sections [6]. Models with dorsal cerebrospinal fluid thicknesses (dCSF) of 2.0, 3.2 and 4.4 mm were made in order to determine the influence of this parameter. This range of dCSF corresponds to its anatomical variation in the chosen spinal segments [6, 8]. A transverse cross-section of the model is shown in **Figure 1A**. Electrical conductivities of the compartments were taken from Struijk et al. [25] with modifications as described in [14]. The volume conductor model had 56x64x80

cubic elements. In order to obtain the stimulation-induced electrical potential field, a discretized form of the Laplace equation was solved numerically. For more details see Struijk et al. [24].

#### Lead models

The influence of contact spacing was evaluated by modeling two commercially available percutaneous lead types with different contact spacing:

- 1) 3487A Pisces Quad® (Medtronic Inc., Minneapolis, MN, USA) – named “PQ”, and
- 2) SC2108 Linear™ (Advanced Bionics Corp., Valencia, CA, USA) – named “LN”.

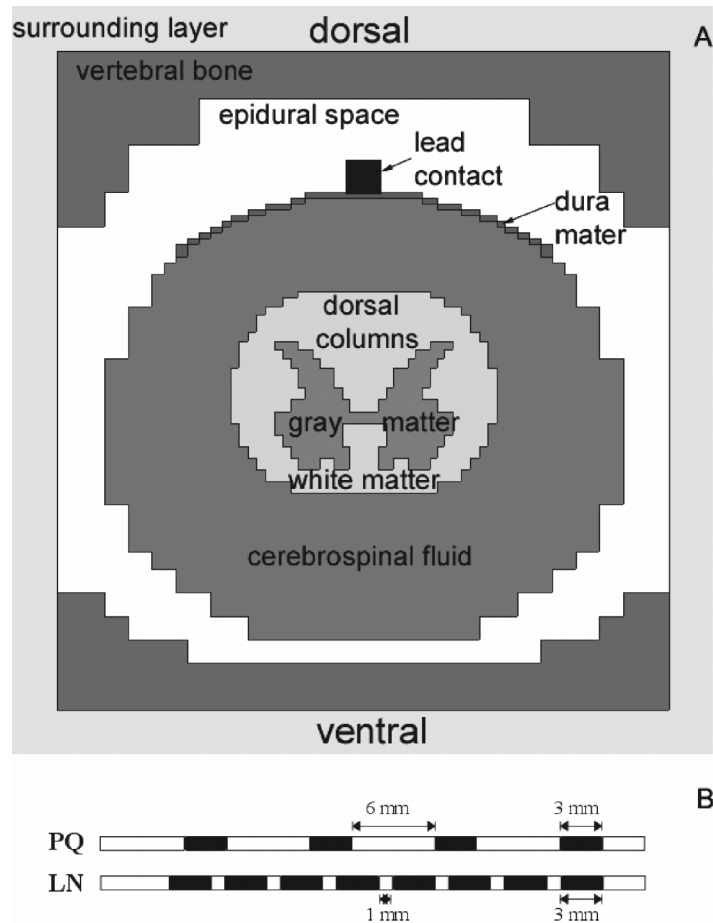


**Figure 1.** a) Transverse cross-section of the low-thoracic spinal cord stimulation model. The anatomical compartments and the epidural lead are labeled. b) Two percutaneous lead models. The lengths of contacts and spacings are specified.



Both lead types have contacts of the same shape and size (3 mm long cylindrical contacts with a diameter of ~1.2mm). The PQ and LN lead have an edge-to-edge contact spacing of 6 mm and 1 mm, respectively. The contacts and leads were modeled as described previously [16] and are shown in **Figure 1B**. Each lead was placed longitudinally at the physiological midline plane of the model, immediately dorsal to the dura mater. The position of the lead is shown in the transverse cross-section in **Figure 1A**.

### **Stimulation strategy**

Stimulation by *current-controlled* pulse generators giving simultaneous pulses of the same pulse width but independent current control at each contact was modeled. In this way the current applied to each contact could be specified.

Dual cathode (- -) and guarded dual cathode (+ - +) stimulation were modeled with 2 and 4 independent current sources, respectively. In both configurations, only adjacent contacts were used. The scheme of the four-contact stimulation (guarded dual cathode) is shown in **Figure 2**.

When calculating the stimulation-induced field in the volume conductor, the total cathodal current was -1 mA. Electronic steering was achieved by varying the cathodal current ratio as follows: 100/0, 80/20, 60/40, 50/50, 40/60, 20/80 and 0/100%, where the first and second number designate the percentage of the total cathodal current applied to the rostral and to the caudal cathodal contact, respectively. This sequence represents steering of the cathodal current from the rostral to the caudal cathodal contact. In this way, the cathodal field could 'smoothly' be shifted from the rostral to the caudal cathode. When a guarded dual cathode configuration was modeled, a current with a fixed magnitude of +0.5 mA was impressed by each anode, thus equilibrating the total cathodal current of -1 mA.

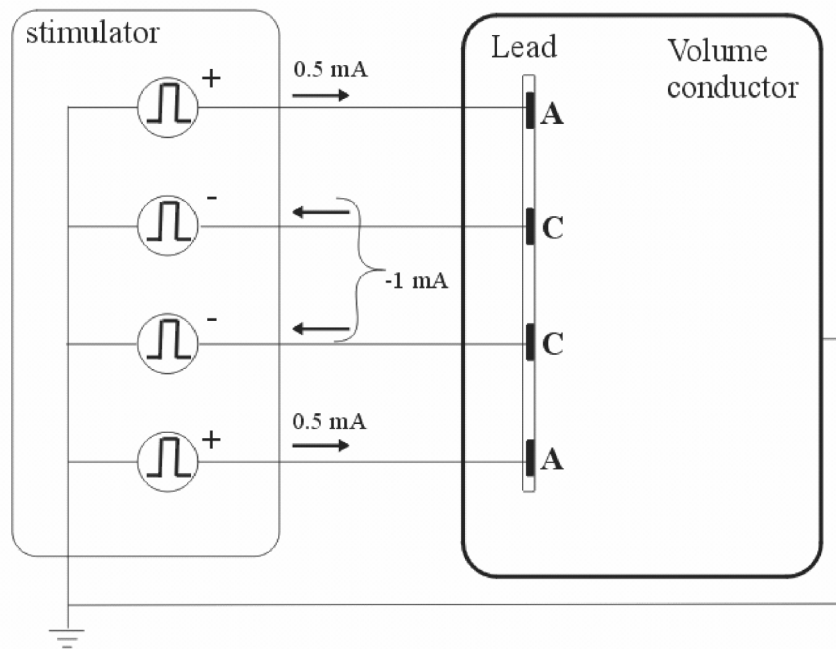


**Figure 2.** Scheme of the connections of the 4-channel stimulator with four lead contacts and the corresponding anodal and cathodal currents. The anodal currents are constant and identical (0.5 mA), whereas the total cathodal current is also constant (-1 mA), but the ratio between the two cathodal currents is variable.

### Fiber models

In order to quantify the effect of shifting the potential field on the recruitment of nerve fibers located in the DCs and DRs, the response of both DC and DR fiber models was simulated. The DC fiber model represented a 12  $\mu\text{m}$  diameter, straight, myelinated fiber whereas the DR fiber model represented a 15  $\mu\text{m}$  diameter, curved, myelinated fiber. The kinetics of the fiber membrane as described by Wesselink et al. was used [29]. Exploiting linearity of the volume conductor model, the electrical field calculated with a total current of 1 mA was scaled up or down in order to calculate the threshold stimulus to excite any DC and DR fiber model. The position of the DC fiber model was varied in order to determine the extent of the fiber recruitment in the DCs. Similarly, the longitudinal span of DR recruitment was determined by varying the rostrocaudal position of the DR fiber model. The DC and DR fiber position was

varied within their anatomical constraints. For details on the fiber models see Manola and Holsheimer [14].

### Evaluation parameters

Several parameters were calculated from the simulation results in order to quantify the effects of electrical field steering:

- *DC fiber threshold [mA]* – total current needed to activate the DC fiber with the lowest threshold
- *DR fiber threshold [mA]* – total current needed to activate the DR fiber with the lowest threshold
- *Discomfort threshold (DT) [mA]* – maximum current that can be applied before the activation of large proprioceptive fibers in the DRs, resulting in uncomfortable sensations and/or reflex responses; according to clinical data this threshold was set at 140% of the DR fiber threshold [5].
- *Maximum recruited DC area [mm<sup>2</sup>]* – part of the DCs within which DC fiber models are recruited at DT, representing the maximum therapeutic DC recruitment. From the somatotopic fiber distribution in the DCs [23] at the level of the stimulating cathodes and the recruited DC area, it can be predicted which dermatomes are most likely covered with paresthesia.
- *Maximum span of DR recruitment [mm]* – longitudinal (rostrocaudal) length over which DR fibers are stimulated at DT. It represents the maximum span of DR recruitment. The recruited DR fibers and the dermatomes of origin will correspond with the perceived paresthesia.

### 4.3. Results

We analyzed the effects of varying the cathodal current ratio on DC and DR fiber thresholds, as well as DC and DR fiber recruitment.

#### DC and DR fiber thresholds

The minimum current necessary to initiate stimulation of DC and DR fibers is shown in **Figure 3A** and **B**, respectively, for the two simulated contact combinations of each lead type and all cathodal current ratios. Both DC and DR threshold currents varied as the ratio of the cathodal currents was changed. They had a minimum value when all current was applied to one of the cathodes (rostral or caudal) and reached a maximum value when the total cathodal current was equally divided between the two cathodes (around 50/50% ratio) (see **Figure 3**). Variations of DC and DR fiber thresholds were larger for the PQ than the LN lead. The ratio of the maximum and minimum threshold value of the DC fibers was 2.5, 1.9, 1.5 and 1.3 for the PQ dual cathode, PQ guarded dual cathode, LN dual cathode and LN guarded dual cathode, respectively. The corresponding threshold ratios of the DR fibers were 1.6, 1.6, 1.1 and 1.3.

Similar ratios were obtained when dCSF was smaller (2.0 mm) or larger (4.4 mm).

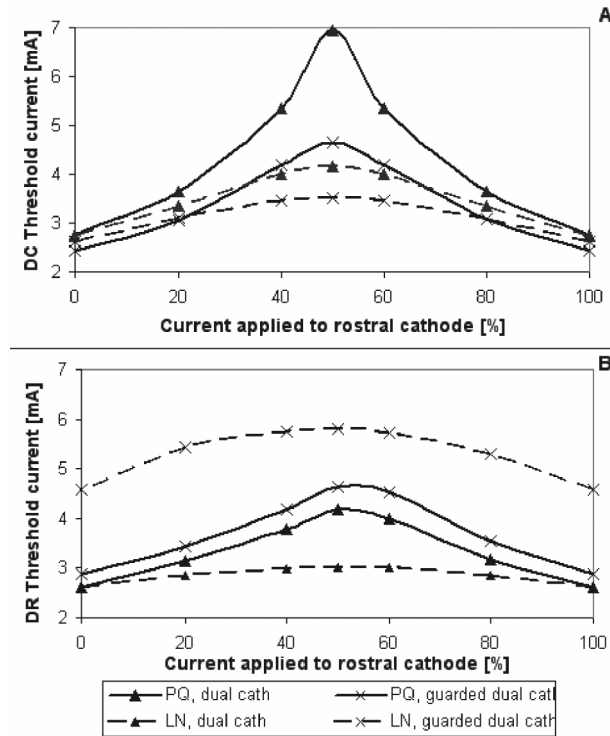


**Figure 3.** DC fiber (A) and DR fiber (B) thresholds for the cathodal current ratio varied over the entire range from 100/0% to 0/100%. dCSF = 3.2 mm.

### Maximum recruited DC area

Recruitment of DC fibers was influenced by the cathodal current ratio. The DC area recruited at DT with dual and guarded dual cathode configurations on each lead type in the model with dCSF = 3.2 mm is shown in **Figure 4A**. The cathodal current ratio was changed from 100/0% towards 0/100%. The recruited DC area did not vary in the same manner for all simulated contact configurations. As the current was distributed more equally between the cathodes, the recruited area decreased for all but the dual guarded cathode configuration programmed on the LN lead. For the latter configuration, it even increased (**Figure 4A**). The shapes of the curves and their relations were similar in models with different CSF thicknesses. **Table 1** shows the range of the recruited areas for each modeled configuration and CSF thickness. With smaller dCSF the range of recruited areas shifted towards larger values. In addition,

when guarding anodes were introduced the recruited areas increased as well. When dCSF was large (4.4 mm) there was virtually no DC recruitment with dual cathode configurations regardless of the lead type. The guarded dual cathode programmed on the LN lead had the largest and least varying recruited DC area over the whole range of cathodal current ratios. Recruitment contours, indicating the ventral boundary of the DC area in which 12  $\mu\text{m}$  fibers are recruited at DT, are shown in **Figure 5** for different cathodal current ratios while stimulating with a guarded dual cathode programmed on the PQ lead in a model with dCSF = 3.2 mm.

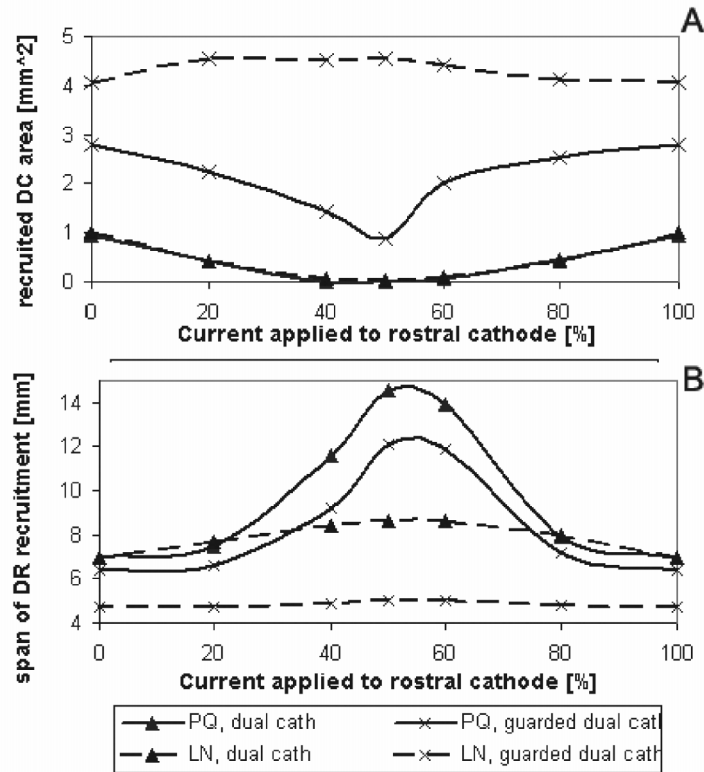


**Figure 4.** Maximum recruited DC area (A) and maximum longitudinal span of DR recruitment (B) when the ratio of the cathodal currents is varied over the entire range. dCSF = 3.2 mm.

**Table 1.** Recruited DC area at DT (in mm<sup>2</sup>) achieved by dual cathode and guarded dual cathode stimulation with PQ and LN lead and different CSF layer thicknesses. The range of values (min-max) covers the entire range of the cathodal current ratios.

Recruited DC area [mm <sup>2</sup> ] at DT for:	PQ dual cath	LN dual cath	PQ guarded dual cath	LN guarded dual cath
dCSF = 2.0 mm	0.4 - 2.0	0.7 - 2.0	2.0 - 3.5	4.7 - 5.2
dCSF = 3.2 mm	0.0 - 1.0	0.0 - 1.0	0.9 - 2.8	4.0 - 4.5
dCSF = 4.4 mm	0.0 - 0.1	0.0 - 0.1	0.0 - 2.0	3.5 - 4.1

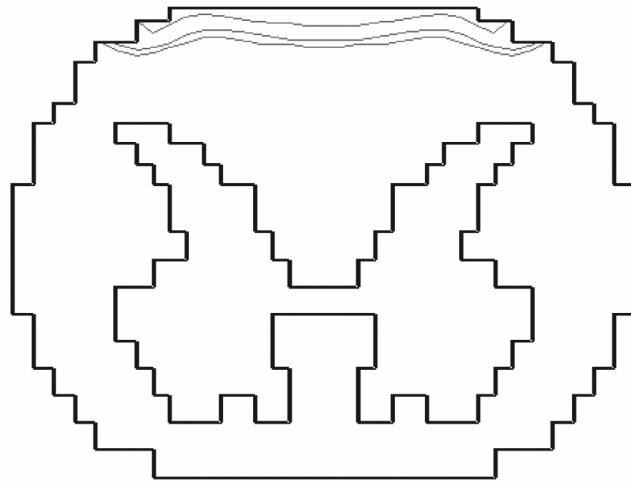


**Figure 5.** Recruitment contours indicating the ventral boundary of the DC area in which 12µm fibers are recruited (superficial part of DCs) at DT. A model with dCSF = 3.2 mm and a PQ lead with guarded dual cathode was used. The lines are shown for 100/0% (largest recruited DC area), 80/20% and 50/50% (smallest recruited DC area).

#### Maximum span of DR recruitment

By varying the cathodal current ratio the recruitment of DR fibers could also be controlled. The span of recruited dorsal rootlets at DT as a function of the cathodal current ratio is shown in **Figure 4B** for all the modeled lead configurations and dCSF = 3.2 mm. The maximum span of DR recruitment was

achieved when the cathodal current was equally distributed over the two cathodes. The variation of the span was nearly twice as large when stimulation was given with the PQ lead than with the LN lead. The ratios of maximum and minimum span were: 2.1 and 1.9 for the dual and guarded dual cathode programmed on the PQ lead and 1.2 and 1.1 for these combinations programmed on the LN lead. In **Table 2** the range of spans of different configurations and different dCSF is presented. As shown, the range of spans was larger with larger dCSF, while it was smaller when the cathodes were flanked by anodes. In addition, the PQ lead generally gave a larger span of DR fiber recruitment than the LN lead (see also **Figure 4B**).

**Table 2.** Span of DR recruitment at DT (in mm) achieved with dual and guarded dual cathode stimulation with PQ and LN lead and different CSF thicknesses. The range of values (min-max) covers the entire range of cathodal current ratios.

Recruited DR span [mm] at DT for:	PQ dual cath	LN dual cath	PQ guarded dual cath	LN guarded dual cath
dCSF = 2.0 mm	6.3 - 14.3	6.1 - 8.1	5.8 - 12.4	4.3 - 5.0
dCSF = 3.2 mm	7.0 - 14.6	7.0 - 8.6	6.4 - 12.1	4.7 - 5.0
dCSF = 4.4 mm	8.1 - 14.8	7.9 - 9.3	7.1 - 11.9	5.0 - 5.3

#### Longitudinal DR fiber threshold profiles

In order to determine these profiles the threshold currents were considered for the DR fiber model at different longitudinal positions between two contacts. For each cathodal current ratio, the stimulation threshold of the DR fiber model was calculated when the fiber model was shifted from the rostral to the caudal end of the model. The results with the dual cathode configuration programmed on the PQ and LN lead and with dCSF = 3.2 mm, are shown in **Figure 6A** and **6B**, respectively. The stimulation thresholds were normalized in such a way that the minimum of each curve (representing the lowest stimulation threshold of DR fibers, from the rostral to the caudal end) had a value 1. In this way the value 1.4 represented the discomfort threshold level as indicated in the Figure. The shift in cathodal current from rostral to caudal was accompanied by a shift of the DR threshold profile in the same direction. In addition, the shape of the PQ threshold profile changed as current was shifted caudally. A second (caudal) minimum occurred at 60/40% and 50/50% (rostral/caudal) current ratios, whereas the first (rostral) minimum disappeared at a current ratio of 40/60% (**Figure 6A-3, -4, -5**). The threshold profile for the LN lead was constant and had only one minimum, regardless of the current ratio (**Figure 6B**).

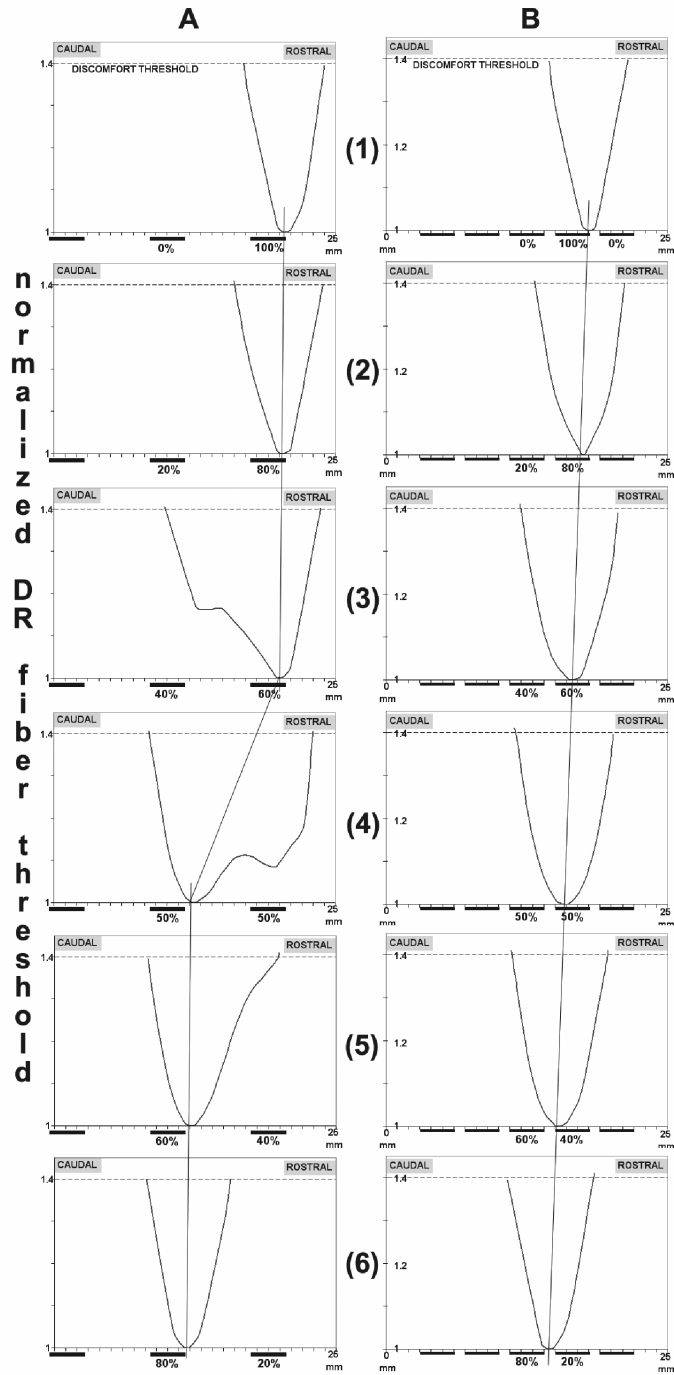




**Figure 6.** (previous page) Longitudinal profile of DR fiber thresholds for different cathodal current ratios applied to the PQ (A) and LN (B) lead. The longitudinal coordinate [mm] is indicated on the x-axis with the contacts represented by bars next to it along with the % of the cathodal current applied. The thresholds are normalized to the minimum value for each plot. Minimum threshold shifts from rostral to caudal (as indicated by straight lines) and the sequence of the profiles repeats. The value of 1.4 represents the discomfort threshold level. dCSF = 3.2 mm.

The straight lines extending from Figure 6A-1 to 6A-6 and from 6B-1 to 6B-6 connect locations of the DR fibers having the lowest threshold as the cathodal field was shifted from rostral to caudal. The rostrocaudal position of the lowest-threshold fiber with varied cathodal current ratio is also shown in **Figure 7** for all four lead configurations in models with dCSF = 3.2 mm. With the PQ lead, the position of the DR fiber having lowest threshold was shifted nearly stepwise when the cathodal current ratio was changed from 60/40% to 50/50%. In contrast, the shift in position of the DR fiber having the lowest threshold was smooth for all cathodal current ratios when modeling stimulation with the LN lead.

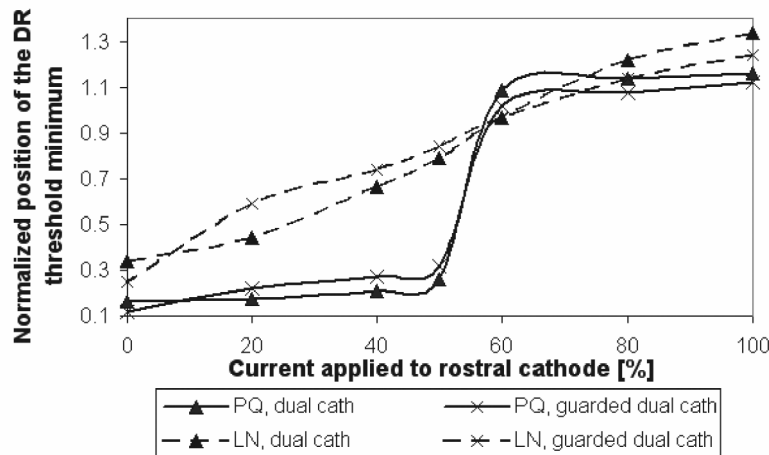


**Figure 7.** Longitudinal excursion of the of DR fiber location having minimum threshold (Figures 5A and 5B) that occurs when the cathodal current ratio of the two adjacent contacts is varied as indicated on the x-axis. The location of the minimum is normalized in respect to contact spacing with 0 representing the longitudinal level of the caudal contact center and 1 of the rostral contact center.

The influence of dCSF was not significant. With a smaller dCSF the minima were more pronounced and the gradients of the curves got steeper (not shown). Similarly, when the dual cathode was flanked by two anodes, the difference was not significant although the curves were smoother. Note that due to an asymmetric orientation of the DR fiber in respect to the contact, the profiles were shifted towards the rostral side of the contacts.

#### 4.4. Discussion

The aim of this modeling study was to investigate a method to control the stimulation field in SCS and to explore its immediate effects on the neural elements.

##### Variation in DC recruitment

By varying the ratio of the cathodal currents, the recruitment of DC fibers varied as characterized by the change in the size of the recruited DC area (**Figure 4A**). As shown in Figure 5, when the recruited DC area was decreased by balancing the currents of the two cathodes, the depth of the recruited area was reduced rather uniformly from medial to lateral. Consequently, paresthesias felt in the most rostral dermatomes (represented most laterally in the DCs) should disappear while paresthesias felt in the other dermatomes should get less intense. The demonstrated variation in the size of the recruited DC area with current steering may or may not be clinically significant taking into account the low density of large DC fibers [11]. Those stimulated fibers contributing to analgesia may or may not be included/excluded when the recruited DC area is changed, depending on their position in the DCs.

##### Variation in DR recruitment

The change in the DR threshold profiles clearly demonstrates the ability to steer the electrical field (and consequently the neural elements stimulated) by varying the cathodal current ratio. However, the different contact spacing of the two leads had a different effect on the recruitment of the DRs during steering. **Figure 6A** shows that the lead with a large contact spacing can only provide a ‘saltatory’ change in the recruitment of the DR fibers. The location of the DR fiber having the lowest threshold was abruptly shifted from a position at the level of the rostral steering cathode (60/40% cathodal current ratio, **Figure 6A - 3**) to a position at the level of the caudal one (50/50% cathodal current ratio, **Figure 6A -4**). Conversely, **Figure 6B** shows that the lead with a small contact spacing could provide a ‘continuous’ change in the rostrocaudal position of the recruited span of DR fibers. In this case the location of the DR fiber initially stimulated was smoothly displaced caudally, following the steering of the cathodal current along the percutaneous array (**Figure 7**).

Obviously, the spacing between the contacts on a lead influences the ability to control the stimulation of DR fibers. With a large contact spacing (9 mm center-

to-center), the electrical fields generated by each cathodal contact are weakly superimposed and stimulation of the fibers positioned between the contacts is less likely. Fibers positioned at the level of the contact delivering the larger percentage of the cathodal current are primarily recruited and superposition of the two cathodal fields only occurs when both cathodes supply nearly equal currents. In contrast, when the contacts are closely spaced (4 mm center-to-center), superposition of the two cathodal fields occurs regardless of the current ratio and control of the resulting electrical field is better.

### **Clinical implications**

The combination of the ‘trolling’ technique with present programming techniques can only achieve 100/0% or 0/100% (when the rostral or caudal cathode, respectively, supplies all current) and roughly 50/50% cathodal current ratio (when both cathodes are fed by the same channel or assigned the same voltage and have the same impedance). We demonstrated that additional recruitment of DR fibers may be achieved with other current ratios. This may have significance in clinical practice if the segmental paresthesia has to be ‘fine-tuned’. If steering of the cathodal current is performed all the way from the rostral to the caudal end of the contact array, all DR filaments between these levels can be stimulated. **Figure 8** shows the scheme of three adjacent spinal cord segments and the shift in DR fiber recruitment as the cathodal current is steered along the contact array. The longitudinal span of both the PQ and the LN lead is ~30 mm. At a low-thoracic level the span of DR filaments of a single root is ~ 10mm (Dr H.K.P. Feirabend, personal communication) and corresponds with the length of the corresponding spinal segment. This means that segmental paresthesias could be induced and electronically shifted over a range of 3-4 adjacent spinal segments. Since the location of DR filaments is discrete (filaments enter the spinal cord at ~1 mm spacing) it may be beneficial to minimize their threshold by shifting the minimum of the DR threshold profile and overlapping it with the position of a particular DR filament. As shown, this can be done with the proposed method. Similarly, the DC and DR threshold ratio can be changed with the proposed method within a range that depends on the relative position of the stimulating contacts and the neural elements. Since there is presumably a small rostrocaudal range (near the T9-T10 intervertebral disc) within which the cathodal field captures the “sweet spot” in the low-back pain syndrome [12], this method may be a solution to fine tune the field. The clinical validity of this hypothesis remains to be tested.

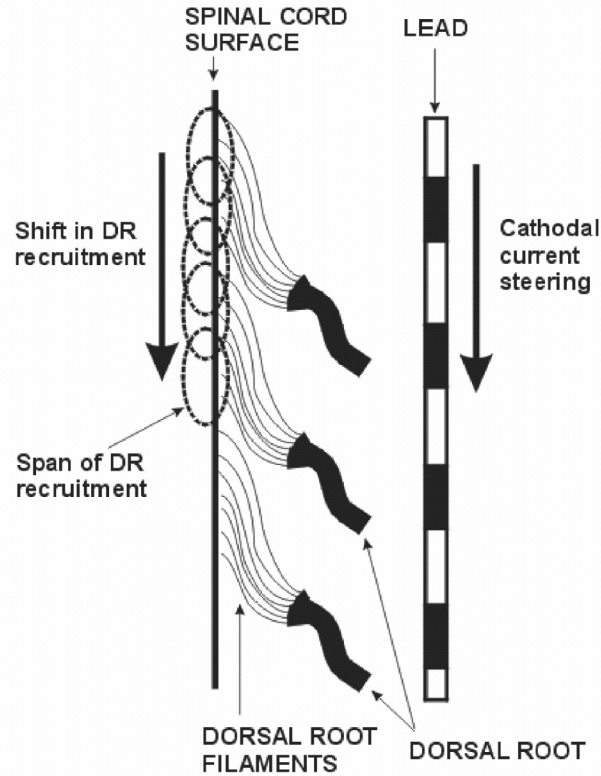


**Figure 8.** DR filament fans of 3 adjacent spinal segments. Their relative positions to the spinal cord are shown. A percutaneous lead is also drawn. The arrows indicate steering of the electrical field and DR recruitment. The DR filaments recruited for each steering step (one cathodal current ratio) are encircled.

North et al. demonstrated a value of ‘automated’ and thorough assessment of contact combination for the clinical outcome [19]. The number of effective contact (or more precisely current) combinations having a distinct influence on DC and DR recruitment is larger if the current of each contact is controlled independently. Therefore, the likelihood that a ‘current combination’ giving a better clinical outcome can be found is increased. A larger number of combinations to be tested demands more sophisticated and automated navigation algorithms and may take more time. However, Oakley et al. showed that in fact less overall time was consumed to test a larger number of combinations if reaching the discomfort threshold was avoided when changing the contact combination during testing [20]. The patients preferred a smooth longitudinal transitioning of the paresthesias while the stimulation amplitude was maintained at a suprathreshold yet subdiscomfort level [20].

Electrical field steering cannot be achieved when a single-source pulse generator is used. With multi-source, *voltage-controlled* devices, when two independent channels are coupled with the contacts intended to be steering cathodes, only the ratio of the cathodal voltages can be controlled. This may not be the same as controlling the current ratio, because the current of each contact would depend on the local load impedance that will depend on the exact position of the lead in the epidural space and the encapsulation tissue [1]. These factors would make ‘fine-tuning’ of the electrical field less well-controlled and the effects of the steering may be masked.

The proposed technique may provide a more flexible and precise way to control the population of stimulated fibers (DRs and DCs) and paresthesia coverage than the combination of “trolling” technique and present programming methods. It also would allow an easy repositioning of the electrical field, should the lead get dislocated along the rostrocaudal axis.

### **Limitations of the model**

The parameters of our SCS model, such as geometries and conductivities of different tissue compartments and nerve fiber parameters were based on their mean values obtained from literature, experiments, approximation techniques etc. Encapsulation tissue was not modeled since little is known about it and its properties change over time [4]. Therefore it is likely that the threshold values and fiber recruitment may be different in reality. However, all the stimulation configurations were tested with the same model and under the same conditions. In this way, the steering phenomena were abstracted and the influence of potentially masking factors (such as the effect of different dCSFs among patients or encapsulation tissue) was minimized. Beneficially, this made a comparison of the steering effects with different leads and contact combinations feasible.

Struijk et al. used several DR fiber models having a different orientation in the coronal and transverse plane [25]. We used the DR fiber model that had approximately 45° inclination in the coronal plane (similar to ‘A1’ type fiber as described by Struijk et al., [25]). Since we modeled the low-thoracic segment of the spine (T9-T12 vertebral level) this fiber model was the most appropriate. However, when the position of the DR fiber (filament) was varied in order to determine the DR fiber threshold profiles it was simply shifted rostrocaudally without changing its orientation. This may not be anatomically completely correct as the DR filaments fan out of the DR bundle and pierce into the spinal cord at different levels in the dorsal root entry zone, presumably having a somewhat different orientation (see **Figure 8**). Struijk et al. [25] have shown that the threshold of a DR fiber does depend on its orientation. In their models, the threshold of the ‘A1’ and ‘A2’ fiber model having respectively a 45° and 0° orientation to the coronal plane differed by ~25% [25]). However, the difference in orientation of the DR filaments within a single DR and adjacent DRs at the low-thoracic level should be less than the difference in orientation

between the ‘A1’ and ‘A2’ fiber model owing to the predominantly rostral direction of the filaments at this level. Therefore, we expect that the variation of the threshold due to the fiber orientation would be less than predicted in the model for ‘A1’ and ‘A2’ fiber type.

#### **4.5. Conclusions**

Conclusions from this modeling study are:

- 1) By means of electrical field steering with two adjacent cathodes (- -) having a variable current ratio it is possible to vary the longitudinal cathodal field and the population of DR/DC fibers stimulated and thereby the induced paresthesia.
- 2) With a large contact spacing (as for most leads used clinically), the cathodal field shifts abruptly from one cathode level to the adjacent one between certain cathodal ratios.
- 3) With a small contact spacing the electrical field can be steered smoothly and stimulation can be focused on just a few DR filaments.
- 4) With a small contact spacing threshold amplitude is fairly constant.
- 5) With a guarded dual cathode (+ - - +) configuration, the recruitment of DC fibers and thus paresthesia coverage is extended, while the field steering properties are preserved.
- 6) The performance of the field steering system is hardly affected by the thickness of the dorsal CSF layer.
- 7) Current-controlled stimulation provides a better control over paresthesia coverage than voltage-controlled stimulation.

---

#### **Acknowledgements**

We would like to thank Dr H.K.P. Feirabend (Neuroregulation Group, Department of Neurosurgery, Leiden University Medical Center (LUMC), Leiden, The Netherlands) for providing information on spinal cord anatomy.

## REFERENCES

- 1 Alo KM and Holsheimer J. New trends in neuromodulation for the management of neuropathic pain. **Neurosurgery**. 50:690-704, 2002
- 2 Barolat G. Spinal Cord Stimulation for Chronic Pain Management. **Archives of Medical Research**. 31:258-262, 2000
- 3 Goodall EV, de Breij F and Holsheimer J. Position-selective activation of peripheral nerve fibers with a cuff electrode. **IEEE Trans Biomed Eng**. 43:851-856, 1996
- 4 Grill WM and Mortimer JT. Electrical properties of implant encapsulation tissue. **Ann Biomed Eng**. 22:23-33, 1994
- 5 He J, Barolat G and Ketcik B. Stimulation usage range for chronic pain management. **Analgesia**. 1:75-80, 1995
- 6 Holsheimer J, Den Boer JA, Struijk JJ and R. RA. MR assessment of the normal position of the spinal cord in the spinal canal. **Am J Neuroradiol**. 15:1994
- 7 Holsheimer J. Computer modelling of spinal cord stimulation and its contribution to therapeutic efficacy (Review). **Spinal Cord**. 36:531-540, 1998
- 8 Holsheimer J and Barolat G. Spinal geometry and paresthesia coverage in spinal cord stimulation. **Neuromodulation**. 1:129-136, 1998
- 9 Holsheimer J, Nuttin B, King GW, Wesselink WA, Gybels JM, *et al*. Clinical evaluation of paresthesia steering with a new system for spinal cord stimulation. **Neurosurgery**. 42:541-549, 1998
- 10 Holsheimer J. Does dual lead stimulation favor stimulation of the axial lower back? (Editorial). **Neuromodulation**. 3:55-57, 2000
- 11 Holsheimer J. Which neuronal elements are activated directly by spinal cord stimulation. **Neuromodulation**. 5:25-31, 2002
- 12 Law J. Targeting a spinal stimulator to treat the 'Failed Back Surgery Syndrome'. **Appl Neurophysiol**. 50:437-438, 1987
- 13 Law JD. Spinal Stimulation: Statistical superiority of monophasic stimulation of narrowly separated, longitudinal bipoles having rostral cathodes. **Appl. Neurophysiol**. 46:129-137, 1983
- 14 Manola L and Holsheimer J. Technical performance of percutaneous and laminectomy leads analyzed by modeling. **Neuromodulation**. 7:231-241, 2004
- 15 Manola L, Holsheimer J, Bradley K and Peterson DK. Electrical steering on percutaneous SCS arrays: a modeling study. Cleveland, OH: 2004.
- 16 Manola L, Holsheimer J and Veltink PH. Technical performance of percutaneous leads for spinal cord stimulation: a modeling study. **Neuromodulation**. 8:88-99, 2005
- 17 Melzack R and Wall P. Pain mechanisms: a new theory. **Science**. 150:971-978, 1965
- 18 North RB, Ewend MG, Lawton MT and Piantadosi S. Spinal cord stimulation for chronic, intractable pain: superiority of "multi-channel" devices. **Pain**. 44:119-130, 1990
- 19 North RB, Calkins S-K, Campbell DS, Sieracki JM, Piantadosi S, *et al*. Automated, patient-interactive, spinal cord stimulator adjustment: a randomized controlled trial. **Neurosurgery**. 52:572-580, 2003

- 20 Oakley J, Varga C, Krames E and Bradley K. Real-time paresthesia steering using continuous electric field adjustment. Part I: intraoperative performance. **Neuromodulation**. 7:157-167, 2004
- 21 Oakley J, Espinosa F, Burchiel K, Bothe H, McKean J, *et al.* Transverse Tripolar Spinal Cord Stimulation: Results of an international multicenter study. **Neuromodulation**. 2005
- 22 Simpson BA. Spinal cord stimulation. **Pain Rev**. 1:199-230, 1994
- 23 Smith MC and Deacon P. Topographical anatomy of the posterior columns of the spinal cord in man. The long ascending fibres. **Brain**. 107:671-698, 1984
- 24 Struijk JJ, Holsheimer J, Barolat G, He J and Boom HBK. Paresthesia thresholds in spinal cord stimulation: a comparison of theoretical results with clinical data. **IEEE Trans Rehab Eng**. 1:101-108, 1993
- 25 Struijk JJ, Holsheimer J and Boom HBK. Excitation of dorsal root fibers in spinal cord stimulation: a theoretical study. **IEEE Trans Biomed Eng**. 40:632-639, 1993
- 26 Struijk JJ and Holsheimer J. Transverse tripolar spinal cord stimulation - Theoretical performance of a dual channel system. **Med. Biol. Eng. Comput**. 34:273-279, 1996
- 27 Sweeney JD, Ksienski DA and Mortimer JT. A nerve cuff technique for selective excitation of peripheral nerve trunk regions. **IEEE Trans Biomed Eng**. 37:706-715, 1990
- 28 Veraart C, Grill WM and Mortimer JT. Selective control of muscle activation with a multipolar cuff electrode. **IEEE Trans Biomed Eng**. 40:640-653, 1993
- 29 Wesselink WA, Holsheimer J and Boom HBK. A model of the electrical behaviour of myelinated sensory nerve fibers based on human data. **Med Biol Eng Comput**. 37:228-235, 1999
- 30 Wesselink WA, Holsheimer J, King GW, Torgerson NA and Boom HBK. Quantitative aspects of the clinical performance of transverse tripolar spinal cord stimulation. **Neuromodulation**. 2:5-14, 1999



# Chapter 5

## **Modelling Motor Cortex Stimulation for Chronic Pain Control: Electrical Potential Field, Activating Functions and Responses of Simple Nerve Fibre Models**

Ljubomir Manola<sup>1</sup> • Bas H. Roelofsen<sup>1</sup> • Jan Holsheimer<sup>1</sup> •  
Enrico Marani<sup>1,2</sup> • Jan Geelen<sup>1,3</sup>

<sup>1</sup>Institute for Biomedical Technology, University of Twente, The Netherlands;  
<sup>2</sup>Neuroregulation group, Dept. of Neurosurgery, Leiden University Medical Centre, The Netherlands; <sup>3</sup>Dept. of Neurology, Medical Spectrum Twente hospital, The Netherlands.

### **Abstract**

This computer modelling study on Motor Cortex Stimulation (MCS) introduced our motor cortex model, developed to calculate the imposed electrical potential field characteristics and the initial response of simple fibre models to stimulation of the precentral gyrus by an epidural electrode, as applied in the treatment of chronic, intractable pain. The model consisted of two parts: 1) a 3-dimensional volume conductor based on tissue conductivities and human anatomical data, in which the stimulation-induced potential field was computed, and 2) myelinated nerve fibre models allowing the calculation of their response to this field. A simple afferent fibre branch and three simple efferent fibres leaving the cortex at different positions in the precentral gyrus were implemented. It was shown that the thickness of the cerebrospinal fluid (CSF) layer between the dura mater and the cortex below the stimulating electrode substantially affected the distribution of the electrical potential field in the precentral gyrus, and thus the threshold stimulus for motor responses and the therapeutic stimulation amplitude. When the CSF thickness was increased from 0 to 2.5 mm, the load impedance decreased by 28% and stimulation amplitude increased by 6.6 V for each mm of CSF. Due to the large anode-cathode distance (10 mm centre-to-centre) in MCS the cathodal fields in mono- and bipolar stimulation were almost identical. By calculating activating functions and fibre responses it was shown that only nerve fibres with a directional component parallel to the electrode surface were excitable by a cathode, while fibers perpendicular to the electrode surface were excitable under an anode.

## 5.1 Introduction

### 5.1.1. General introduction

Motor Cortex Stimulation (MCS) has been applied in the last twelve years as a treatment for several types of chronic, intractable pain. Nearly 300 cases of MCS have been published. Although the clinical results are variable, the number of published cases in which MCS was applied successfully in the treatment of central post stroke pain (CPSP) and trigeminal neuralgia (TGN) allows the conclusion that these indications are validated for MCS treatment [1].

In MCS, an electrode is placed epidurally over the location on the precentral gyrus where the contralateral painful body area is represented. The surgical procedure has been described by e.g. Garcia-Larrea et al. [2] and Nguyen et al. [12]. Neurophysiological stimulus-response methods and advanced neuro-navigation techniques support the precise placement of the stimulating electrode, reported to be critical for successful MCS [11, 17].

As a first step to unravel the analgesic mechanism of MCS, PET scans have been made after implantation [2]. The most significant increase in regional cerebral blood flow, which corresponds to an increase in metabolism as a result of increased neuronal activity, has been observed in the ventro-anterior (VA) and the ventro-lateral (VL) nuclei of the thalamus.

The aim of this study is to predict the immediate bioelectrical effects of MCS by computer modelling. Apart from the analysis of the stimulation induced field, this study also aims to explore the resulting response of simple fibre models in the precentral gyrus. More sophisticated fibre models are still being developed.

### 5.1.2. Anatomical aspects

The brain surface is covered by membranes that enclose the cerebrospinal fluid. The inner membrane, or pia mater, covers the cortical surface completely into the various sulci and fissures. It is connected by thin filaments to the arachnoid, forming the middle membrane. The outer and thickest membrane, the dura mater, is covered by a thin layer of epidural fat and follows the bony structure of the skull.

At the pial surface the precentral gyrus is situated between the precentral sulcus and the central sulcus on its anterior and posterior side, respectively. The lateral fissure and, at the interhemispheric side, the sulcus cinguli form its inferior and superior anatomical borders, respectively [13].

The primary motor cortex constitutes of a thin layer of grey matter and its afferent and efferent fibres in the white matter beneath. The primary motor cortex (Brodmann's area 4), which is characterised by the presence of the giant cells of Betz, partly covers the precentral gyrus. Near the lateral fissure it is practically limited to the anterior wall of the central sulcus. Superiorly, the primary motor cortex increasingly widens and covers the whole convexity of

the precentral gyrus at its border with the interhemispheric fissure. The complementary part of the precentral gyrus is covered by the premotor cortex or Brodmann's area 6 (see Zilles [30]). Both the primary and the premotor cortex have a somatotopic organisation. The face is represented most inferiorly, while the lower extremities project to the superior area of the precentral gyrus, which extends into the wall of the interhemispheric fissure [24, 29].

The motor cortex has a laminated structure of six layers, as shown in **Figure 1a**. In this figure cell bodies, dendrites and axons are made visible by different staining methods. Main inputs of the motor cortex originate from the cerebellum and the pallidum via the ventro-anterior (VA) and ventro-lateral (VL) nuclei of the thalamus. The ramifications of these thalamocortical fibres constitute parts of the 'horizontal' sheets of myelinated fibres in primarily layer IV of the motor cortex [30]. Corticothalamic neurons in layers V and VI project to the VA-VL complex, thus closing the corticothalamic loop [10, 15].

No data was found in the literature on the distribution of nerve fibre diameters in the various layers of the motor cortex. In particular the largest fibres in each afferent and efferent pathway are of interest, because these fibres need the lowest stimulus for their excitation. The largest fibre diameter measured in a study on human brain white matter (not including the axons of Betz cells) is 4  $\mu\text{m}$  [23]. Some Betz cell efferents are among the largest fibres in the pyramidal tract and may have diameters up to 13  $\mu\text{m}$  [24, 27]. Since the mean size of Betz cells (in layer V) is larger in the superior part (limbs) than in the inferior part (face) of the precentral gyrus, it is likely that the mean calibre of their efferents is also larger in the superior part.

All pyramidal cells have a long apical dendritic tree perpendicular to the cortical layers and extending into layer I. Their efferents have the same orientation with respect to the cortical layers, thus creating a 'fountain' of nerve fibres emerging from the white matter into the grey matter of the precentral gyrus, as shown in **Figure 1b** (see also Villiger [26]).

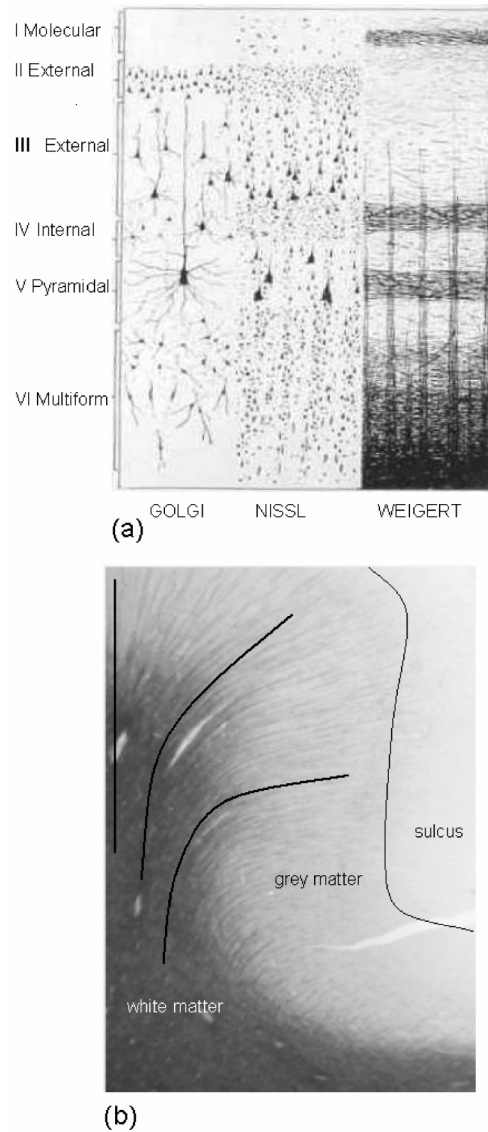


**Figure 1.** (a) Layered structure of the motor cortex (laminae I-VI); cortical afferents from various parts of the brain ascend and bifurcate into a specific layer parallel to the cortical surface; the giant cells of Betz are located in layer V; (b) efferents of the pyramidal neurons leave the cortex into the white matter below, creating a 'fountain' of fibres in the gyrus.

## 5.2. Methods

### 5.2.1. Volume conductor model

#### *Geometry*

A 3D inhomogeneous and partly anisotropic volume conductor model, representing the grey and white matter of the precentral gyrus, as well as the surrounding anatomical structures, has been constructed. **Figure 2** shows a transverse cross-section of this 3D model which represents part of the gyrus with the precentral and the central sulcus on the left and the right side, respectively.

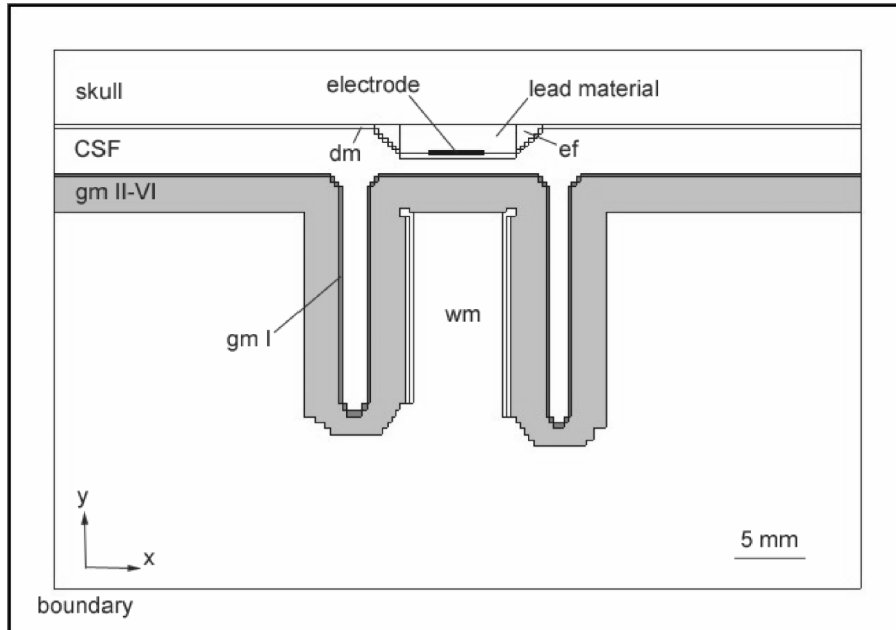


**Figure 2.** Transverse section (x-y plane) of the 3-dimensional volume conductor model through the centre of the epidural electrode; **dm**: dura mater, **CSF**: cerebrospinal fluid, **ef**: epidural fat, **gm I**: cortical layer I, **gm II-VI**: layers II-VI.

The 80 layers that compose the model from inferior to superior (z-direction) have the same geometry, except for the outer ones, which are used as boundary layers. Each layer consists of 6300 cubic elements, each defined by an (an)isotropic conductivity. The length of the rib of a cube was chosen smallest (0.3 mm) in the vicinity of the epidural electrode, where the voltage gradient is largest. The implanted stimulating device was modeled according to the dimensions of the paddle of a Resume II lead (Medtronic Inc., Minneapolis,

MN), generally used in MCS: a 2 mm thick, 8 mm wide and 44 mm long insulator. This paddle model was placed between the skull and the dura mater from inferior to superior above the precentral gyrus. Each metal electrode was a disc with a diameter of 4 mm on the lower side of the paddle and directly above the dura mater. To model monopolar or bipolar stimulation, one electrode or two electrodes at a center-to-center distance of 10 mm on the paddle were defined.

The dimensions of the model in x-, y- and z-direction are 60.8 x 42.6 x 57.4 mm respectively. **Table 1** presents an overview of the geometries of the modelled anatomical compartments. The arachnoid and the pia mater were not incorporated in the model as separate compartments.

**Table 1.** Human anatomical data implemented in the MCS model.

Parameter	mean [mm]	s.d. [mm]	n	reference
skull thickness (over motor cortex)	5		93	van Veenendaal, 1982 (unpublished)
dura mater thickness	0.36		>10 0	[7, 8]
CSF layer thickness (over precentral cortex)	3.1	0.8	6	Roelofsen, 2003 (unpublished) (T2 weighted MRI density profiles)
motor cortex layer I thickness layers II-IV layers V- VI	0.2 1.4 2.1			(Brodmann area 4) [30]
precentral gyrus width				Roelofsen, 2003 (unpublished)
central sulcus width	11.7	4.9		(all parameters measured at 5 positions along the precentral gyrus of 6 fixated hemispheres; corrected for 15% shrinkage)
precentral sulcus width	2.7 2.3	0.73 1.1		
central sulcus depth	16.4	4.0		
precentral sulcus depth	15.6	4.0		

### **Conductivities**

The electrical conductivities of the anatomical model compartments are presented in **Table 2**. The conductivities of most compartments were taken from the Spinal Cord Stimulation model developed in our group. The conductivity of the grey matter, however, was inhomogeneous with layer I

having a ~60% lower value than layers II-VI. This value was estimated from empirical data by Haberly and Shepherd [4] and Hoeltzell and Dykes [6]. In both studies, a large gradient in conductivity was reported from layer I to layer II. The conductivity of the white matter was anisotropic, having the higher value in the direction of the myelinated fibres.

**Table 2.** Conductivities in the MCS model.

Compartment	Conductivity [S/m]
Skull	0.02
Epidural fat ( <b>ef</b> )	0.04
Lead material	0.0001
Dura mater ( <b>dm</b> )	0.065
Cerebrospinal fluid ( <b>CSF</b> )	1.7
Grey matter	
layer I ( <b>gm I</b> )	0.14
layer II –VI ( <b>gm II-VI</b> )	0.36
White matter	
parallel to fibers	0.6
perpendicular to fibers	0.083
Boundary layer	0.0009

The conductivity of the boundary layer, representing distant tissues, was chosen such that the model impedance matches the mean empirical value when stimulating monopolarly (~750 Ohm). The conductivity of the dura mater was given a value at which the model impedance matches the mean empirical value in bipolar stimulation (~1000 Ohm).

#### ***Computation of the 3D potential field***

A finite difference method was implemented in the simulation software to solve the potentials at the grid-points of the model resulting from the voltage(s) allocated to the electrode(s). These grid-points are the vertices of the cubic elements assembling the volume conductor model. For each volume element, conservation of charge applies as expressed by

$$\nabla \cdot \mathbf{J}^{\text{total}} = 0 \quad (1)$$

The total current density  $\mathbf{J}^{\text{total}}$  includes a conduction current density and an impressed current density. The latter arises from bioelectric sources within the tissue. In the MCS model, the assumption is made that bioelectrical sources have a negligible influence on the stimulation induced electrical field.

Therefore, only the conduction current density is left which can be written as the product of the conductivity vector  $\boldsymbol{\sigma}$  and the electrical field vector  $\mathbf{E}$

$$\mathbf{J}^{\text{total}} = \boldsymbol{\sigma}\mathbf{E} \quad (2)$$

With  $E$  expressed as the negative gradient of the potential field

$$\mathbf{J}^{\text{total}} = -\boldsymbol{\sigma}\nabla\Phi \quad (3)$$

Substitution of (3) into (1) yields the Laplace equation of the potential field

$$\nabla \cdot \boldsymbol{\sigma}\nabla\Phi = 0 \quad (4)$$

The boundary conditions applied are of the Dirichlet type:

at the electrode surface:  $\Phi = \text{constant}$

at the model surface:  $\Phi = 0$

Taylor's theorem was utilised to provide the finite difference representation of (4) in which the potentials at the individual grid-points appear. Thus, a second order approximation of the equation for the potential at grid-point  $(x,y,z)$  with a homogeneous medium and a uniform grid becomes

$$\begin{aligned} \sigma_x \frac{\Phi_{x-1,y,z} - 2\Phi_{x,y,z} + \Phi_{x+1,y,z}}{(\Delta x)^2} + \sigma_y \frac{\Phi_{x,y-1,z} - 2\Phi_{x,y,z} + \Phi_{x,y+1,z}}{(\Delta y)^2} \\ + \sigma_z \frac{\Phi_{x,y,z-1} - 2\Phi_{x,y,z} + \Phi_{x,y,z+1}}{(\Delta z)^2} = 0 \end{aligned} \quad (5)$$

Each of the three terms of (5) belongs to an orthogonal direction. The square of the local resolution is the denominator of each term. Each nominator contains the appropriate conductivity vector component and the potentials at three successive grid-points along an axis. The equations for all grid-points in the model constitute the linear system

$$\mathbf{A}\boldsymbol{\Phi} = \mathbf{b} \quad (6)$$

in which matrix  $\mathbf{A}$  contains the grid spacing and vertex conductivity information,  $\boldsymbol{\Phi}$  the potentials at the non-boundary grid-points and  $\mathbf{b}$  the information about the Dirichlet conditions.

The matrix equation (6) was solved for the potentials at the grid-points according to the Red-Black Gauss-Seidel algorithm with variable over-relaxation. In order to obtain a reliable solution, the procedure was implemented in such a way that two independent iterations with different initial guesses of  $\boldsymbol{\Phi}$  converge to the final solution. The stopping criterion was defined as

$$\frac{\sum_{i=1}^n |\Phi_i' - \Phi_i''|}{n} < 0.0001V \quad (7)$$



with  $\Phi_i'$  and  $\Phi_i''$  as the potentials on grid-point  $i$  calculated by each iteration procedure and  $n$  as the number of grid-points of the model.

### 5.2.2. Nerve Fibre model

A McNeal-type cable model [9] with sealed ends (infinite termination impedance) was incorporated in the simulation software to predict the response of myelinated nerve fibres to the external potential field. All nodes of Ranvier of the fibre were made excitable, having modified Frankenhaeuser-Huxley membrane kinetics adjusted to experimental data of human sensory fibres at 37°C. The internodal portion of the fibre was assumed to be an ideal insulator. For a detailed description of the fibre model see Wesselink et al. [28].

Four fibre types were modelled as shown in **Figure 3**. All fibre models were placed in the transverse cross-section (x-y plane) through the centre of the electrode (**Figure 2**). The course of fibre model A1 is parallel to the cortical surface at a depth of 1.4 mm and represents a thalamocortical (afferent) fibre branch in layer IV. Fibre models E1 – E3 represent cortical efferents arising in layer V with orientations based on their course in the cortex and the white matter below, as depicted in **Figure 1b**.

According to the inverse recruitment principle, the threshold stimulus of a fibre group is related to the excitation of the largest fibres in this group. To obtain the threshold stimuli of the efferent fibre groups represented by fibre models E1–E3, these fibre models should be considered as efferents of the giant cells of Betz in layer V, that project into the corticofugal motor system. Based on neuroanatomical studies (see section 5.1.2) it is assumed that these axons have a diameter exceeding the size of the efferents projecting from laminae V and VI to the VA-VL complex of the thalamus.

Each efferent fibre model E1-E3 originates in layer V and leaves the cortex at a different location, thus resulting in different orientations of the initial parts of these fibre models. Fibre model E1 originates in the convexity of the precentral gyrus and its course is perpendicular to the electrode surface. Fibre model E2 originates at a location where the cortex bends from a horizontal to a vertical orientation, forming the anterior wall of the central sulcus. The initial part of this fibre model is at an angle of 45 degrees to the electrode surface. Fibre model E3 leaves the cortex deeper in the anterior wall of the central sulcus and the orientation of its initial part is parallel to the electrode surface. Note that fibre type E1 is only present in the superior region of the precentral gyrus, where Brodmann area 4 extends over the convexity of the gyrus (see section 5.1.2).

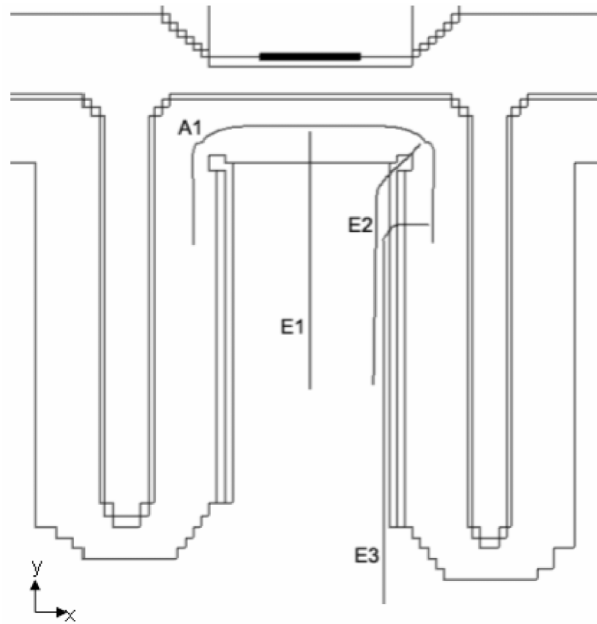


**Figure 3.** Cortical fibre models; A1: ‘horizontal’ branch of a cortical afferent at a depth of 1.4 mm in the cortex; E1–E3: cortical efferents of Betz cells in layer V, leaving the cortex at different locations in the gyrus.

### 5.3. Results

#### 5.3.1. Influence of the grid on the calculated electrical potential field

The total grid size (number of gridpoints) and the grid spacing in each orthogonal direction of the model were chosen such that all anatomical structures could be represented with a satisfactory resolution while limiting the computational load, which is a power function of the total number of grid points. To test how sensitive the calculated electrical potential field is to the chosen grid, the grid was refined twice in all three directions. When calculating with the finer grid the iterative Gauss-Seidel procedure was stopped when the average final residuals of the discrete equation were 4 times less than those obtained with the coarser grid which took ~16 times longer to accomplish.

The two field solutions resulted in a small mean difference (<2.5%) and a maximum of about 10% only around the edge of the electrode. However, this was not considered to be relevant as the neural structures to be stimulated are far more distant from the electrode. Indeed, model output parameters such as

fibre model thresholds and the lumped tissue impedance differed by less than 3% (and all had a deflection of the same sign).

Based on these sensitivity tests we concluded that the original model with  $91 \times 71 \times 81$  grid points provides a sufficiently accurate solution obtained within a reasonable computation time ( $\sim 4000$  iterations and 60-90 min. depending on PC). All results presented were calculated with this model.

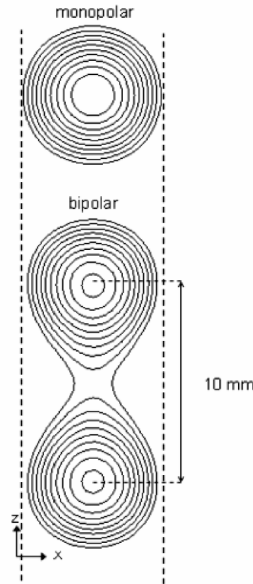


**Figure 4.** Iso-current density lines in the x-z plane of the model parallel to the electrode surface(s) at a depth of 1.4 mm in the cortex; 10 equidistant lines ( $4.5\text{--}7.5 \mu\text{A}/\text{mm}^2$ ); mono- and bipolar stimulation (1 mA).

### 5.3.2. Cathodal field at monopolar and bipolar stimulation

Since MCS is applied both monopolarly and bipolarly we compared the corresponding fields in the precentral gyrus. To eliminate the effect of different load impedances in mono- and bipolar stimulation, a 1 mA current was applied in both cases and each stimulation-induced field was represented by an identical set of 10 iso-current density lines in a plane parallel to the surface of the electrode(s) and a depth of 1.4 mm in the cortex.

As shown in **Figure 4**, the current density field is circular when stimulating monopolarly. At bipolar stimulation the symmetry in the x-direction is maintained, but the current density field is slightly more confined towards the axis of the bipole. In the z-direction, the outmost iso-lines of the bipolar field (representing the lowest current densities) extend more towards the other pole,

while the iso-lines representing higher current densities are still circular, virtually creating a monopolar current density field.

### **5.3.3. Sensitivity of the current density field to the width of the sulci**

The widths of the precentral and the central sulcus have a standard deviation of 41 % and 30 % of the corresponding mean values (see **Table 1**). In order to investigate the influence of this variability on the current density field in the cortex below an electrode, models were made in which the average width of each sulcus was increased by the standard deviation. The current density field was quantified by calculating the average of the normal current-density component in two y-z planes in the cortex situated on the edges of the electrode (see **Figure 2**). Stimulation was applied monopolarly (-1 V).

On the side of the precentral sulcus the average normal current density component in the cortical y-z plane was 1.3 % higher as a result of a 41 % wider precentral sulcus. Similarly, a 30 % wider central sulcus resulted in a 1.0 % increase of the average normal current density component in the cortical y-z plane on the side of the central sulcus.

### **5.3.4. Influence of the CSF layer below the electrode on the current density field**

In **Figure 5a** and **5b** iso-current density lines are depicted in a transverse (x-y) and a longitudinal (y-z) plane through the centre of the electrode in monopolar (cathodal) stimulation. Due to the inhomogeneous medium the iso-lines are not circular around the electrode (as would be expected in a homogeneous medium). The highest current densities are in the well-conducting CSF layer covering the cortex, as shown by the iso-current density lines in this layer and their orientation perpendicular to this layer. (The direction of the current is normal to the direction of the iso-current density lines.) Note that little current flows into the sulci. Efficacy calculations at both monopolar and bipolar stimulation in models with a 3.1 mm CSF layer thickness yielded that about 60% of the total cathodal current does not enter the cortex, but flows parallel to the electrode surface in the CSF-layer. Below the electrode the current also spreads approximately radially into the cortex, as shown in **Figure 5a-b**. The current densities in the cortex are, however, substantially lower than in the overlying CSF layer, as shown by the low values of the iso-current density lines (5–14  $\mu\text{A}/\text{mm}^2$ ).

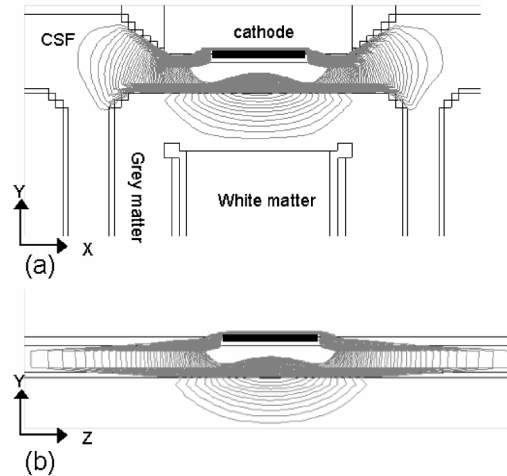


**Figure 5.** Iso-current density lines in the x-y plane (a) and the y-z plane (b) through the centre of the cathode; 55 equidistant lines ( $5\text{-}60 \mu\text{A}/\text{mm}^2$ ); monopolar cathodal stimulation (1 V).

Due to its thickness (2 mm), the implantation of a lead for MCS will most probably reduce the thickness of the (highly conductive) CSF layer under the paddle. Because it is unknown how much the thickness of this layer will be reduced, we modelled several thicknesses to predict the effects on the current density distribution and the load impedance in monopolar stimulation. If no CSF is present between the dura mater and the cortex under the lead paddle (**Figure 6**, upper left plot), current penetrates deep into the cortex and the underlying white matter and enters the CSF on both sides of the paddle via the dura mater and the cortex. In this condition the load impedance is high (975 Ohm). If a small CSF layer of 0.5 mm is present between the dura mater under the lead paddle and the cortex (**Figure 6**, upper right plot), the iso-current density lines penetrate less deep into the white matter, indicating a reduced current density in the cortex and the underlying white matter. Moreover, the current density in the CSF on both sides of the paddle becomes higher and the load impedance is reduced by  $\sim 20\%$  as compared to the model without CSF below the paddle. A further increase of the CSF layer thickness up to 2.5 mm results in a continued reduction of the current density in the cortex and white matter below the cathode and a further reduction of the load impedance, as shown in **Figure 6**.

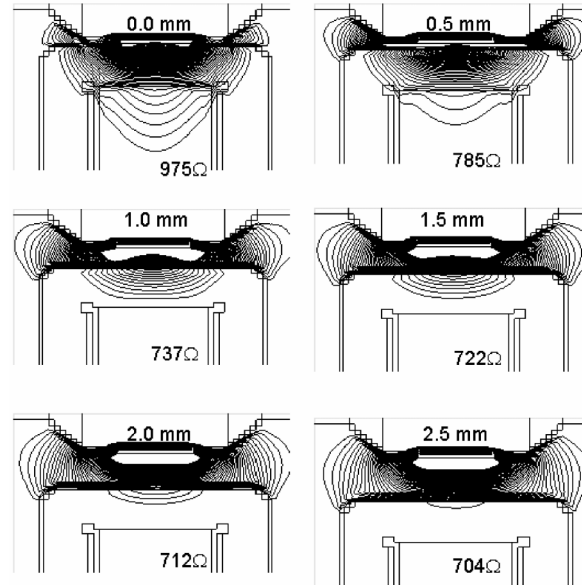


**Figure 6.** Iso-current density lines in the x-y plane through the centre of the cathode in six models having different thicknesses of the CSF-layer between electrode and cortex; 55 equidistant lines ( $5\text{-}60 \mu\text{A}/\text{mm}^2$ ); monopolar cathodal stimulation (1 V); thickness of the CSF layer and load impedance are indicated in each plot.

### 5.3.5. Activating functions

A first-order approximation of the effect of the stimulation-induced potential field on the membrane voltage of a nerve fibre is given by the activating function (AF), defined as the second order difference of the nodal field potentials of a myelinated fibre [19]. A positive AF indicates membrane depolarisation and possibly excitation, whereas a negative value indicates hyperpolarisation. The change in membrane potential increases with increasing value of AF.

AF's were calculated parallel to and perpendicular to the electrode surface, as shown in **Figure 7**. The AF's were calculated along lines in the plotted model sections which coincide with the horizontal axes of the graphs. **Figure 7a** shows the AF along a line in the x-y plane parallel to the cathodal surface at a depth of 1.4 mm in the cortex, while stimulating monopolarly. The region in which the AF has a positive value is confined to a circular area under the cathode of about 6 mm (2 mm wider than the diameter of the cathode) and its

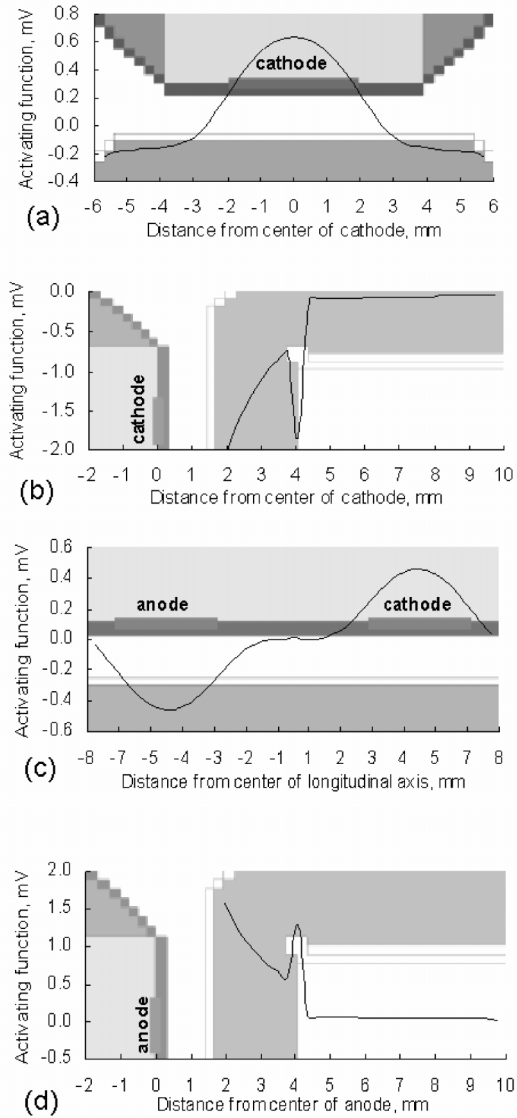


**Figure 7.** Activating functions along a line in the plotted model sections coinciding with the horizontal axis of each graph; (a-b) monopolar cathodal stimulation (1 V); (c-d) bipolar stimulation (1 V).

maximum is located under the centre of the cathode. More distant from the cathode the AF gets slightly negative. **Figure 7b** presents the AF along a line normal to the cathodal surface and crossing the centre of the cathode, while stimulating monopolarly. Its value is most negative in layer I of the cortex and gets almost zero in the underlying white matter. The sharp negative peak arises from the sudden change in electrical conductivity at the border of the cortex and the white matter.

At bipolar stimulation, the two cathodal AF's are identical to those at monopolar stimulation (shown in **Figure 7a,b**), except for their slightly lower absolute values. **Figure 7c** shows the AF along a line at a depth of 1.4 mm in the cortex and parallel to the line connecting the centres of the two electrodes. Its maximum and minimum are located under the centre of the cathode and the anode, respectively. In a region of ~3 mm centered between the electrodes the AF value is almost zero. This means that the anodal and cathodal fields hardly overlap and that the anode and cathode can be considered as virtual monopoles (see also Section 3.2). The two anodal AF's are mirror images of the cathodal ones: positive and negative along a line normal and parallel to the anodal surface, respectively (see **Figure 7c** and **7d**).

The AF curves in **Figure 7c** and **7d** were calculated in a bipolar stimulation model which was calibrated at a ~200 Ohm higher load impedance than the monopolar model (see *Conductivities* section in 5.2.1). Because the same voltage was applied between cathode and anode in both models (the model boundary being the anode in monopolar stimulation), the current density near the cathode was higher in the monopolar case. Consequently, monopolar voltage-controlled stimulation results in somewhat higher potential gradients and higher absolute AF values than bipolar stimulation.

### 5.3.6. Threshold stimuli for fibre excitation

The threshold stimuli of the fibre types shown in **Figure 3** were calculated for monopolar (cathodal), voltage-controlled stimulation with monophasic pulses of 0.21 msec duration. Under these stimulation conditions efferent fibres of type E1 were hyperpolarized, which is in accordance with the negative AF values calculated in the previous section (only fibres with a direction component parallel to the electrode surface are excitable by a cathode).

**Figure 8** shows the normalized threshold stimuli of the fibre types E2, E3 and A1 as a function of their diameter (5–15  $\mu\text{m}$ ). As shown by the shape of the curves, the threshold amplitudes of the three fibre types have a similar dependence on their diameter. Efferent fibre type E2 (with an initial angle of 45 degrees to the electrode surface) has the highest threshold. Although further away from the electrode, efferent fibre type E3 has a lower threshold, which should be attributed to its initial orientation parallel to the cathodal surface. Fibre type A1 has the lowest threshold, probably because it is nearest to the cathode and oriented parallel to the electrode surface. Note that the thresholds



were calculated for simple fibre models (see Discussion) and that they will likely be different when more realistic fibre models are applied.

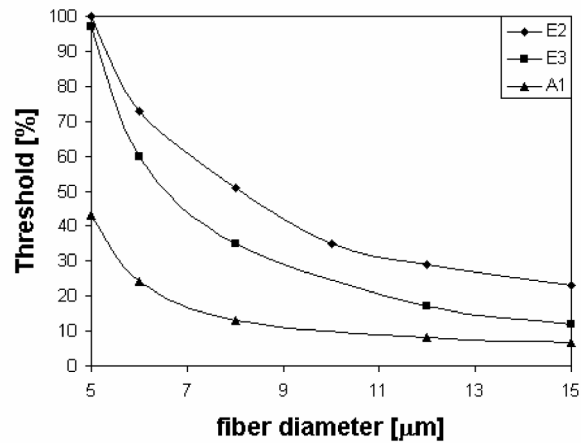


**Figure 8.** Normalized threshold voltages of the cathodally excitable fibre types (A1, E2, E3) as a function of their diameter (5-15  $\mu\text{m}$ ) in monopolar stimulation.

The excitation threshold of a 5  $\mu\text{m}$  type A1 fibre was calculated in models with each of the six CSF layer thicknesses depicted in **Figure 6**. A linear fit of the data points ( $R^2=0.97$ ) yielded a sensitivity of  $6.6 V_{\text{threshold}}/\text{mm CSF}$ . The excitation threshold of the type A1 fibre varies also linearly with its depth in the cortex ( $R^2=1$ ), yielding a sensitivity of  $3.3 V_{\text{threshold}}/\text{mm depth}$ .

In bipolar voltage-controlled stimulation at a pulsewidth of 0.21 ms the threshold curves have the same shape as in monopolar stimulation. Due to a 33% higher load impedance of the bipolar model the threshold voltages are proportionately higher. When fibre type E1 was placed below the centre of the anode it could be excited in contrast to the situation when it was placed under the cathode. Moreover, its threshold stimulus was lower than for fibre type E2 and E3 with the same diameter placed under the cathode.

## 5.4. Discussion

### 5.4.1. Volume conductor model

Since the compartments filled with CSF have a much higher electrical conductivity than the other anatomical compartments of the model (see **Table 2**), their geometry may be a critical factor. In contrast to the width of the sulci, which hardly affects the current density field in the cortex below an electrode,

this field is affected substantially by varying the thickness of the CSF layer between the cortex and the dura mater under the electrode. In our standard model the thickness of the Resume lead paddle (2 mm) was subtracted from the (mean) CSF layer thickness (3.1 mm). Since no imaging data are yet available on the thickness of the CSF layer and the shape of the cortex below the implanted lead paddle, improvements in modelling MCS should be focused primarily on these anatomical aspects.

#### **5.4.2. Nerve fibre models**

##### ***Efferent fibres***

All fibre types modelled in this study have been represented by a simple, straight or curved, myelinated nerve fibre model. In reality, a nerve fibre originates from a neuronal cell body having dendritic extensions as well. A complete neuron model would be most appropriate to simulate the electrical behaviour of pyramidal cells in the precentral cortex. Nevertheless, even with our simple efferent fibre models E1, E2 and E3, an initial comparative guess of threshold stimuli can be obtained. Because in neocortical cells the time constant of soma-dendritic membrane ( $15 \pm 7$  msec) is generally more than 160-fold the time constant of nodal membrane [14], a short stimulation pulse (0.1-0.2 msec) just exciting a myelinated fibre will hardly affect the soma-dendritic membrane potential of the same neuron. Empirical studies have confirmed that axons are the targets of external stimulation of brain tissue [14, 18]. Computer modelling of a complete neuron has shown that action potentials were neither initiated at the soma nor in dendritic tree branches, but always at (the initial segment of) the axon, irrespective of the stimulus polarity and the orientation of the neuron in the extracellular field [20]. To yield a proper estimate of the threshold stimulus when using a simple efferent fibre model, the termination impedance at its proximal end should equal the input impedance of the missing soma-dendritic part of the neuron.

##### ***Afferent fibres***

The type A1 afferent has been modelled as a simple 'horizontal' fibre at a depth of 1.4 mm in the cortex. In reality, on leaving the white matter afferents ascend normal to the laminated structure of the cortex up to a layer where they bifurcate. The fibre branches extend within this layer and make en-passage synaptic contacts with local cortical neurons. In a modelling study on the recruitment of dorsal column fibres in the spinal cord it has been shown that the presence of collaterals normal to the dorsal column fibre (radial to the cathode) reduce the threshold stimulus by up to 50% compared to an unbranched fibre [22]. Since a similar geometrical situation would exist when a cortical afferent would be modelled as a branched fibre, its threshold stimulus would be reduced substantially as compared to the value of the simple A1 fibre model we used.

##### ***Fibre diameters***

Another crucial aspect in the comparison of threshold stimuli of different fibre types in the motor cortex is the maximum of their diameter distributions, which

determines the threshold stimulus of each fibre type. However, data about fibre calibres of afferents and efferents in the various layers of the human primary motor cortex are still missing.

The goal of this initial modelling study was to develop a MCS model and test the influence of certain model parameters on the imposed electrical potential field. The further development of this model will primarily be focused on more sophisticated fibre models with realistic diameters in order to allow an improved prediction of their recruitment.

#### **5.4.3. Empirical and modeled stimulation amplitude data**

MCS is generally applied bipolarly with the cathode over the cortical region corresponding to the painful body area [11, 25] at an amplitude ranging from 2 to 8 V [21]. Taking into account the high sensitivity of the stimulation threshold of cortical fibres to the thickness of the overlying CSF layer (6.6 V/mm CSF for fibre type A1), such a wide range is likely to occur. Even more when the effects of other variables, such as the pulsewidth (0.06-0.5 msec [21]) and the percentage of the motor threshold voltage chosen as the chronic stimulation level (20-50%) are considered as well. These variables prevent a meaningful comparison of empirical and calculated stimulation voltages.

The low threshold for excitation of the efferent type E1 fibre under the anode as predicted by modelling is consistent with empirical studies reporting that *anodal* stimulation on the convexity of the precentral gyrus directly activates cortical efferents at a lower stimulus amplitude than *cathodal* stimulation does [3, 5, 16].

The diameter of Betz cells varies from ~60 to ~120  $\mu\text{m}$  with the smallest cells located in the inferior part of the precentral gyrus, and the largest ones in the superior part [24]. Under the assumption that the axon diameter is correlated with the size of the cell body, the motor threshold would be higher when stimulating the facial area than e.g. a limb area. However, no empirical data are yet available to test this hypothesis.

#### **5.4.4. Which cortical fibres may mediate the analgesic effect of MCS?**

Since it has been shown by brain imaging that the thalamic VA-VL complex is activated by MCS [2], cortical nerve fibres most likely mediating the analgesic effect are either cortico-thalamic fibers or thalamo-cortical fibers, the latter by antidromic propagation of the stimulation-induced action potentials towards the collateral fibre terminals in these thalamic nuclei.

In clinical practice MCS is applied cathodally at 20–50% of the motor threshold. This motor threshold is most likely related to the stimulation of large type E2 or type E3 corticospinal fibres arising from Betz cells in layer V. Because these fibres have a larger diameter than corticothalamic fibres arising in layers V and VI, it is unlikely that the latter are *directly* activated and induce the analgesic effect at a stimulation amplitude 50-80% below the threshold of

motor responses. Future modelling work should provide an answer to this question.

### **5.5. Conclusions**

- 1) The thickness of the CSF-layer between the dura mater and the cortex below the cathode affects the threshold amplitude for motor responses and the therapeutic stimulation amplitude in MCS substantially.
- 2) Due to the large centre-to-centre distance of the electrodes currently applied in MCS, the anodal and cathodal fields hardly interfere in bipolar stimulation. Accordingly, there will be virtually no difference between the responses to monopolar (cathodal) and bipolar stimulation, except for a higher voltage (and energy) needed in bipolar stimulation.
- 3) Bipolar stimulation with the anode placed over the superior region of the precentral gyrus should be avoided, since cortical efferents in the convexity of the gyrus have a low threshold when stimulated by an anode. The anode should thus not be considered an indifferent (inactive) electrode contact. Both cathode and anode position can be relevant for the clinical effects of MCS.

---

### **Acknowledgments:**

The authors gratefully thank Dr. Kees Venner (Mechanical Engineering Dept., University of Twente, The Netherlands) for his valuable advices on numerical algorithms.

## REFERENCES

- 1 Brown J and Barbaro N. Motor cortex stimulation for central and neuropathic pain: current status. **Pain**. 104:431-435, 2003
- 2 Garcia-Larrea L, Peyron R, Mertens P, Gregoire MC, Lavenne F, *et al.* Electrical stimulation of motor cortex for pain control: a combined PET-scan and electrophysiological study. **Pain**. 83:259-273, 1999
- 3 Gorman ALF. Differential patterns of activation of the pyramidal system elicited by surface anodal and cathodal cortical stimulation. **J Neurophysiol**. 29:547-564, 1966
- 4 Haberly L and Shepherd G. Current-density analysis of summed evoked potentials in Opposum prepyriform cortex. **J Neurophysiol**. 36:789-803, 1973
- 5 Hern JEC, Landgren S, Phillips CG and Porter R. Selective excitation of corticofugal neurones by surface-anodal stimulation of the baboon's motor cortex. **J Physiol**. 161:73-90, 1962
- 6 Hoeltzell P and Dykes R. Conductivity in the somatosensory cortex of the cat: evidence for cortical anisotropy. **Brain Res**. 177:61-82, 1979
- 7 Jiang D. Study of some morphologic aspects of the human dura mater. **Chin J Surg**. 28:108-109, 1990
- 8 McComb J, Withers G and Davis R. Cortical damage from Zenker's solution applied to the dura mater. **Neurosurg**. 8:68-71, 1981
- 9 McNeal D. Analysis of a model for excitation of myelinated nerve. **IEEE Trans Biomed Eng**. 23:329-337, 1976
- 10 Na J, Kakei S and Shinoda Y. Cerebellar input to corticothalamic neurons in layers V and VI in the motor cortex. **Neurosci Res**. 28:77-91, 1997
- 11 Nguyen J-P, Lefaucheur J-P, Decq P, Uchiyama T, Carpentier A, *et al.* Chronic motor cortex stimulation in the treatment of central and neuropathic pain. Correlations between clinical, electrophysiological and anatomical data. **Pain**. 82:245-251, 1999
- 12 Nguyen J-P, Lefaucheur J-P, LeGuerinel C, Eizenbaum J, Nakano N, *et al.* Motor cortex stimulation in the treatment of central and neuropathic pain. **Arch Med Res**. 31:263-265, 2000
- 13 Nieuwenhuys R, Voogd J and van Huijzen C. The human central nervous system. A synopsis and atlas., 3rd ed. Berlin: Springer Verlag, 1988.
- 14 Nowak LG and Bullier J. Axons but not cell bodies are activated by electrical stimulation in cortical gray matter. I. Evidence from chronaxie measurements. **Exp Brain Res**. 118:477-488, 1998
- 15 Ohye C. Thalamus. In: Paxinos G. The human nervous system. San Diego: Academic Press., 1990: 439-468.
- 16 Phillips CG and Porter R. Unifocal and bifocal stimulation of the motor cortex. **J Physiol**. 162:532-538, 1962
- 17 Pirotte B, Voordecker P, Joffroy F, Massager N, Wikler D, *et al.* The Zeiss-MKM system for frameless image-guided approach in epidural motor cortex stimulation for central neuropathic pain. **Neurosurg Focus**. 11:1-6, 2001
- 18 Porter R. Focal stimulation of hypoglossal neurons in the cat. **J Physiol**. 169:630-640, 1963

- 19 Rattay F. Analysis of models for external stimulation of axons. **IEEE Trans Biomed Eng.** 33:974-977, 1986
- 20 Rattay F. The basic mechanism for the electrical stimulation of the nervous system. **Neurosci.** 2:335-346, 1999
- 21 Smith H, Joint C, Schlugman D, Nandi D, Stein J, *et al.* Motor cortex stimulation for neuropathic pain. **Neurosurg Focus.** 11:2001
- 22 Struijk J, Holsheimer J, van der Heide G and Boom H. Recruitment of dorsal column fibers in spinal cord stimulation: Influence of collateral branching. **IEEE Trans Biomed Eng.** 39:903-912, 1992
- 23 Tang Y and Nyengaard J. A stereological method for estimating the total length and size of myelinated fibers in human brain white matter. **J Neurosci Methods.** 73:193-200, 1997
- 24 Truex R and Carpenter M. Human anatomy, Baltimore: Williams&Wilkins Company, 1964.
- 25 Tsubokawa T, Katayama Y, Yamamoto T, Hirayama T and Koyama S. Chronic motor cortex stimulation in patients with thalamic pain. **J Neurosurg.** 78:393-401, 1993
- 26 Villiger L. Gehirn and Ruckenmark, Leipzig: Wilhelm Engelmann Verlag, 1940.
- 27 von Keyserlingk DG and Schramm U. Diameter of axons and thickness of myelin sheaths of the pyramidal tract fibres in the adult human medullary pyramid. **Anat Anz, Jena.** 157:97-111, 1984
- 28 Wesselink WA, Holsheimer J and Boom HBK. A model of the electrical behaviour of myelinated sensory nerve fibres based on human data. **Med Biol Eng Comput.** 37:228-235, 1999
- 29 Zeffiro T. Motor cortex. In: Paxinos G. The human nervous system. San Diego: Academic Press, 1990: 803-810.
- 30 Zilles K. Cortex. In: Paxinos G. The human nervous system. San Diego: Academic Press, 1990: 757-802.

# Chapter 6

## **Anodal vs Cathodal stimulation of Motor Cortex: a modeling study**

Ljubomir Manola • Jan Holsheimer • Peter Veltink • Jan R. Buitenweg

Biomedical Signals & Systems Group, University of Twente,  
The Netherlands

### **Abstract**

**Objective.** To explore the effects of electrical stimulation performed by an anode, a cathode or a bipole positioned over the motor cortex for chronic pain management.

**Methods.** A realistic 3D volume conductor model of the human precentral gyrus (motor cortex) was used to calculate the stimulus-induced electrical field. The subsequent response of neural elements in the precentral gyrus and in the anterior wall and lip of the central sulcus was simulated using compartmental neuron models including the axon, soma and dendritic trunk.

**Results.** While neural elements perpendicular to the electrode surface are preferentially excited by anodal stimulation, cathodal stimulation excites those with a direction component parallel to its surface. When stimulating bipolarly, the excitation of neural elements in parallel to the bipole axis is additionally facilitated. The contact over the precentral gyrus determines the predominant response. Inclusion of the soma-dendritic model generally reduces the excitation threshold as compared to simple axon model.

**Conclusions.** The different electrode position and polarity over the PCG and near the CS have a large and distinct influence on the response of cortical neural elements to stimuli.

**Significance.** Modeling studies like this can help to identify the effects of electrical stimulation on cortical neural tissue, elucidate mechanisms of action and ultimately to optimize the therapy.

## 6.1. Introduction

Motor Cortex Stimulation (MCS) is a promising therapy in the treatment of chronic, otherwise intractable pain. Introduced by Tsubokawa and his colleagues [31], it was accepted and developed in several centers worldwide [6, 18, 20]. Until now, about 350 cases have been reported [17] and so far central and facial pain are considered to be the main indications for MCS [3, 20].

Because the electrode lead is implanted epidurally (i.e. between the dura mater overlying the sensorimotor cortex and the skull), the technique is generally safe and therefore attractive. Since the brain surface is not exposed, visual guidance cannot be used for target localization. Therefore, the central sulcus is identified using somatosensory evoked potentials and neuronavigation data. The somatotopy of the motor cortex is mapped for each patient individually as it is important that the electrodes used in chronic stimulation are positioned over the cortical representation of the painful body part [19, 20]. This is generally done peroperatively using bipolar stimulation. In chronic stimulation, the stimulus amplitude is typically set at 20-50% of the motor threshold, a value large enough to cause analgesia without any motor effects. The lead most commonly used for stimulation is the Resume<sup>TM</sup> (Medtronic Inc., Minneapolis, MN, USA). This lead has a paddle with 4 disc electrodes having a diameter of 4 mm and spaced by 10 mm (center-center). The insulating paddle has a thickness of ~2 mm.

The mechanism by which MCS alleviates pain is not known. PET studies have shown an increase in cerebral blood flow during MCS in the VA-VL complex of the ipsilateral thalamus, the cingulate gyrus and the brainstem. However, it remains unknown which neural elements are activated immediately by the stimulus-induced electrical field in the region of the motor cortex [20]. Acquiring this knowledge is important because: 1) the neural elements in the cortex affected by the stimulus induce the analgesic effect and 2) the clinical result may be improved when the stimulation technique (lead, its position and the stimulation parameters) can be optimized based on knowledge of the neural elements which should be targeted.

Computer modeling is a method that may help to answer these questions. In the past, our spinal cord stimulation (SCS) model was validated and helped to identify important parameters influencing the results of SCS [10]. In a previous paper [15], our model of MCS was introduced and described. Model predictions regarding the stimulus-imposed electrical field and activating functions were presented. Simple nerve fiber models were used to simulate the response of neural elements to the applied electrical field. However, instead of just axons (as in SCS) the motor cortex also includes *cell bodies* and *dendrites* of several types of neurons. Among these neurons are pyramidal cells having an apical dendritic tree proximal to the electrode which may alter the axonal response to the applied field. In this modeling study, a pyramidal cell model including a cell



body (soma) and a dendritic trunk representing the apical dendritic tree is introduced.

The aim of this study was to evaluate the effect of anodal and cathodal stimulation with a lead placed over the precentral gyrus and over the central sulcus on collaterals of afferents parallel to the laminated structure of the cortex and pyramidal cells oriented perpendicular to those laminae. So far only cathodes are assumed to initiate a neural response, whereas anodes are considered to be indifferent electrodes. The model predictions have been validated by experimental data from animal studies and clinical data.

## 6.2. Methods

### Models

Similar to our SCS models, the MCS model comprises two parts:

1) *3D volume conductor model* with stimulating *electrode(s)*:

The 3D volume conductor had a size of 66x43x57 mm and was represented by 121x73x80 cubic elements. The precentral gyrus (PCG) flanked by the precentral sulcus on the anterior and the central sulcus (CS) on the posterior side constitute the central part of the model (**Figure 1**).

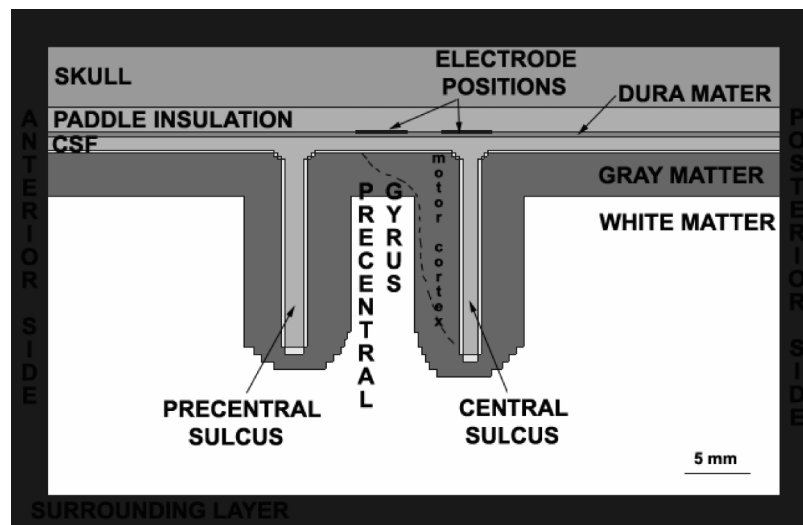


**Figure 1.** Anterior-posterior cross-section of the model. Model compartments are labeled. Electrode positions and approximate position of the motor cortex are indicated.

The PCG includes the premotor cortex (Brodmann area 6) anteriorly and the primary motor cortex (area 4) posteriorly and in the anterior wall of CS [35]. A layer of highly conductive cerebrospinal fluid (CSF) separates the dura mater from the cortical surface. The thickness of the CSF varies among patients and is likely reduced by the thickness of the lead placed between the dura mater and the skull compartment in the model. Models with a CSF thickness ranging from 0.5 to 2.0 mm were made in order to assess the influence of this parameter. Contrary to our previous MCS model, the model presented here had the lead paddle oriented *perpendicular* to CS as commonly used in clinical practice [20]. *Monopolar* stimulation with a single *cathode* or *anode* positioned over the center of PCG and over CS was modeled. The electrode diameter was 4 mm (see Introduction). The potential at the boundary of the model was set at 0 Volts (Dirichlet boundary condition), thus providing the return path for the stimulation-induced current. In addition, *bipolar* stimulation with poles positioned over PCG and CS (electrode diameter 4 mm, center-to-center spacing 7 mm) was modeled. The *electrical potential field* induced by the stimulus pulse in the 3D space of the model was calculated at the vertices of the cubes forming the model by solving a discrete form of the Laplace equation using numerical techniques. A detailed description of the volume conductor model and the calculation methods are presented in our previous publication [15].

## 2) Models of cortical neural elements:

The same myelinated fiber types as in our previous model were considered. They include afferent ('A') fibers *parallel* and efferent ('E') fibers *perpendicular* to the cortical laminae. However, the 'E' fibers originating from *pyramidal cells* have an apical *dendritic tree* extending up to lamina I. Their position is between the axon and the stimulating electrode(s) and therefore their presence might affect the stimulation conditions and outcome. In order to account for these aspects, the 'E' *fiber* models were extended with a (simple) model of the *cell body (soma)* and *apical dendritic trunk*. Hence such a complex structure is referred to as a *pyramidal neuron*. The modeled neural elements are shown in **Figure 2**. The 'A' fiber is parallel to the cortical surface and was placed at 1.1 mm depth in the cortex which approximately corresponds to lamina IV. 'E' neurons were represented by three distinct neurons: 'E1' on top of PCG, 'E2' in the lip of CS and 'E3' – in the wall of CS. Each 'E' neuron was perpendicular to the local cortical laminae. All neural elements ('A', 'E1'-'E3') were placed in the plane passing through the center of the electrode.

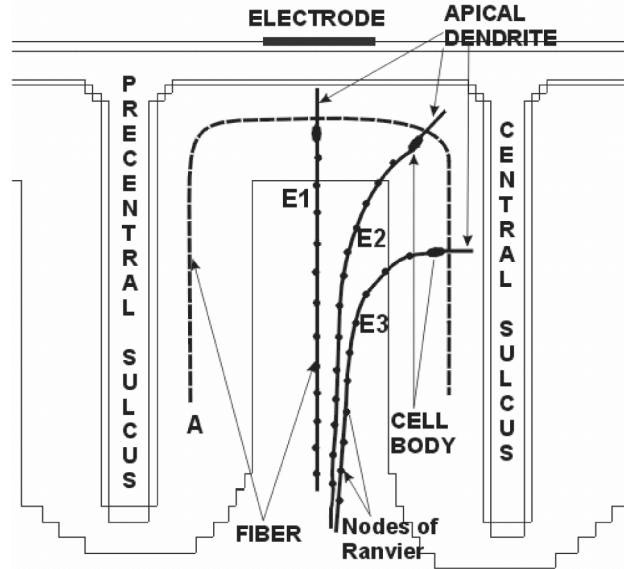


**Figure 2.** Neural elements in the motor cortex as modeled in the standard model: 'A' - nerve fiber parallel to the cortical laminae, 'E1' - neuron on top of the precentral gyrus, 'E2' - neuron in the lip of the central sulcus, 'E3' - neuron in the wall of the central sulcus.

The *myelinated axon (nerve fiber)* model consisted of nodal compartments connected with internodal resistors. It had a uniform structure along its length. The internodal distance and axonal diameter had a logarithmic and a linear relation, respectively, with the fiber diameter, as described by Wesselink et al [34]. The nodal membrane described by Wesselink et al. included non-linear  $\text{Na}^+$  and  $\text{K}^+$  channel kinetics as well as linear leakage channels. The *soma* was modeled as a tapered cylinder (frustum) with the larger base on the axon side. The size of the soma was chosen such that its volume matched its mean value ( $86800 \mu\text{m}^3$ , [27]). The *apical dendritic trunk* was modeled as a membrane cylinder extending from the soma towards the cortical surface. The membrane of both soma and dendritic trunk was considered to be *passive* (no voltage-sensitive ionic channels) with a time constant of 10 msec. This time constant fits experimental data of hippocampal pyramidal cells [32]. The geometrical and electrical properties of the axon hillock and axonal *initial segment* (IS) of human pyramidal cell were not found in literature, but have been described for other species and neuron types, often ambiguously [4, 14, 16, 21, 26]. Because IS is most likely significantly longer than a node of Ranvier, it was estimated to be 10 times longer than a node ( $15 \mu\text{m}$ , [5]), while its other characteristics were the same as in the model of a node of Ranvier. The axon hillock was not

presented separately in the models, but was lumped with the somatic compartment. In **Table 1** the geometrical and electrical parameters of the IS, somatic and dendritic compartments in the standard model are presented.

**Table 1.** Geometrical and electrical parameters of the *standard* neuron model. The majority of the parameters in IS-soma-dendritic part were inherited from the axon model [34]. References are included if applicable, whereas the other parameters were estimated.

Neuron part	Parameter	Value	Reference
AXON NODE	Length [ $\mu\text{m}$ ]	1.5	[34]
	Diameter [ $\mu\text{m}$ ]	$0.8 \cdot \text{fibdiam} - 1.8e^{-6}$	
	Number of compartments	1	
	Membrane kinetics	active	
INITIAL SEGMENT	Length [ $\mu\text{m}$ ]	15	[5, 14]
	Number of compartments	1	-
	Membrane kinetics	same as axon node	-
SOMA	Larger base diameter [ $\mu\text{m}$ ]	60	[27]
	Smaller base diameter [ $\mu\text{m}$ ]	8	
	Length [ $\mu\text{m}$ ]	80	
	Number of compartments	1	-
	Leakage conductance [ $\text{S}/\text{m}^2$ ]	2.8	[32]
	Membrane kinetics	passive	-
APICAL DENDRITIC TRUNK	Length [mm]	1	-
	Diameter [ $\mu\text{m}$ ]	8	-
	Number of compartments	15	-
	Leakage conductance [ $\text{S}/\text{m}^2$ ]	2.8	[32]
	Membrane kinetics	passive	-

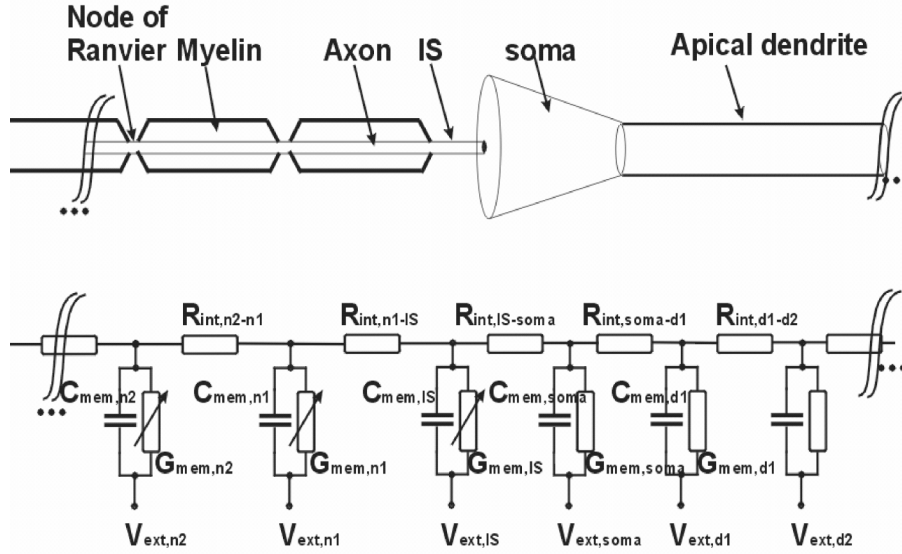


**Figure 3.** Geometry of the pyramidal neuron as modeled. Soma modeled as a frustum, apical dendrite as a cylinder. Electrical equivalent of the model shown:  $V_{ext}$  – extracellular field potential at the model compartment,  $R_{int}$  – intracellular resistance between two adjacent membrane compartments,  $C_{mem}$  – capacitance of the compartment membrane,  $G_{mem}$  – conductance of the compartment membrane, variable with voltage and time for nodal and IS compartments. The ends of the neuron model were sealed (infinite impedance).

In **Figure 3** the equivalent electrical circuit of a pyramidal neuron is shown. According to Kirchoff's law, the outward current of each membrane compartment should equal the sum of the intracellular currents flowing from the adjacent compartments. The membrane current consists of a capacitive and a resistive component. These currents and their relation are described by the following equation:

$$C_{mem,i} \frac{dV_{mem,i}}{dt} + I_{resistive,i} = \frac{V_{int,i-1} - V_{int,i}}{R_{int,i-1}} + \frac{V_{int,i+1} - V_{int,i}}{R_{int,i+1}} \quad (1)$$

with index  $i$  indicating  $i^{\text{th}}$  compartment,  $V_{int,i}$  equals intracellular potential ( $V_{int,i} = V_{ext,i} + V_{mem,i} + V_{rest}$ ),  $V_{rest}$  is resting membrane potential,  $V_{mem,i}$  is a deflection of the membrane potential from the resting value,  $V_{ext,i}$  is extracellular potential,  $R_{int,i-1}$  is intracellular resistance between  $i^{\text{th}}$  and  $i-1^{\text{th}}$  compartment,  $C_{mem,i}$  is membrane capacitance,  $I_{resistive,i}$  is resistive current component which equals the sum of  $\text{Na}^+$ ,  $\text{K}^+$  and leakage currents when voltage-sensitive ionic channels

were present (node and IS) and is voltage and time dependent [34]. Because the somatic and dendritic compartments of the standard neuron model were described by a passive model (very low channel density, [4, 14], their  $I_{resistive,i}$  equaled the leakage current  $I_{leakage,i} = G_{leakage} * (V_{mem,i} + V_{rest} - V_{leakage})$  with  $G_{leakage}$  (equivalent leakage conductance) calculated from the membrane time constant ( $\tau_{mem,i}$ ) as  $C_{mem,i} / \tau_{mem,i}$ .

### Simulations

Spline interpolation was used to calculate the stimulus-induced field potentials at positions corresponding to the nerve cell compartments. These values were used as perturbations ( $V_{ext}$ ) for the system made up of differential equation (1) for each neuron compartment. To solve this system, we used MATLAB® (MathWorks Inc, Natick, MA, USA). The numerical method “ode15s” from SIMULINK with a variable step, suitable for stiff problems, was applied as a solver for integration. Excitation of a neural element was assumed only when propagation of an action potential (AP) was observed *in the axon*. In order to determine the *excitation threshold*, an arbitrary range of voltages (0-30 Volts) was considered and the bisection method was applied until the lowest stimulus voltage resulting in AP generation and propagation was determined with a resolution of 0.1 Volt. The axonal compartment having the largest depolarization at the end of the stimulus pulse (with the excitation threshold voltage applied as the stimulus) was considered the *site of AP initiation*.

## 6.3. Results

### Electrical potential fields and subthreshold response

An important model outcome is the *stimulus-induced electrical potential field*. This field represents the ‘driving force’ for the stimulation of neurons in the proximity of the electrode(s). As shown in **Figures 4A-C**, a different electrode position, polarity or electrode combination influences the shape of the field markedly. When the electrode was over PCG the iso-potential lines were nearly symmetrical on the anterior and posterior side (**Figure 4A**), whereas with the electrode over CS the iso-lines penetrated PCG from the posterior side (**Figure 4B**). The electrical field profile for the bipole differed from either of the monopolar fields, indicating a superposition of the monopolar fields (**Figure 4C**).

The membrane voltage deflections in several compartments of the ‘E1’-‘E3’ neurons during the stimulus pulse of 1 Volt are shown in **Figures 4D-F**. The stimulus was applied as shown in the corresponding **Figures 4A-C**.

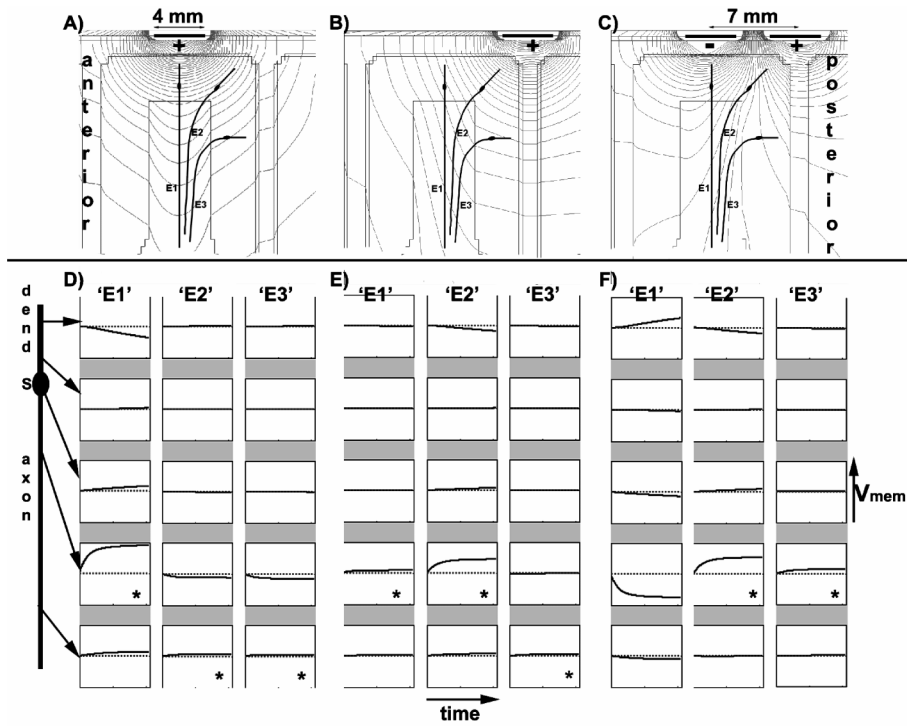


**Figure 4.** A-C: Iso-potential lines for the stimulus of 1 Volt: A) anodal stimulation centered on PCG, B) anodal stimulation centered on CS, C) bipolar stimulation with cathode centered on PCG. 50 iso-lines between 0.4 and 0.6 Volt in monopolar and -0.1 and 0.1 Volt in bipolar stimulation are shown (4.1 mV distance between lines). D-F: Membrane potentials of the 'E' neurons during the stimulus pulse of 1 Volt applied by the electrodes shown in A-C. Time courses of the membrane potentials of a dendritic compartment far from soma, near soma, somatic, an axon node near soma and an axon node far from soma as indicated on the lefthand side by arrows are shown in top to bottom rows. X-axis: time interval 0:210  $\mu$ sec, Y-axis: voltage -10:10 mVolt range. Zero voltage level is indicated by the dashed line. Asterisks indicate compartments where excitation will most likely take place at an adequately high stimulation level.

Since the stimulus amplitude was subthreshold the membrane response was a result of the stimulus-induced extracellular field (shown in **Figures 4A-C**) and the neuron structure. Membrane kinetics did not influence the response much (voltage-gated ion channels are generally closed in the subthreshold regime). Therefore, the response obtained with the opposite stimulus polarity was nearly reversed for each compartment and is not shown. Depending on the electrode

position and stimulus polarity, different membrane compartments along the neurons had either a positive (depolarization) or a negative (hyperpolarization) response of a different magnitude. The axonal compartments having the largest depolarization at the end of the stimulus pulse are most likely the sites of excitation (indicated by an asterisk in **Figures 4D-F**). This subthreshold analysis shows that the axon nodes close to the soma of the 'E1', 'E2' and 'E2' neurons, respectively, will most easily respond to stimuli applied by the electrode configurations in **Figures 4A-C**. These effects were explored in more detail and more accurately by calculating the excitation thresholds.

#### **Excitation threshold and site of excitation**

To predict how a specific neural element responds to the stimulus-induced field, the most exact way is to solve the system of differential equations (eq 1) of each model compartment. The solution represents a temporal excursion of the membrane potential of each compartment for a given stimulus pulse of 210  $\mu\text{sec}$  duration and constant amplitude. In this way, the excitation threshold was determined for neurons parallel and perpendicular to the cortical laminae. The 'A', 'E1', 'E2' and 'E3' neurons in the plane passing through the center of the electrode and perpendicular to CS were considered only. Monopolar stimulation with the electrode over PCG and CS as well as bipolar stimulation were modeled. The standard thickness of the CSF layer was 1.1 mm, being equal to the mean value (3.1 mm - unpublished data, 6 measurements) subtracted by the thickness of the lead (2.0 mm). The fiber diameters were between 5 and 15  $\mu\text{m}$ . The results on excitation thresholds are presented in **Figure 5** whereas the corresponding sites of excitation are indicated in **Figure 6** for all fiber diameters. Note that the exact node of excitation is not well defined because there may often be several adjacent nodes with almost identical thresholds. The excitation of perpendicular fibers often took place at axonal nodes near the place where the electrical tissue conductivity changes (boundary between gray and white matter). Following the fold of the gyrus, the orientation of the neurons with respect to the electrode changes and therefore their excitation conditions were altered. By changing the electrode polarity/position, the group of neurons preferentially excited and the relative order of recruitment with increasing stimulus amplitude changed as well (**Figure 5**).



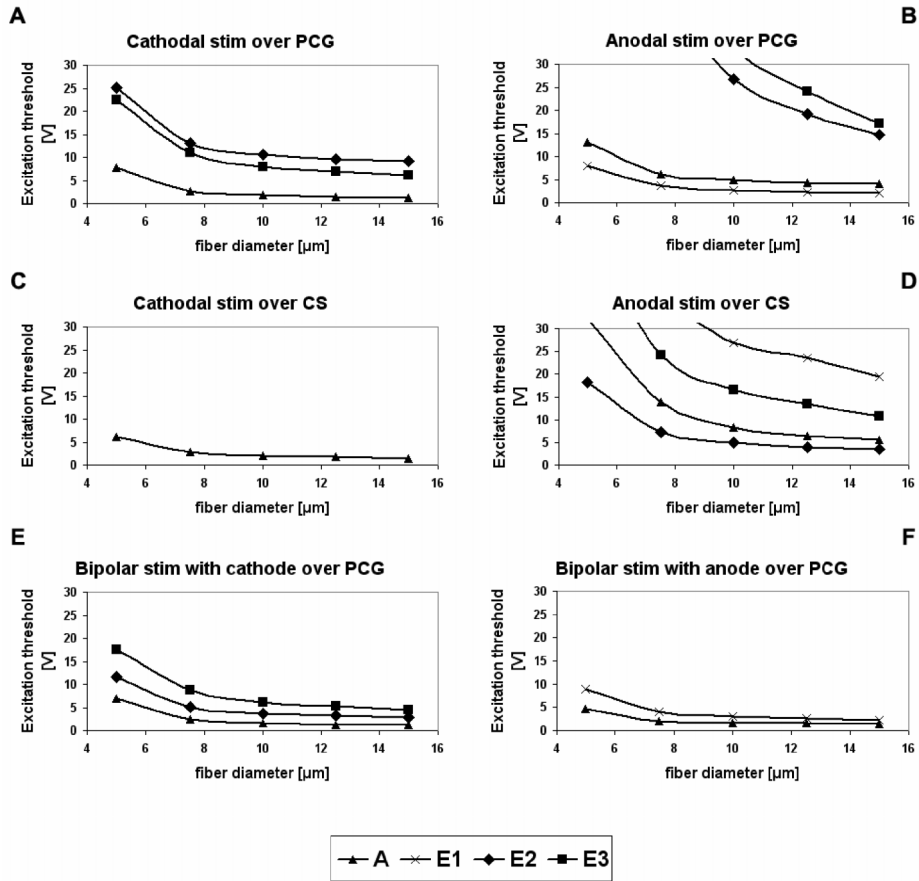


**Figure 5.** Excitation thresholds [Volts] of the ‘A’ fiber and ‘E’ neuron models (Figure 2) when stimulated by the electrodes having different positions and polarities. The fiber diameter was varied in the range 5-15 μm.

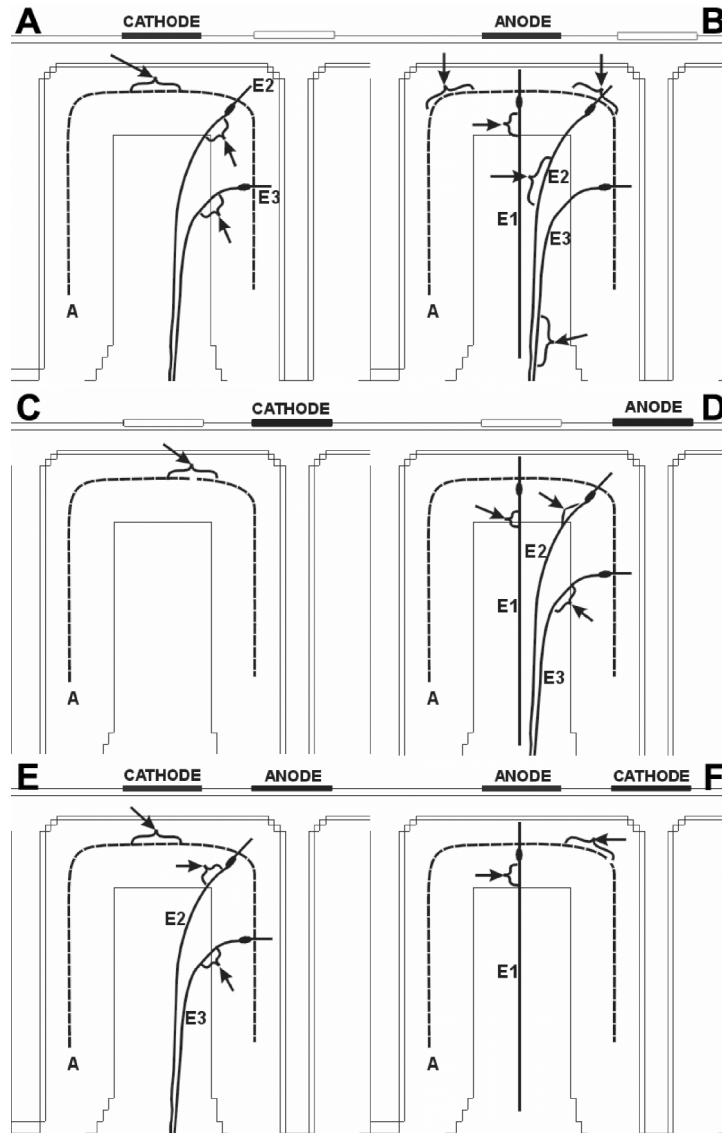


**Figure 6.** Sites of excitation in the ‘A’ fiber and ‘E’ neurons when stimulated by the electrodes having different positions and polarities. For each electrode configuration, only those neurons that are activated below 30 Volts are shown. Often a few nodes have a similar threshold; therefore a span of excitation sites is indicated for each neural element.

### Effect of the soma-dendritic compartments

The presence of the IS-soma-dendritic part in the standard neuron model may have changed the excitation threshold of the simple fiber model used in a previous paper [15]. To obtain a simple fiber model the IS-soma-dendritic part was substituted by a single node of Ranvier. The excitation threshold of this model was calculated and compared with the threshold of the standard neuron model. The excitation thresholds increased by up to 17% for the simple fiber models as shown in **Table 2**. The change was largest when the excitation took place electrically close to the soma i.e. when excitation was only a few nodes distally and the fiber diameter was small. Conversely, if the distance between the excitation site and the soma was large, the influence of the IS-soma-dendritic compartments was negligible. When a large depolarization (and excitation) took place at the first node of the simple fiber model, it was substituted by a depolarization of the dendrite in the corresponding standard neuron model and did therefore lack excitation at stimuli below 30 Volts.

**Table 2.** Percentage increase in excitation threshold when the standard IS-soma-dendritic model was substituted by a node of Ranvier. The results for the extremes of the modeled fiber diameter range (5 - 15  $\mu\text{m}$ ) are shown. ‘-’ indicates that the threshold for excitation exceeded 30 Volts.

Neuron type & fiber diam: electrode:	‘E1’		‘E2’		‘E3’	
	5 $\mu\text{m}$	15 $\mu\text{m}$	5 $\mu\text{m}$	15 $\mu\text{m}$	5 $\mu\text{m}$	15 $\mu\text{m}$
Cathode over PCG	-	-	1 %	5 %	0 %	2 %
Anode over PCG	12 %	5 %	-	0 %	-	0 %
Cathode over CS	-	-	-	-	-	-
Anode over CS	-	1 %	17 %	3 %	0%	0 %
Bipole with cathode over PCG	-	-	9 %	4 %	0 %	0 %
Bipole with anode over PCG	13 %	7 %	-	-	-	-

### Influence of the neuron model position

The neuron models described in the previous paragraphs had fixed positions within PCG. The cell bodies of ‘E’ neurons were  $\sim 1.4$  mm under the cortical surface (approximately in lamina V). In order to test the sensitivity of the excitation threshold, the position of the neuron models was varied within an anatomically constrained range as shown in **Figure 7A**. The electrode was centered on PCG and the stimulus polarity was chosen such that it had the lowest threshold for the particular neuron model (i.e. a cathode for ‘A’, ‘E2’

and 'E3' and an anode for 'E1', see **Figures 5A-B**). As shown in **Figure 7B** the excitation thresholds increased with increasing distance from the stimulating electrode. For the 'E1' neuron, the trendlines showed a linear increase in excitation threshold of 0.5 Volts per mm displacement in the x direction away from the center of the electrode. Similarly, the threshold of the 'A' fiber increased by 1 Volt per mm depth in the cortex (y direction). The 'E2' and 'E3' neuron threshold increased by 1.2 Volt per mm depth in the sulcus wall (y direction). However, due to the variable position of the Ranvier nodes (at which initiation of AP occurred) with respect to the abrupt change of the grey matter orientation, the thresholds of the 'E2' neurons in the lip of the sulcus wall were variable and were therefore excluded when calculating the trendline (**Figure 7B**).

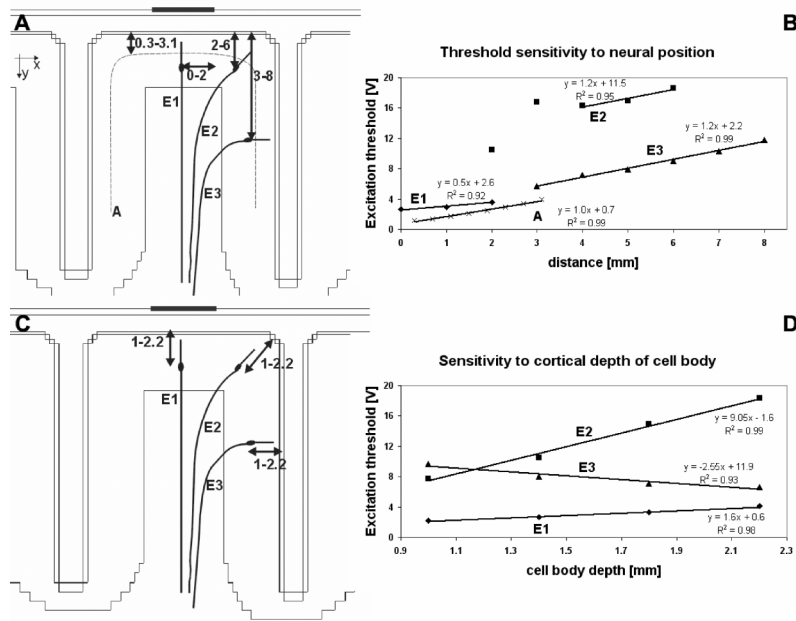


**Figure 7.** Influence of the neuron model position on the excitation threshold. **A, C:** Simulated variations of the position as indicated (in mm). The electrode was centered on PCG. Variations of the excitation threshold with: **B)** varied distance from the center of the electrode ('E1') or cortical surface ('A', 'E2', 'E3') and **D)** varied cortical depth of the soma.

The formulas for the linear fits are given. For the 'E2' neuron two points are excluded when calculating the linear fit (figure B) for the reasons explained in the text. Results from anodal stimulation for 'E1' neuron and cathodal stimulation for 'A', 'E2' and 'E3' neurons are shown because they had smaller excitation thresholds than with the opposite polarity. Nerve fiber diameter was 10  $\mu\text{m}$ .

Similarly, cortical depth of the cell body was varied in the range 1.0 - 2.2 mm (**Figure 7C**), representing approximately the boundaries of cortical lamina IV-V where the large pyramidal cells of the motor cortex are present. The length of the dendritic trunk was adjusted so that it always reached the same cortical level regardless of cell body depth. The excitation threshold changed with 1.6, 9 and -2.5 Volts per additional mm cortical depth for the 'E1', 'E2' and 'E3' neuron, respectively (see **Figure 7D**).

**Sensitivity of thresholds to the neuron model parameters**

In order to determine which parameters of the IS-soma-dendritic compartments influenced the neural response of the 'E1'-'E3' neurons, and to which extent, their parameters were varied as shown in **Table 3**. The same volume conductor model and stimulus polarity as described in the previous paragraph were used.

**Table 3.** IS-soma-dendrite model parameter ranges tested. Parameters were varied one at a time. Responses of 'E1' – 'E3' neurons having fiber diameters in the range of 5-15  $\mu\text{m}$  with an electrode over PCG were simulated. In the last two columns, the influence of anodal stimulation on the 'E1' neuron threshold is reported only, because for other conditions changes did not affect the result substantially. Results obtained from models with the lowest parameter value tested were taken as the baseline when calculating % change.

Neuron part:	Parameter:	Range:	Influence on 'E1' threshold:	
			5 [ $\mu\text{m}$ ]	15 [ $\mu\text{m}$ ]
INITIAL SEGMENT	Length [ $\mu\text{m}$ ]	1.5-60	15 %	0 %
	Permeability $\text{Na}^+$ -channels [ $\text{dm}^3/\text{m}^2\text{s}$ ]	0.00704-0.704	0 %	0 %
SOMA & APICAL DENDRITIC TRUNK	Soma volume [ $\mu\text{m}^3$ ]	62000-116000	0 %	0 %
	Intracellular resistance [ $\text{Ohm} \cdot \text{m}$ ]	0.1-1.0	50 %	12 %
	Membrane time constant [msec]	1-100	-10 %	-10 %
	Dendrite diameter [ $\mu\text{m}$ ]	2-32	-55 %	-17 %
	Permeability $\text{Na}^+$ -channels [ $\text{dm}^3/\text{m}^2\text{s}$ ]	0.0 (passive membrane) -0.00704	0 %	0 %

The model outcome was marginally sensitive (<5%) to variations of the parameters tested. Only the response of the ‘E1’ neuron in anodal stimulation had a higher sensitivity to certain parameters (see **Table 3**). This is likely due to the proximity of the IS-soma-dendritic part to the stimulating electrode and the proximity of the excitation site to the IS-soma-dendritic part. The influence was typically largest in neurons with the smallest fiber diameter, also because higher voltage levels were needed for their excitation which resulted in a more significant response of the IS-soma-dendritic part.

#### **Sensitivity of thresholds to volume conductor model parameters**

With an increase in the CSF thickness, there was less penetration of current into PCG [15]. Consequently, the excitation threshold of the neural elements increased, whereas the site of excitation remained unchanged. The % increase in threshold is summarized in **Table 4**. As shown, substantially larger (typically more than 100 %) thresholds can be expected when the CSF thickness is increased from 0.5 to 2.0 mm. Since the relative increase in threshold value was unequal for different neurons having the same diameter, the ratio of their thresholds also changed with increasing CSF thickness. For the modeled range of CSF thicknesses, however, this did not result in a change of the qualitative relation between the threshold curves in **Figure 5**.

**Table 4.** Percentage increase of the excitation threshold when the thickness of the CSF layer between electrode and cortical surface was increased from 0.5 to 2.0 mm. The *average* increase for fiber diameters 5-15  $\mu\text{m}$  is shown. ‘-’ indicates that the threshold for excitation exceeded 30 Volts.

<b>neural element: electrode:</b>	<b>‘E1’ neuron</b>	<b>‘E2’ neuron</b>	<b>‘E3’ neuron</b>	<b>‘A’ fiber</b>
<b>Cathode over PCG</b>	-	170 %	105 %	180 %
<b>Anode over PCG</b>	165 %	80 %	40 %	200 %
<b>Cathode over CS</b>	-	-	-	100 %
<b>Anode over CS</b>	<5%	120 %	105 %	100 %
<b>Bipole with cathode over PCG</b>	-	130 %	110 %	175 %
<b>Bipole with anode over PCG</b>	190 %	-	-	130 %

The thickness of the gray matter (GM) in PCG of humans is ~3.8 mm [35]. Below it the white matter (WM) is found. Models with a GM thickness in the range 3.2 – 4.4 mm were made. A model with 3.2 mm GM was taken as a baseline in the following analysis. Thresholds of the ‘A’ fibers were not substantially influenced by the thickness of GM (<5% deviation from the baseline) nor did the site of excitation change. Because the ‘E’ neurons intersect the GM-WM boundary, their excitation was influenced by the position of this boundary. When increasing the GM thickness from 3.2 to 4.4 mm, the excitation threshold did not change for the ‘E1’ neuron in anodal stimulation whereas it decreased by 15% and increased by 80% for the ‘E2’ and ‘E3’ neuron, respectively, in cathodal stimulation. The values reported are mean values for the range of fiber diameters simulated.

In addition, the transition between the GM and WM conductivity is most likely not as abrupt as in our models. Models with an intermediate layer having a thickness of 0.6 - 1.8 mm and an arbitrary conductivity of 0.48 S/m (the mean value of the GM and WM conductivities) were made. The thickness of GM was kept at an arbitrary 2.6 mm. The thresholds were compared with the results of models with PCG consisting of GM and WM only. There was a maximum decrease of 10% for the ‘E1’ and a maximum increase by 5% for the ‘E2’ and ‘E3’ neuron in anodal and cathodal stimulation, respectively. Thresholds of ‘A’ fibers increased by up to 3%.

#### 6.4. Discussion

##### Neurons represented by models

Understanding which cortical neural elements the models actually represent may help to identify the input elements of the pain relieving circuitry in stimulation. Fibers defined as *perpendicular* to the cortical laminae may constitute descending (cortico-thalamic, cortico-pontine, cortico-spinal, cortico-cortical etc.) and ascending (thalamo-cortical, cortico-cortical, reticulo-cortical etc.) pathways, whereas fibers *parallel* to the cortical laminae may represent their collaterals, bifurcations or, alternatively, intrinsic cortical axons. The models of the fibers having cell bodies in the cortex are not representative for the ascending fibers whose cell bodies are located in other parts of brain. The modeled somata and dendritic trunks may represent pyramidal cell bodies and their apical dendritic trees from which the descending pathways stem. Largest among the pyramidal cells are the Betz cells in cortical lamina V.

##### Model predictions

By varying the stimulation conditions the group of excited neural elements may change. In *anodal stimulation* either neurons oriented perpendicular to the electrode surface (‘E1’ in **Figure 5B** and ‘E2’ in **Figure 5D**) or nerve fibers parallel to the cortical laminae (‘A’ in **Figure 5B** and **D**) have the lowest threshold. *Cathodal stimulation* favors excitation of nerve fibers parallel to the

cortical laminae. The thresholds for stimulation of these fibers are lower than in anodal stimulation. Because the fibers parallel to the cortical laminae were modeled as being parallel to the bipole axis, their stimulation was facilitated with either polarity orientation of the bipole as compared to the corresponding monopolar case. Similarly, an additional anode over CS facilitated excitation of neurons in the anterior wall and lip of CS as compared to cathodal stimulation over PCG (**Figure 5E**). The effect on these neurons was opposite when a cathode was added over CS (**Figure 5F**). Qualitatively, the neural response to bipolar stimulation resembles that of monopolar stimulation with the same polarity over PCG. This indicates that the effect of the electrode over PCG dominates, whereas the electrode over CS may facilitate or suppress stimulation of certain neuron groups.

In order to make comparative predictions, it was assumed that all nerve fibers had the *same diameter* regardless of the neuron type. To our knowledge, the diameter distributions of most human cortical nerve fibers (both efferents and afferents and their arborizations) are not well known. Nerve fibers parallel to the cortical laminae likely have smaller diameters because of their local function (see previous section), whereas pyramidal tract fibers most likely have the largest diameters (up to 13  $\mu\text{m}$  in humans [33]). It is expected that the diameter of a nerve fiber varies with its allocation to a muscle representation in the motor cortex [27]. To be able to determine which fiber types are excited at a given stimulus, the largest corresponding fiber size in a specific part of motor cortex should be known.

#### **Parameter sensitivity of the model outcome**

Terminating the nerve fiber model with a simple node of Ranvier was a less favorable condition for excitation than terminating it with an IS-soma-dendritic part. To explain this phenomenon the time integral of the intracellular current flowing from the proximal end of the nerve fiber (i.e. IS in standard neuron model and node in simple fiber model) into the fiber during the stimulus pulse (the displaced electrical charge) was calculated. This parameter had a larger value when the axon ended with an IS-soma-dendritic part than in case the axon ended with a node (results not shown). For some stimulation conditions the latter was even negative, indicating an overall opposite current flow. Since the current flowing into the axon during the stimulus pulse contributes to its depolarization and facilitates its excitation, these calculations make plausible why the inclusion of the IS-soma-dendritic model generally reduces the excitation threshold.

When the electrical and geometrical parameters of the IS-soma-dendritic model were varied, the response of the 'E1' neuron at anodal stimulation was influenced most, as shown by the sensitivity analysis. With the electrode over PCG the IS-soma-dendritic part of the 'E2' and 'E3' neurons was hyperpolarized or weakly depolarized because of their orientation nearly parallel to the iso-lines. Another reason for some influence on the excitation



threshold is the electrical separation between the excitation site (several nodes away from the soma) and the compartments whose parameters were changed (IS-soma-dendrite). Similar was noted by Rothwell [29] and Rubenstein [30] too. Finally, as the threshold stimuli of fibers with larger diameters are smaller, the response of the IS-soma-dendritic part was smaller and therefore affected the membrane voltage course in the axon part to a lesser extent (**Table 3**).

Varying the IS-soma-dendritic parameters did, however, influence the membrane response of this neuron part. E.g. backpropagation of the AP and its invasion into the soma-dendritic part could be influenced, as concluded by Luscher and Larkum [13]. However, these were all post-excitation events (after an AP has been initiated) and were therefore not of interest for this analysis. In addition, these effects are just local and do not affect other neurons.

### **Model constraints**

Since neuronal excitation was always initiated at an axon node and there was a limited influence of the IS-soma-dendritic parameters, the application of axon model parameters that ensure the model to match the behavior of human cortical fibers is essential in the prediction of excitation thresholds. Instead of a cortical fiber, the nerve fiber model used in this article was fitted to mimic the behavior of the human peripheral sensory fiber. To our knowledge, electrical and geometrical parameters (diameter, orientation, location, length of ‘parallel’ fibers, degree of myelination, ion-channel density, excitability of the IS etc.) of human cortical fibers are still unknown. As a consequence and due to similar uncertainties on parameters of the volume conductor model (e.g. tissue conductivities, thickness of CSF etc.), some of the predicted excitation thresholds are beyond the output range of a pulse generator and are most likely overestimated. The motor thresholds obtained from one series of patients at bipolar stimulation were between 10 and 21 Volts (J-P Nguyen, personal communication). The calculated excitation thresholds would have been even larger, if the pulsewidth corresponded with the smaller values used in these patients (60-150  $\mu$ sec).

### **Comparison with empirical data**

Hern et al. reported that the anodal thresholds to excite neurons in the motor cortex were lower than the cathodal ones, whereas there was no significant difference in the thresholds of a motor response following anodal and cathodal stimulation [9]. In order to elicit movements, a number of neurons belonging to the same muscle representation presumably need to be activated. Because it is not known which cortical neurons should be recruited to elicit motor effects and what their mutual relations are, we explored the individual cell responses only. Patton and Amassian [22] were the first to discern an initial *D-wave* (direct response) followed by an *I-wave(s)* (indirect response) in the corticofugal tract response to electrical stimulation of the motor cortex in anesthetized monkeys and cats. These responses were confirmed by intra- and extra-cellular

recordings from cortical neurons [1, 23, 24, 28]. The short latency D-wave results most probably from direct activation of pyramidal cells (initiated in the axon or IS) whereas the I-wave follows from their indirect, longer latency, transsynaptic activation. With a supraliminal stimulus both anodal and cathodal stimulation evoked D- and I-wave responses, the anodal stimulus usually evoking a D-wave at a lower amplitude than an I-wave and the cathodal stimulus evoking an I-wave at a lower amplitude than a D-wave [1, 7].

The empirical results led to the conclusion that descending tract fibers approximately perpendicular to the surface of the electrode are excited at a lower amplitude in anodal than in cathodal stimulation [1, 9, 29]. Hern et al. reported that in the primate cortex the cathodal threshold for a cortico-fugal response was typically 1.5-5 times larger than the anodal threshold [9]. From **Figure 5A** and **B** a range of 1.3 – 4 was calculated as the ratio between the cathodal threshold of the ‘A’ fiber having a diameter of 5-7.5  $\mu\text{m}$  and the anodal threshold of the ‘E1’ neuron having a fiber diameter of 10-15  $\mu\text{m}$ . This range calculated for the model matches the experimental range.

The optimal cortical foci for cathodal stimulation were located anterior to those for anodal stimulation when the arm area in primates was stimulated [9]. On the inferior side the primary motor cortex (Brodmann area 4) extends less over the convexity of PCG than on the superior side [35]. The representation of the arm may thus be centered on the anterior lip of CS. Therefore, it is likely that efferent neurons belonging to the arm representation (‘E2’) have the lowest threshold when the anode is positioned over the CS region (**Figure 5D**). A cathode positioned over PCG, though, will likely stimulate either fibers parallel to the cortical laminae (‘A’) or neurons in the sulcus wall (‘E2’, ‘E3’) at comparable amplitudes (**Figure 5A**). Parallel fibers (‘A’) innervate descending neurons (‘E’) either monosynaptically or via one or more interneurons (polysynaptically). When ‘A’ fibers are activated by a single stimulus pulse, the consecutive response in the descending pathway(s) (one or more I-waves) is complex and delayed as compared to the direct or D-response. The stimulus amplitude needed to generate an I-wave with surface anodal stimulation was larger than with surface cathodal stimulation [7] which is in accordance with our model predictions assuming similar fiber size (‘A’ fibers, **Figure 5A vs B** and **C vs D**).

Modeling results are also confirmed by the experimental finding that anodal stimulation depolarizes the axonal part of neurons perpendicular to the electrode while hyperpolarizing their dendritic part [1, 2, 7, 29]. The opposite was observed in cathodal stimulation. The preference to excite the neuron pointing with its dendritic tree towards an anode is also known from publications on other modeling studies [25, 26].

According to our modeling results site of initial excitation following anodal stimulation was generally several nodes distant from the soma (deeper in WM) compared to cathodal stimulation (e.g. ‘E2’ and ‘E3’ neuron at monopolar stimulation over PCG, **Figure 6A vs B**). Gorman reported a latency of  $\sim 0.1$  msec

between D-waves elicited at anodal and cathodal stimulation, respectively [7]. Assuming a 10  $\mu\text{m}$  fiber with an internodal distance of  $\sim 1$  mm and a conduction velocity of  $\sim 50$  m/s, this latency would correspond to 5 internodal distances or  $\sim 5$  mm which is close to our model predictions.

Direct cortical stimulation and recording of nerve responses from the spinal cord in human subjects confirmed the existence of D- and I-waves with similar characteristics as observed in animals, including lower anodal than cathodal thresholds for a direct pyramidal cell response [11]. Therefore, model predictions confirmed by animal experiments are likely to apply here as well. Based on chronaxie and refractory period measurements, Hanajima et al. concluded that cortical elements initially activated by stimulation are myelinated axons [8]. However, it was observed that muscle twitch responses produced by stimulation of the exposed motor cortex in awake humans had a lower (or similar) threshold in cathodal than in anodal stimulation [8, 12]. According to Patton and Amassian a simple D-response is not a sufficient condition to elicit muscle responses [22]. Therefore, in these experiments cortical neural elements must have been stimulated at the motor threshold level. The conclusion by Hern et al. on similar anodal and cathodal motor thresholds [9] is thus in accordance with the results of Libet and Hanajima.

#### **Mechanism and neural elements excited in chronic therapeutic stimulation**

Chronic stimulation inducing analgesic effects is applied at 20-50% of the motor threshold. It has been shown recently that in bipolar stimulation the anode of the bipole evoking the largest motor response in the painful body area should be programmed as a cathode to obtain pain relief during chronic stimulation. An electrode positioned posteriorly to this electrode over CS or the postcentral gyrus is generally programmed as an anode (J-P Nguyen, personal communication). Our modeling results have shown that this electrode polarity reversal will likely influence the thresholds and recruitment order of the neural elements underneath the active electrodes. When the anode over PCG was replaced by a cathode, neurons perpendicular to the electrode did not have the lowest threshold anymore, whereas stimulation of those neurons with a direction component parallel to the electrode was promoted. Creating a bipole by adding an anode posteriorly over CS, will also facilitate the excitation of those neurons with a direction component parallel to the bipole axis and those perpendicular to the anodal surface. Any neurons with different orientations are expected to have higher excitation thresholds. With increasing distance between the electrodes, bipolar stimulation may become bifocal with both cathode and anode having separate effects on the underlying parts of the cortex (motor and possibly sensory). Several questions have not yet been answered, such as: Will the cathode recruit nerve fibers parallel to the cortical laminae or neurons with a direction component parallel to the cathode? Or will anodal stimulation of neurons in the anterior wall of CS pointing at the anode (or similar neurons in the sensory cortex) prevail? Or could, alternatively, changes in polarization of

the soma-dendritic part induced by stimulus pulses give rise to neuronal plasticity? Although these effects were not modeled in the present study they cannot be excluded from having an influence on analgesia. This theoretical approach is helpful in asking the right questions. It helps to limit and focus the empirical studies to be performed on relevant questions.

### **6.5. Conclusions**

A set of computer modeling results on excitation of motor cortex region have been presented. A simple nerve fiber model was extended with a soma-dendritic model which generally resulted in a facilitated excitation. It was shown that the relative position and orientation of a neural element in respect to the stimulating electrode(s) influences its excitation threshold vastly. This fact can be used in clinical practice to enhance the response of desired and suppress the response of unwanted neural elements. Contrary to common belief, an anode positioned over the cortex cannot be considered an indifferent electrode because it can stimulate neural elements at a comparable or even lower threshold level.

---

### **Acknowledgements:**

We would like to thank Prof. J-P Nguyen (Department of Neurosurgery, Hôpital Henri Mondor, Créteil, France) and Dr. J-P Lefaucheur (Department of Neurophysiology, Hôpital Henri Mondor, Créteil, France) for providing us with clinical data.

## REFERENCES

- 1 Amassian VE, Stewart M, Quirk GJ and Rosenthal JL. Physiological basis of motor effects of a transient stimulus to cerebral cortex. **Neurosurgery**. 20:74-93, 1987
- 2 Basser PJ and Roth BJ. New currents in electrical stimulation of excitable tissues. **Ann Rev Biomed Eng**. 2:377-397, 2000
- 3 Brown JA and Barbaro NM. Motor cortex stimulation for central and neuropathic pain: current status. **Pain**. 104:431-435, 2003
- 4 Colbert CM and Johnston D. Axonal action-potential initiation and Na<sup>+</sup> channel densities in the soma and axon initial segment of subicular pyramidal neurons. **J Neurosci**. 16:6676-6686, 1996
- 5 Farinas I and DeFelipe J. Patterns of synaptic input on corticocortical and corticothalamic cells in the cat visual cortex. II. The axon initial segment. **J Comp Neurol**. 304:70-77, 1991
- 6 Garcia-Larrea L, Peyron R, Mertens P, Gregoire MC, Lavenne F, *et al*. Electrical stimulation of motor cortex for pain control: a combined PET-scan and electrophysiological study. **Pain**. 83:259-273, 1999
- 7 Gorman ALF. Differential patterns of activation of the pyramidal system elicited by surface anodal and cathodal cortical stimulation. **J Neurophysiol**. 29:547-564, 1966
- 8 Hanajima R, Ashby P, Lang AE and Lozano AM. Effects of acute stimulation through contacts placed on the motor cortex for chronic stimulation. **Clin Neurophysiol**. 113:635-641, 2002
- 9 Hern JEC, Landgren S, Phillips CG and Porter R. Selective excitation of corticofugal neurones by surface-anodal stimulation of the baboon's motor cortex. **J Physiol**. 161:73-90, 1962
- 10 Holsheimer J. Which neuronal elements are activated directly by spinal cord stimulation. **Neuromodulation**. 5:25-31, 2002
- 11 Katayama Y, Tsubokawa T, Maejima S, Hirayama T and Yamamoto T. Corticospinal direct response in humans: identification of the motor cortex during intracranial surgery under general anaesthesia. **J Neurol Neurosurg Psychiatry**. 51:50-59, 1988
- 12 Libet B, Albert WW, Wright EW, Delattre LD, Levin G, *et al*. Production of threshold level of conscious sensation by electrical stimulation of human somatosensory cortex. **J Neurophysiol**. 27:546-578, 1964
- 13 Luscher HR and Larkum ME. Modeling action potential initiation and back-propagation in dendrites of cultured rat motoneurons. **J Neurophysiol**. 80:715-729, 1998
- 14 Mainen ZF, Joerges J, Huguenard JR and Sejnowski TJ. A model of spike initiation in neocortical pyramidal neurons. **Neuron**. 15:1427-1439, 1995
- 15 Manola Lj, Roelofsen BH, Holsheimer J, Marani E and Geelen J. Modelling motor cortex stimulation for chronic pain control: electrical potential field, activating functions and responses of simple nerve fibre models. **Med Biol Eng Comput**. 43:335-343, 2005

- 16 McIntyre CC and Grill WM. Excitation of central nervous system neurons by nonuniform electric fields. **Biophys J.** 76:878-888, 1999
- 17 Meyerson B. Motor cortex stimulation - effective for neuropathic pain but the mode of action remains illusive. (Editorial). **Pain.** 118:6-7, 2005
- 18 Meyerson BA, Lindblom U, Linderöth B, Lind G and Herregodts P. Motor cortex stimulation as treatment of trigeminal neuropathic pain. **Acta Neurochir (Wien).** 58:150-153, 1993
- 19 Nguyen J-P, Lefaucheur J-P, Decq P, Uchiyama T, Carpentier A, *et al.* Chronic motor cortex stimulation in the treatment of central and neuropathic pain. Correlations between clinical, electrophysiological and anatomical data. **Pain.** 82:245-251, 1999
- 20 Nguyen J-P, Lefaucheur J-P and Keravel Y. Motor cortex stimulation. In: Simpson B. *Electrical Stimulation and the relief of Pain*, Pain Research and Clinical Management. Elsevier Science, 2003:
- 21 Palay SL, Sotelo C, Peters A and Orkand PM. The axon hillock and the initial segment. **J Cell Biol.** 38:193-201, 1968
- 22 Patton HD and Amassian VH. Single- and multiple-unit analysis of cortical stage of pyramidal tract activation. **J Neurophysiol.** 17:345-363, 1954
- 23 Phillips CG and Porter R. Unifocal and bifocal stimulation of the motor cortex. **J Physiol.** 162:532-538, 1962
- 24 Purpura DP and Mc Murtry JG. Intracellular activities and evoked potential changes during polarization of motor cortex. **J Neurophysiol.** 28:166-185, 1965
- 25 Ranck JB. Which elements are excited in electrical stimulation of mammalian central nervous system: A review. **Brain Res.** 98:417-440, 1975
- 26 Rattay F. Analysis of the electrical excitation of CNS neurons. **IEE Trans Biomed Eng.** 45:766-772, 1998
- 27 Rivara C-B, Sherwood CC, Bouras C and Hof PR. Stereologic characterization and spatial distribution patterns of Betz cells in the human primary motor cortex. **The anatomical record part A.** 270A:137-151, 2003
- 28 Rosenthal J, Waller HJ and Amassian VE. An analysis of the activation of motor cortical neurons by surface stimulation. **J Neurophysiol.** 30:844-858, 1967
- 29 Rothwell JC. Techniques and mechanisms of action of transcranial stimulation of the human motor cortex. **J Neurosci Methods.** 74:113-122, 1997
- 30 Rubenstein JT. Axon termination conditions for electrical stimulation. **IEEE Trans Biomed Eng.** 40:654-663, 1993
- 31 Tsubokawa T, Katayama Y, Yamamoto T, Hirayama T and Koyama S. Chronic motor cortex stimulation in patients with thalamic pain. **J Neurosurg.** 78:393-401, 1993
- 32 Turner D and Schwartzkroin PA. Steady-state electrotonic analysis of intracellularly stained hippocampal neurons. **J Neurophysiol.** 44:184-199, 1980
- 33 von Keyserlingk DG and Schramm U. Diameter of axons and thickness of myelin sheaths of the pyramidal tract fibres in the adult human medullary pyramid. **Anat Anz, Jena.** 157:97-111, 1984

- 34 Wesselink WA, Holsheimer J and Boom HBK. A model of the electrical behaviour of myelinated sensory nerve fibres based on human data. **Med Biol Eng Comput.** 37:228-235, 1999
- 35 Zilles K. Cortex. In: Paxinos G. The human nervous system. San Diego: Academic Press, 1990: 757-802.





# Chapter 7

**Final remarks**

Although SCS and MCS are being used for quite some time in clinical practice to treat various chronic, neuropathic pain syndromes, the therapies and their outcome can still be improved. Improvements should be focused on: a) increasing knowledge of mechanism of action (especially in MCS), b) diagnostics and patient selection, c) lead design (to selectively stimulate the required population of neurons), d) methods for lead positioning and programming and e) pulse generator design and versatility. These improvements should stem from clinical, neurophysiological, technological and biophysical knowledge, all of which is continuously being improved yet often misunderstood or underrated.

In this thesis a theoretical approach towards optimization of SCS and MCS is presented. Computer modeling may contribute to a better understanding of the immediate biophysical mechanisms following the application of electrical stimuli to neural structures and to determine the influence of geometrical, physiological, electrical and other parameters. Bearing in mind that the influence of these parameters is often difficult to determine by *in vivo* experiments, the role of computer modeling is invaluable for the optimization process. Unlike clinical experiments, parameters of the model are fully controlled and therefore the influence of each parameter can be assessed independently. However, the results should not be taken for granted as some model parameters are not exactly known, not known at all or have a natural variation. In addition, the structure, neuroanatomical composition of the model and modeled mechanisms may not be correct although best knowledge is used in making models. Hence, the predictions should be considered as relative (not absolute) and esteemed in relation to other model predictions. Because computer modeling can predict the level of discrimination regarding the outcome under different experimental conditions, it is instructive in selecting which (clinical) experiments are useful to perform. Combining theoretical findings with clinical data and experience is of immense importance for future SCS and MCS systems design.

Both clinical studies and previous modeling work on SCS have shown that stimulation with leads having small center-to-center contact spacings favors recruitment of the dorsal columns (DCs), and thus paresthesia coverage, versus stimulation of the dorsal roots (DRs). Our modeling study of stimulation with commonly used percutaneous leads (Chapter 3) confirms these findings. However, although leads having a small contact spacing are available since some 10 years, the clinical environment is often reluctant to use them. This is in part attributable to the marketing strategy of the companies. A main reason is that clinicians are reluctant to use new equipment when they 'believe' that the old system helps their patients adequately. If this is not the case for some patients they might consider other equipment. From a point of view of product validation and innovation this is unfortunate, because it limits among others the verification of model predictions e.g. on the effects of contact spacing. The optimal contact spacing also depends on the distance from the lead contacts to

the neural target (spinal cord). Consequently, the contact spacing considered optimal at a low-thoracic level of implantation may be too large and thus suboptimal for implantation at the cervical level where the distance to the spinal cord is generally smallest [5]. A solution of this problem would be a lead with a dense distribution of contacts on the array (high spatial resolution). By selecting more or less close contacts on such a lead, the clinical results might be optimized.

However, a small center-to-center contact spacing and an increased recruitment of DC fibers is accompanied by an increased energy consumption as shown by our modeling (Chapter 3). Although the shape of the electrical field favors the stimulation of nerve fibers running in parallel with the contact array (DCs), the penetration of current into the spinal cord is less efficient than with large contact spacings. On the other hand, stimulation of DR fibers is less efficient, resulting in a larger threshold. This is beneficial for the clinical outcome as the therapeutic range is increased (due to a larger increase of the discomfort threshold). An increased energy consumption may be acceptable if it brings benefits for the patient, especially as a new generation of implantable pulse generators has rechargeable batteries with yet a larger capacity than the former ones. In addition, most manufacturers have recognized that a decreased conducting wire resistance reduces energy consumption by decreasing the energy they dissipate. Most leads now have low-resistance conducting wires.

Apart from the influence of the geometry of the lead, we have shown that its position within the dorsal epidural space is crucial (Chapter 2 and Chapter 3). Any displacement of the lead laterally from the physiological midline and/or dorsally from the dura mater results in a decreased ability to recruit DC fibers and a relative increase of the ability to recruit DR fibers. As a result the therapeutic range is reduced, which is unfavorable in the treatment of complex, multi-dermatomal pain syndromes that require a broader recruitment of the DCs. Techniques to fully control the position of a percutaneous lead during insertion and to preserve this position postoperatively are not yet available. Implanting a surgical paddle lead provides better control of the lead position and stability in the epidural space.

A comparison of percutaneous and surgical leads with a similar center-to-center contact spacing (Chapter 2) revealed that this parameter is still crucial for the ability to recruit fibers in the DCs versus DRs. Two different lead types with the same contact spacing had a similar performance in the recruitment of fibers in the DCs and DRs. Clinically, however, a better performance of the surgical lead was observed by North et al. [6], presumably due to its larger volume, resulting in a displacement of the dura mater in a ventral direction, towards the spinal cord. According to our model predictions a reduced distance from the lead most likely accounts for a better performance, i.e. an increased paresthesia coverage.

A smaller dorsal CSF thickness indicates a smaller distance to the neural target and reduced stimulation thresholds. Because DC fiber thresholds

are reduced more steeply than DR fiber thresholds when the distance is reduced this will result in an increased therapeutic range and thus an increased paresthesia coverage. Moreover, the energy consumption is reduced. A natural variation of the dorsal CSF thickness exists among individuals, as well as an intra-individual variation related to the spinal level and to posture. Although these variations cannot be controlled, the CSF thickness can be reduced by using bulkier leads or by inserting sham material (mass) in the dorsal epidural space. A pilot study by Khan et al. using this approach has been shown to be beneficial (personal communication). The latter approach would be particularly attractive as it utilizes a less-traumatic and simpler surgical technique than a paddle lead.

The performance of a single percutaneous lead positioned over the physiological midline and two (aligned or staggered) percutaneous leads of the same type positioned in parallel on either side of the physiological midline were compared (Chapter 3). In both cases a single channel pulse generator was used. The “dual lead” is increasingly popular nowadays. We predicted that the single lead would have a larger recruitment of DC fibers. This model prediction has recently been confirmed in a study by North et al. [7]. However, sometimes the dual lead has a better clinical outcome [1]. This is not attributable to a technical advantage of a dual lead as indicated by our modeling results, but to both a higher likelihood that one of the leads resides in the immediate vicinity of the physiological midline and to a ventral displacement of the dura due to the additional mass inserted in the epidural space (two leads instead of one).

A step forward to compensate for a suboptimal lead position (due to malpositioning during implantation or to migration) may be electrical field steering. We demonstrated how the field can be steered rostrocaudally using multiple pulse generators and independent control of the current applied to different cathodes (Chapter 4). Steering the electrical field along the rostrocaudal axis altered primarily the population of stimulated DR fibers. A similar concept could be implemented with e.g. two or three percutaneous leads inserted in parallel. By changing the amplitude ratio of the stimuli applied to different leads at the same rostrocaudal level the electrical field can be steered in the mediolateral plane. This concept is similar to transverse tripole steering as introduced earlier [8], but may avoid the mechanical and implantation problems that the transverse tripolar surgical lead featured. The attractiveness of the electrical field steering concept resides in its ability to steer the field in a continuous, predictable way. Theoretical and clinical work to develop and validate this concept is proceeding.

In MCS a contact array is placed on the dura mater near the neural target(s), a stimulus pulse is applied repeatedly at a certain frequency and a neural response is provoked. In contrast to SCS no paresthesias are felt in MCS. Therefore, the target area has to be identified differently (imaging, MEPs). However, we recognized that the stimulation approach was essentially the same as in SCS and therefore we were able to use the same approach to model the

effects of MCS (Chapter 5). Although the model is in an early phase as many parameters are not yet known, some predictions have already been made and validated.

Unlike SCS there is no valid theory that explains the mechanism of action in MCS. This makes it difficult to decide which population of neurons or fiber tracts should be modeled. Moreover, lack of knowledge of the neural targets to be stimulated in order to elicit analgesia prevents us from optimizing the therapy (lead design, orientation, stimulus parameters) in a systematic and knowledge-based way. Therefore, a reversed approach should be applied: all relevant cortical elements that may respond to the stimulus should be modeled and their thresholds and stimulation conditions compared. In this way, it could be possible to determine which neural elements most likely respond directly to the applied stimulus. Based on chronaxie measurements it was concluded that large cortical myelinated axons are most likely to respond directly to the stimulus as applied in MCS [4]. This was confirmed by our modeling results (Chapter 6). The site of action potential initiation was always at one of the axonal nodes, even when the cell body and apical dendrite were included in the model. This fact stresses the importance of having a nerve fiber model that mimics the behavior of cortical nerve fibers. We used a peripheral sensory nerve fiber model in our MCS models [9]. It is known that peripheral sensory and motor fibers exhibit a different behavior and characteristics. It may thus be expected that cortical nerve fibers also have a distinct behavior that demands different model parameters. In addition, the diameters, position and orientation of cortical nerve fibers should be known better in order to predict the excitation thresholds more accurately. Neuroanatomical work on nerve fiber distributions in the cortex should give answers to these questions.

Similar to SCS, the distance between the lead and the neural targets (determined mainly by the thickness of the CSF in between) influences the excitation thresholds vastly (Chapter 6). Having a thinner CSF layer implies lower thresholds for excitation. However, just as in SCS where the excitation thresholds of DC and DR fibers do not have the same sensitivity to the thickness of the CSF, a different behavior can be expected in MCS for different groups of nerve fibers as shown by modeling. Moreover, the population of nerve fibers stimulated may be influenced by controlling the CSF thickness. Similar to SCS, the CSF thickness can presumably be controlled by the volume of the inserted lead. Unfortunately, measuring the thickness of the CSF under the lead in MCS and SCS, is hardly possible due to the artifacts in CT and MRI images.

Both cathodes and anodes are used in MCS, just as in SCS. With amplitudes and duration of pulses applied in SCS, an anode only modulates the effects of stimulation and never directly stimulates neural elements nor blocks their excitation. However, in MCS an anode cannot be considered an indifferent lead contact. In fact, a neuron (pyramidal cell) oriented perpendicular to the anodal surface may have a low excitation threshold. The opposite happens with

cathodal stimulation where perpendicular nerve cells cannot be excited due to hyperpolarization of the axon. This behavior as predicted by modeling has also been observed in animal experiments. Due to a curvature of the cortical surface, different groups of pyramidal cells may or may not be perpendicular to the anodal/cathodal surface, depending on the lead contact position in respect to the precentral gyrus. Consequently, by varying the position of cathodes and anodes, the group of pyramidal cells perpendicular to the cortical surface that responds most readily or does not respond at all to the stimulus can be varied. The anodal contact is often located over the sensory cortex (postcentral gyrus) or in its vicinity (over the central sulcus). Therefore, pyramidal cells in the sensory cortex perpendicular to the anode may be excited and the role of sensory cortex in analgesia cannot be simply discarded especially as spinothalamic input via thalamus ends in sensory cortex. It has been shown that stimulating exclusively the sensory cortex may also result in pain relief [2].

The mechanisms of analgesic action of MCS remain unknown. PET scan studies performed during MCS have shown an increased cellular activity in those thalamic nuclei having connections with the motor cortex [3]. Activation of these nerve cells may be either due to antidromically or orthodromically propagated action potentials from neural elements excited in the (motor) cortex. Similarly, activity of the sensory cortex may be modulated by MCS. Alternatively, since MCS for chronic pain is applied below the motor threshold level, the analgesic effects may be linked to neuronal plasticity either mediated by the repeated stimulus-imposed extracellular field or by backpropagation and invasion of the action potentials caused by this field.

Lack of knowledge on the mechanisms of action is an extremely limiting factor. Knowledge of these mechanisms or at least a good working hypothesis (as the ‘gate-control’ theory in SCS) is crucial for the optimization of the therapy. A working hypothesis on the neural network involved in analgesia and monitoring the neuronal activities in parts of this network concurrent with and without MCS would help to elucidate these mechanisms. These activities can be measured either by means of novel imaging techniques (PET, fMRI) or by ‘on-spot’ electrophysiological recording. Although they are being used in clinical practice, these imaging techniques may still not have a sufficient resolution and reliability. For ethical reasons, clinical experiments involving ‘on-spot’ electrophysiological recording may not be an option (although they have been performed in deep brain stimulation). However, MCS experiments on primates may be adequate.

In conclusion, the computer modeling results presented in this thesis can be successfully used to explore effects of both SCS and MCS (as well as other electro-neuromodulative techniques). While SCS model predictions were validated in the past, the MCS model still needs to face validation. In collaboration with clinical and (neuro)physiology/anatomy centers, refinements and improvements of the MCS model should be sought in order to obtain better model predictions. Nevertheless, computer modeling represents an invaluable

tool that may contribute significantly to unravel the effects of stimulation and subsequently to the improvement and innovation of these neuromodulative therapies.

## REFERENCES

- 1 Alo K, Redko V and Chornov J. Four year follow-up of dual electrode spinal cord stimulation for chronic pain. **Neuromodulation**. 5:79-88, 2002
- 2 De Ridder D, De Mulder G, Sunaert S and Moller A. Somatosensory cortex stimulation for deafferentation pain. **Neuromodulation**. 9:(in press), 2006
- 3 Garcia-Larrea L, Peyron R, Mertens P, Gregoire MC, Lavenne F, *et al.* Electrical stimulation of motor cortex for pain control: a combined PET-scan and electrophysiological study. **Pain**. 83:259-273, 1999
- 4 Hanajima R, Ashby P, Lang AE and Lozano AM. Effects of acute stimulation through contacts placed on the motor cortex for chronic stimulation. **Clin Neurophysiol**. 113:635-641, 2002
- 5 Holsheimer J and Wesselink W. Optimum electrode geometry for spinal cord stimulation: the narrow bipole and tripole. **Med Biol Eng Comput**. 35:493-497, 1997
- 6 North R, Kidd D, Olin J and Sieracki J. Spinal cord stimulation electrode design: prospective, randomized, controlled trial comparing percutaneous and laminectomy electrodes - Part I. Technical outcomes. **Neurosurgery**. 51:381-390, 2002
- 7 North R, Kidd D, Olin J, Sieracki J and Petrucci L. Spinal cord stimulation for axial low back pain: a prospective controlled trial comparing 16-contact insulated electrodes with 4-contact percutaneous electrodes. **Neuromodulation**. 9:56-67, 2006
- 8 Struijk J and Holsheimer J. Transverse tripolar spinal cord stimulation - Theoretical performance of a dual channel system. **Med Biol Eng Comput**. 34:273-279, 1996
- 9 Wesselink WA, Holsheimer J and Boom HBK. A model of the electrical behaviour of myelinated sensory nerve fibres based on human data. **Med Biol Eng Comput**. 37:228-235, 1999



---

## Summary of the thesis

### Computer modeling of neuromodulation in the management of chronic pain

Neuromodulation is an important and frequent therapy applied, among others, in the management of chronic pain. Neuromodulation is defined as “a therapeutic alteration of activity in the central, peripheral or autonomic nervous systems, electrically or pharmacologically, by means of implanted devices”. It encompasses a focal, minimal invasive and reversible approach. Due to its invasive character with some more risks than other modalities of pain treatment, neuromodulation is generally applied as the last option when all other therapies have failed. The overall success rate of this treatment modality is about 50%. It is often the only modality that may help a particular patient. However, there are still many chronic pain patients in whom neuromodulation was attempted with suboptimal or even less than satisfactory results. For the sake of this pool of patients it is an imperative to understand the effects occurring during a neuromodulation therapy and to design stimulation in such a way that a larger number of patients can be treated, while giving them an improved satisfaction with the therapy.

This thesis is focused on spinal cord and motor cortex stimulation therapies for chronic, otherwise intractable pain management. The influence of various stimulation and volume conductor parameters on the neural response was investigated by means of realistic computer models.

In **Chapter 1** neuromodulation is presented as one of the treatment modalities for the management of various chronic pain syndromes. Further, the clinical methods named spinal cord stimulation and motor cortex stimulation are introduced. Details are given on working hypotheses (when existing), main indications, surgical procedures and technical aspects, difficulties and challenges encountered in the therapies. The chapter is completed by introducing the computer model as an invaluable tool to mimic/simulate the biophysical effects of neurostimulation.

The technical performance of two different lead types commonly used in the clinical practice of spinal cord stimulation, the paddle (or surgical) lead and the percutaneous lead has been modeled and evaluated in **Chapter 2**. In addition to the thickness of the dorsal cerebrospinal fluid and the lead distance from the dura mater, the contact spacing on the lead was identified as the most important parameter influencing the performance. Despite a similar contact spacing and technical performance, a superior clinical performance of paddle leads was observed in clinical practice. This superiority is most likely attributable to the larger volume of a paddle and a consequent ventral displacement of the dura mater. The secure fixation of the paddle in close

---

contact with the dura mater is most likely an additional factor determining the superior clinical performance as discussed in the chapter.

In **Chapter 3** the technical performance of percutaneous leads for spinal cord stimulation having various contact spacings is modeled and compared. While reducing the contact spacing the recruitment of dorsal column fibers is increased, though with larger energy expenditure. The effect on the recruitment of dorsal root fibers is opposite. Modelling predicts that a displacement of the lead dorsally or laterally in the dorsal epidural space results in a reduction of the ratio of dorsal root and dorsal column fiber thresholds and thereby in less paresthesia coverage (when the stimulus is just at the discomfort threshold). When two leads are connected in parallel modelling predicts that dorsal column recruitment is reduced. This prediction has recently been confirmed empirically.

Owing to technical advances the concept of electrical field steering has recently emerged in spinal cord stimulation. A method to electronically shift the electrical field rostrocaudally along the spinal cord, resulting in predictable changes in the population of recruited sensory nerve fibres and thus the position of paresthesia is described in **Chapter 4**. It is predicted that a smaller contact spacing allows a better control of the stimulation field. This may be crucial in the treatment of pain syndromes such as chronic low-back pain, as discussed in this chapter.

In **Chapter 5**, the first model of electrical stimulation of human motor cortex is introduced. The region of the precentral gyrus and surrounding sulci with an electrode array (paddle lead) on the overlying dura mater represents the core of the model's volume conductor. A simple fiber model was taken from the spinal cord stimulation model and used to assess the neural response to the stimulation induced field. It was predicted that the thickness of the cerebrospinal fluid layer underneath the active contact influences the stimulation threshold considerably. In addition, nerve fibers oriented perpendicular to an anode above the cortical surface could be activated at a low amplitude. As a consequence, an anode cannot be considered an indifferent contact in motor cortex stimulation, contrary to common belief.

A refined and extended model of motor cortex stimulation is described in **Chapter 6**. When the myelinated axon model was extended with a frustum and another cylindrical membrane structure, representing a pyramidal cell and its apical dendrite, respectively, the stimulation threshold was generally reduced. By changing the polarity and/or position of the stimulating contact array, stimulation thresholds of pyramidal cells varied and the population of recruited cells was changed as well. The model predictions have been shown to be qualitatively in accordance with empirical data from the literature.

Finally, the thesis is completed in **Chapter 7** with a discussion of the most prominent effects in spinal cord and motor cortex stimulation that have been analyzed by computer modeling. In addition, recommendations for future theoretical and empirical studies are proposed.

---

## Samenvatting

### De computer modellering van neuromodulatie in het beheer van chronische pijn

Neuromodulatie is een belangrijke en veel toegepaste therapie die, onder ander, in het beheer van chronische pijn wordt toegepast. Neuromodulatie wordt gedefinieerd als "de therapeutische wijziging van activiteit in het centrale, perifere of autonome zenuwstelsels, elektrisch of farmacologisch, met behulp van geïmplanteerde apparaten". Het omvat een brandpunts, minimale invasieve en omkeerbare benadering. Wegens zijn invasieve karakter met meer risico's dan andere modaliteiten van pijn wordt neuromodulatie over het algemeen toegepast als laatste optie wanneer al andere therapieën niet succesvol zijn geweest. Het totale succes percentage van deze behandelingsmodaliteit is ongeveer 50%. Het is vaak de enige modaliteit die een bepaalde patiënt kan helpen. Nochtans, zijn er nog vele chronische pijnpatiënten bij wie neuromodulatie met suboptimaal of zelfs minder dan bevredigende resultaten werd geprobeerd. Omwille van deze pool van patiënten is het belangrijk om de effecten te begrijpen die tijdens een neuromodulatietherapie voorkomen en een stimulatie methode te ontwikkelen, zodanig dat een groter aantal patiënten kan worden behandeld en de tevredenheid over de therapie wordt verhoogd..

Dit proefschrift geconcentreerd zich op ruggemerg en motorschors stimulatie voor chronisch, anders hardnekkig, pijnbeheer. De invloed van diverse stimulatie en volumeleiderparameters op de neurale reactie werd onderzocht door middel van realistische computermodellen.

In **Hoofdstuk 1** wordt neuromodulatie voorgesteld als één van de behandelingsmodaliteiten voor het beheer van diverse chronische pijnsyndromen. Verder worden de klinische methodes, ruggemergstimulatie en de stimulatie van de motorschors, geïntroduceerd. De details worden gegeven op werkhypothesen (wanneer het bestaan), hoofdaanwijzingen, chirurgische procedures en technische aspecten, moeilijkheden en uitdagingen die in de therapie worden ondervonden. Het hoofdstuk wordt voltooid door het computermodel te introduceren als een onschatbaar hulpmiddel om de biofysische gevolgen van neurostimulation te simuleren.

De technische prestaties van twee verschillende elektrode types die algemeen in de klinische praktijk van ruggemergstimulatie worden toegepast, het peddel (of chirurgisch) elektrode en het percutane elektrode, worden gemodelleerd en geëvalueerd in **Hoofdstuk 2**. Naast de dikte van de dorsale cerebro-spinale vloeistof en de elektrode afstand van de dura mater, is de contactafstand tussen de elektrode delen geïdentificeerd als belangrijkste parameter die de prestaties beïnvloedt. Ondanks de gelijkaardige contactafstand en technische prestaties, werden superieure klinische prestaties van peddel elektrode waargenomen in de klinische praktijk. Deze superioriteit is het meest waarschijnlijk toe te schrijven

---

aan het grotere volume van een peddel en een voortvloeiende buikverplaatsing van dura mater. De veilige bevestiging van de peddel in dicht contact met dura mater is waarschijnlijk een extra factor die de superieure klinische prestaties bepaalt, zoals deze in het hoofdstuk wordt besproken.

In **Hoofdstuk 3** worden de technische prestaties van percutane elektrode voor ruggemergstimulatie bij diverse contactafstand gemodelleerd en vergeleken. Terwijl het verminderen van het contact dat de rekrutering van dorsale kolom uit elkaar plaatst wordt de vezels verhoogd, niettemin met grotere energieuitgaven. Het effect op de rekrutering van dorsale wortelvezels is tegenovergesteld. De modellering voorspelt dat een verplaatsing van het elektrode dorsaal of lateraal in de dorsale epidurale ruimte in een vermindering van de verhouding van dorsale wortel en de dorsale drempels van de kolomvezel en daardoor in minder paresthesiadekking resulteert (wanneer de stimulus enkel bij de ongemakdrempel is). Wanneer twee elektroden in parallelle modellering worden verbonden voorspelt het model dat de dorsale kolomrekrutering wordt verminderd. Deze voorspelling is onlangs empirisch bevestigd.

Ten gevolge van technische vooruitgang is het concept ‘electrische sturing’ onlangs in ruggemergstimulatie tevoorschijn gekomen. Een methode om rostro-caudaal het elektrisch veld langs het ruggemerg te verplaatsen, die leidt tot een voorspelbare veranderingen in de bevolking van aangeworven sensorische zenuwvezels resulteert en zo de positie van paresthesia veranderd wordt beschreven in **Hoofdstuk 4**. Het wordt voorspeld dat het kleinere contactafstand een betere controle van het stimulatiegebied toestaat. Dit kan in de behandeling van pijnsyndromen zoals chronische low-back pijn essentieel zijn, zoals besproken in dit hoofdstuk.

In **Hoofdstuk 5**, wordt het eerste model van elektrostimulatie van menselijke motorschors geïntroduceerd. Het gebied van precentral gyrus en de omringende groeven met een elektrodenserie (peddel elektrode) op het bedekken dura mater vertegenwoordigt de kern van de het volumeleider van het model. Een eenvoudig vezelmodel werd genomen uit het model van de ruggemergstimulatie en werd gebruikt om de neurale reactie op het stimulatie veroorzaakte gebied te beoordelen. Het wordt voorspeld dat de dikte van de cerebro-spinale vloeibare laag onderaan het actieve contact de stimulatie drempel aanzienlijk beïnvloedt. Bovendien zou de zenuwvezels georiënteerde aan een anode boven de corticale oppervlakte bij een lage amplitude kunnen worden geactiveerd. Bijgevolg, kan een anode als een onverschillig contact in de stimulatie van de motorschors worden beschouwd niet, strijdig met gemeenschappelijk geloof.

Een geraffineerd en uitgebreid model van de stimulatie van de motorschors wordt beschreven in **Hoofdstuk 6**. Toen het myelinated model werd uitgebreid met frustrum en een andere cilindrische membraanstructuur, die een pyramidal cel en zijn apicale dendriet vertegenwoordigt, respectievelijk, werd de stimulatie drempel over het algemeen verminderd. Door de polariteit en/of de positie van de bevorderende contactserie te veranderen, variëerden de

---

stimulatierempels van pyramidal cellen en werd de bevolking van aangeworven cellen eveneens veranderd. De modelvoorspellingen zijn getoond om kwalitatief overeenkomstige empirische gegevens van de literatuur te zijn.

Tot slot wordt het proefschrift voltooid in **Hoofdstuk 7** met een bespreking van de prominentste gevolgen in ruggemerg en motorschors stimulatie die door computer te modelleren zijn geanalyseerd. Bovendien worden de aanbevelingen voor toekomstige theoretische en empirische studies voorgesteld.



---

## **Curriculum Vitae**

The author of this thesis was born on 14 March 1977 in Belgrade, Serbia. Having completed the high school as a student of generation he joined the Faculty of Electrical Engineering in Belgrade in 1996. During the studies he did a practical training in the Lighting Laboratory of the Helsinki University of Technology, Finland and at the Beckman Institute of the University Urbana, USA. Towards the end of the studies he gained interest in biomedical engineering because of the inherent multidisciplinary nature of the field. In 2002 he defended diploma thesis with the title “ECG Virtual Instrument using LabView®”.

In the same year he joined Biomedical Signals&Systems Group of the University of Twente, The Netherlands as a PhD student. The main part of the time was spent on research for the project comprising computer modeling of neurostimulation, while the rest was dedicated to teaching duties and education. The research results were presented through a number of publications and presentations in (inter)national meetings and conferences. The ultimate result of the four-year research lies before you in the form of this thesis.

---

## List of publications

- *Refereed journal papers*

1. Manola Lj., Roelofsen B.H., Holsheimer J., Marani E., and Geelen J. Modelling motor cortex stimulation for chronic pain control: characteristics of the electrical field, activating function and nerve fibre responses. *Med Biol Eng Comput* 2005; 43:335-343.
2. Manola Lj., Holsheimer J and Veltink P.H. Technical performance of percutaneous leads for spinal cord stimulation: a modeling study. *Neuromodulation* 2005; 8:88-99.
3. Manola Lj. and Holsheimer J. Technical performance of percutaneous and laminectomy leads analyzed by modeling. *Neuromodulation* 2004; 7:231-241.
4. Nakazato M., Manola Lj. and Huang T.S. *ImageGrouper*: a group-oriented user interface for content-based image retrieval and digital image arrangement. *J Visual Lang Comput* 2003; 14:363-386.
5. Jiang X., Holsheimer J., Manola Lj., Wagner G., Wijkstra H., Knipscheer B., Meuleman J.H. Application of correlation techniques in the analysis of corpus cavernosum electromyographic signals. (*submitted*).
6. Manola Lj., Holsheimer J., Veltink P, Bradley K and Peterson D. Theoretical investigation into longitudinal field steering in spinal cord stimulation. (*submitted*).
7. Manola Lj., Holsheimer J., Buitenweg JR. and Veltink P. Anodal vs cathodal stimulation of motor cortex: a modeling study. (*submitted*).

---

- *Other*

**Book chapter:**

1. Manola, Lj. and Holsheimer, J. Motor cortex stimulation: role of computer modeling. *Neuromodulation* eds. Simpson B, Krames E and Sakas D. 2006 (*submitted*)

**Abstracts, posters and oral presentations at international conferences and meetings:**

1. Manola Lj., Roelofsen B., Holsheimer J., Marani E. (2005) A computer modeling study on motor cortex stimulation. In (Ed.), *Abstract 7th INS World Congress*, Rome, Italy. (*abstract + oral presentation*)



- 
2. Manola Lj., Holsheimer J., Veltink P. (2005) Dual percutaneous leads for SCS – single vs dual mode. In (Ed.), *Abstract 7th INS World Congress*, Rome, Italy. (abstract + oral presentation)
  3. Manola Lj., Holsheimer J. (2005) Technical performance of percutaneous and laminectomy leads with similar contact spacing. In (Ed.), *Abstract 7th INS World Congress*, Rome, Italy. (abstract + poster)
  4. Manola Lj. (2005) A computer modelling study on motor cortex stimulation. *International PhD student summer school*, Kotor, Montenegro. Organizers: Prof Dr Dejan Popovic and Prof Dr Thomas Sinkjaer. (poster + oral presentation)
  5. Manola, Lj., & Holsheimer, J. (May, 2005). *Electrical steering with two tripoles on a dual percutaneous lead*. Valencia, Calif., Advanced Bionics Corp.
  6. Holsheimer, J., Roelofsen, B.H., Manola, L., & Marani, E. (2004). Electrical fields and neural responses in motor cortex stimulation. In (Ed.), *Abstracts Meeting European Society Stereotactic and Functional Neurosurgery Vol. 146. Acta neurochirurgica. Supplementum (ISSN 0065-1419)* (pp. 900) Vienna. (abstract)
  7. Holsheimer, J., Roelofsen, B.H., Manola, L., & Marani, E. (2004). Field modelling in motor cortex stimulation. In (Ed.), *Proceedings 1st Scientific Meeting Benelux Neuromodulation Society Vol. 7. Neuromodulation (ISSN 1094-7159)* (pp. 147) Leuven. (abstract)
  8. Holsheimer, J., & Manola, Lj. (Nov, 2005). *Does it matter that the contact impedance of SCS electrodes is variable?* Ghent, Belgium, 3rd Meeting Benelux Neuromodulation Society.
  9. Manola, Lj., & Holsheimer, J. (Nov, 2005). *Single vs dual mode stimulation in SCS - what is the difference?* Ghent, Belgium, 3rd Meeting Benelux Neuromodulation Society.
  10. Holsheimer, J., Os, R. van, & Manola, Lj. (Oct, 2005). *Cathodal and anodal effects in bipolar motor cortex stimulation: which cortical fibres are activated?* Paris, France, European Continuous Medical Training (ECMT) course on motor cortex stimulation for the treatment of central and peripheral pain.
  11. Manola, L., Holsheimer, J., Bradley, K., & Peterson, D.K. (2004). Electrical steering on percutaneous SCS arrays: a modelling study. In (Ed.), *Abstract 16th Congress American Society Stereotactic and Functional Neurosurgery* Cleveland, OH. (abstract)
  12. Manola, L., & Holsheimer, J. (2004). Mediolateral electrical steering with two guarded cathodes on two parallel percutaneous spinal cord stimulation leads: a modelling study. In W.M.G.F. Pontenagel & J. Feijen (Eds.), *Proceedings of the Dutch Annual Conference on BioMedical Engineering* Papendal: University of Twente (ISBN 90-365-2102-5). (oral presentation)
  13. Manola, L., Roelofsen, B.H., & Holsheimer, J. (2004). Motor Cortex Stimulation: a computer modelling study. In Duncan Wood & Paul Taylor

- 
- (Eds.), *9th Annual IFESS Conference* (pp. 20-22) Bournemouth, UK: IFESS (ISBN 1-85899-191-9). (*abstract + oral presentation*)
14. Manola, Lj., & Holsheimer, J. (May, 2004). *Electrical steering with dual AB SC2108 leads*. Valencia, Calif., Advanced Bionics Corp.
  15. Manola, L., & Holsheimer, J. (2003). The technical performance of different lead types for spinal cord stimulation with similar contact spacing analysed by modeling. . In W.M.G.F. Pontenagel & J. Feijen (Eds.), *Proceedings of the Dutch Annual Conference on BioMedical Engineering* Papendal: University of Twente (ISBN 90-365-1973-x). (*abstract + oral presentation*)
  16. Holsheimer, J., Manola, L. (2003) Technical performance of percutaneous leads in SCS. In (Ed.), *Abstract 6th INS World Congress*, Madrid, Spain. (*abstract*)
-